

¹
²

Conceptual Design Report The Neutrino Experiment

³ Volume: The Liquid Argon Detector at the Far Site

⁴

February 9, 2015

Editor's Note: This document has been prepared in an ad hoc manner to provide a summary of the scope of the LBNE project as of January 2015. It pulls content from version 8 of LBNE's CDR vol 4 and includes some changes made since 2012, with notes added; the changes may not be reflected consistently throughout the document, as a thorough editing pass has not been made. It is planned to update this document in 2015 consistent with the plan resulting from the iIEB's efforts. Changes to note in particular about the current plan relative to the 2012 design include:

- House two detectors, of fiducial mass 10 kton and 30 kton, respectively, in separate, parallel caverns. Outfit the smaller cavern as soon as possible and outfit the larger in a later phase of work. (The 30-kton detector was not part of the 2012 design; its configuration, to be determined by the international collaboration, is not discussed in this interim report.)
- Place the compressors for the nitrogen refrigeration system on the surface, and place the remainder of the refrigeration system in the 10-kton cavern. Deliver argon and nitrogen in gas form to the smaller cavern, where liquification will take place. Liquid will be transferred to and from the detector in the 30-kton cavern.
- Make detector shallower and longer. Build APAs of width 2.3 m and height 6 m (2012 dimensions were 2.5 m × 7 m). Increase the length of the 10-ton detector from 25 m to 30 m.
- Replace the far detector prototyping plan known as LAr1 by a plan to build and test a prototype with full-size TPC components at CERN.

Contents

2	1 Introduction	1
3	1.1 Introduction to the LBN Project	1
4	1.1.1 About this Conceptual Design Report	1
5	1.1.2 LBN and the U.S. Neutrino-Physics Program	2
6	1.1.3 LBN Project Organization	3
7	1.1.4 Principal Parameters of the LBN Project	4
8	1.1.5 Supporting Documents	4
9	1.2 Introduction to the Liquid Argon Far Detector	5
10	1.2.1 Overview	5
11	1.2.2 Cavern Layout	9
12	1.2.3 Cryostat Construction	12
13	1.2.4 Cryogenic Systems	14
14	1.2.5 LAr Purification	14
15	1.2.6 Time Projection Chamber	14
16	1.2.7 Electronics, Readout and Data Acquisition	15
17	1.2.8 Photon-Detection System	18
18	1.2.9 Detector Installation and Operation	19
19	1.3 Principal Parameters	19
20	1.3.1 Design Considerations	20
21	1.4 Detector Development Program	22
22	1.5 Participants	23
23	2 Time Projection Chamber and Electronics	25
24	2.1 Introduction	25
25	2.2 Design Considerations	28
26	2.3 Anode Plane Assemblies	30
27	2.3.1 Wires	30
28	2.3.2 Wire Planes	32

1	2.3.3	APA Frame	35
2	2.3.4	Wire Wrapping Around an APA	35
3	2.3.5	Wire Supports on Inner Frame Members	38
4	2.3.6	Wire-Winding Machines	39
5	2.3.7	Alternative APA Construction	39
6	2.4	Cathode Plane Assemblies	44
7	2.5	Field Cage	45
8	2.6	TPC Assembly in the Cryostat	46
9	2.7	In-Vessel Front-End Electronics	47
10	2.7.1	Architecture	47
11	2.7.2	Data Rates	49
12	2.7.3	CMOS Circuit Design	51
13	2.8	TPC Infrastructure	55
14	2.8.1	Design Considerations	55
15	2.8.2	Reference Design	56
16	2.8.3	TPC High Voltage	56
17	2.8.4	Wire-Bias Voltages	57
18	2.8.5	Power for the Cold Electronics	57
19	2.8.6	Digital Data IO Feedthroughs	58
20	2.9	TPC Prototyping, Test and Checkout	59
21	2.9.1	TPC Prototyping	59
22	2.9.2	Assembly Testing	60
23	2.9.3	Checkout	61
24	3	Data Acquisition	62
25	3.1	Introduction	64
26	3.2	Design Considerations	65
27	3.2.1	Physics Considerations	65
28	3.2.2	Technical Considerations	65
29	3.2.3	Event Rates and Timing	66
30	3.3	Architecture Summary	68
31	3.4	Data Concentrator Module	69
32	3.4.1	Data Processing/Handling	70
33	3.4.2	Timing, Control and Configuration Signals	71
34	3.5	Ethernet Switch Network	71
35	3.6	Event Building and Triggering	71
36	3.6.1	Event Building	71
37	3.6.2	Event Data Model	72

1	3.6.3 Triggering and Selection for Output Streams	72
2	Rejection of Event Records	72
3	Event selection for Physics-Specific Streams	73
4	3.7 Timing System	73
5	3.8 Run Control	73
6	3.9 Slow Control Systems	74
7	3.10 DAQ Infrastructure	74
8	3.10.1 Wide Area Network	74
9	3.10.2 Online Data Storage	74
10	3.10.3 Power and Cooling	75
11	4 Photon Detector	76
12	4.1 Introduction	76
13	4.2 Requirements and Goals	76
14	4.2.1 Beam-based physics	76
15	4.2.2 Proton decay and atmospheric physics	77
16	4.2.3 Low-energy physics	77
17	4.2.4 General Considerations	77
18	4.3 Cast or Bulk doped acrylic bars	77
19	4.3.1 Current status of design	79
20	5 Installation and Commissioning	84
21	5.1 Introduction	84
22	5.2 Above-ground Pre-Installation	87
23	5.2.1 Cryostat Materials	87
24	5.2.2 TPC Materials	87
25	5.2.3 Liquid Argon Receipt	89
26	5.3 Below-ground Pre-Installation	92
27	5.3.1 Equipment Required for Detector Installation	92
28	5.3.2 Clean Area	92
29	5.3.3 Rails for TPC-Panel Support and Transfer	94
30	5.3.4 Detector Electrical Ground	98
31	Reference Design	98
32	Features	99
33	5.4 Below-ground Installation Activities	102
34	5.5 TPC Installation	102
35	5.6 Installation Prototype	107
36	5.7 Training and Access Control	107

1	5.8	Detector Commissioning	108
2	5.9	ES&H	110
3	6	Detector Development Program	111
4	6.1	Introduction	111
5	6.2	Components of the Development Program	112
6	6.3	Scope and Status of Individual Components	112
7	6.3.1	Materials Test System	112
8	6.3.2	Electronics Test Stand	116
9	6.3.3	Liquid Argon Purity Demonstrator	116
10	6.3.4	Photon Detection R&D	120
11	6.3.5	TPC Design	120
12	6.3.6	Electronics Development	121
13		CMOS Transistors: Lifetime Verification and Technology Evaluation	121
14		Readout Architectures, Multiplexing and Redundancy	123
15	6.3.7	Cryostat Development: 35-ton Prototype	123
16	6.3.8	One-kiloton Engineering Prototype: LAr1	125
17	6.3.9	Physics Experiments with Associated Detector-Development Goals	126
18		ArgoNeuT - T962	127
19		MicroBooNE E-974	127
20	6.4	Summary	131
21	7	Alternatives Not Selected	132
22	7.1	Detector Configuration	132
23	7.1.1	Double Phase Readout	132
24	7.1.2	Cryostat Shape	132
25	7.1.3	Modular Cryostat	133
26	7.2	Depth Options	134
27	7.2.1	Surface and 300L	134
28	7.2.2	800L	134
29	7.3	Cryogenics Plant	135
30	7.3.1	LAr Supply using a Temporary Air-Separation Plant	135
31	7.3.2	LAr Storage	135
32	7.3.3	Common Riser for LAr and LN	136
33	7.3.4	Common Vent Lines	136
34	7.4	Cryostat Insulation	136
35	7.5	TPC	137
36	7.5.1	TPC Configuration	137

1	Reference Design 1a	137
2	Reference Design 2a	137
3	7.5.2 Wire Spacing	138
4	7.5.3 Number of Wire Planes	139
5	7.5.4 Drift Length	139
6	7.6 DAQ Cable Routing	139
7	7.7 Installation & Commissioning	140
8	7.8 Photon Detection	140
9	7.9 LAr1 Prototype	140

List of Figures

1.1	Location of LAr-FD caverns at the 4850L	6
1.2	Detector configuration within the cavern	7
1.3	Fiducial mass of 10-kton detector	8
1.4	Parameters for 10-kton detector cavern and pit, 2014	10
1.5	Parameters for 30-kton detector cavern and pit, 2014	11
1.6	Dimensions for 10-kton detector cavern and cryostat, 2014	13
1.7	TPC modular construction concept; the APA and CPA arrangement has been changed to two APAs and three CPAs as of 2014, see Figure 1.8.	16
1.8	APA and CPA arrangement, 2014	17
1.9	Conceptual front-end electronics architecture	18
1.10	Organization chart for the Far Detector subproject	24
2.1	Cross section of the TPC inside the cryostat	27
2.2	Illustration of the APA wire wrapping scheme	29
2.3	Plot of electric potential distribution near the wire planes	31
2.4	Illustration of ambiguity problem if U & V wire angles are equal	33
2.5	Conceptual design of a wire frame	34
2.6	Conceptual design of a wire bonding board for the x wires	35
2.7	Concept of wire wrapping board for U wires on long edge of APA	37
2.8	Closeup view of a partially assembled corner of an APA	37
2.9	Conceptual design of the wire support for the U, V & X wires	38
2.10	Two winding machine concepts	39
2.11	Concept of the alternative APA wiring scheme	41
2.12	Illustration of dead space above FR-4 boards and possible solution	41
2.13	Conceptual designs of the wire winding machine and wire module storage fixture	42
2.14	Assembly table with equipment for stretching wires.	43
2.15	Conceptual design of a cathode plane assembly	44

1	2.16 Electrostatic simulation of electric field near a section of field cage	45
2	2.17 A partial assembly of the TPC showing all major components	46
3	2.18 Conceptual architecture of the front-end electronics operating in LAr	48
4	2.19 Architecture and layout of the 16-channel front-end mixed-signal ASIC	49
5	2.20 Conceptual architecture of zero-suppression	51
6	2.21 Measured pulse response with details	53
7	2.22 Measured ENC vs filter time constant	54
8	2.23 ICARUS HV feedthrough; concept of new feedthrough	57
9	2.24 Conceptual design of signal/power feedthrough	58
10	3.1 Block diagram depicting the DAQ reference-design architecture	68
11	3.2 Photograph of several prototype NO ν A Data Concentrator Modules.	70
12	4.1 Schematic drawing of cast acrylic light guide	78
13	4.2 IU dewar paddle frame showing movable alpha source	80
14	4.3 Left: Stacked waveforms for 11 positions of the α source along the bar. Right: The results of fitting a single exponential to the measurements on the left. The attenuation length is \sim 37 inches.	81
15		
16		
17	4.4 Left: Monte Carlo simulations of the 420 nm light seen by the SiPMs as a function of distance along the bar. Right: Increase in the light due to reflections in the TallBo dewar for the different light guide technologies.	82
18		
19		
20	4.5 Comparison of several light guide technologies including the CSU fiber technology in the TallBo dewar. The corrections for systematics in Fig- ure 4.4 (right) have been applied.	82
21		
22		
23	5.1 Cutaway view of two cryostats with TPC detectors installed	86
24	5.2 Cryostat components staged in a LNG transport ship	88
25	5.3 Concept for APA shipping containers - cross section view	90
26	5.4 TPC-panel containers exiting the Yates shaft	91
27	5.5 Raised-panel floor to protect the cryostat's primary membrane	93
28	5.6 Support rails inside cryostat	95
29	5.7 Feedthroughs	96
30	5.8 TPC installation monorail with APA moving to support rail	97
31	5.9 Block diagram of the AC power for one cryostat	100
32	5.10 TPC panels installed in cryostat	103
33	5.11 The three main work zones for TPC Installation	106
34	5.12 Startup and Commissioning Sequence	109
35	6.1 Liquid argon area at the Proton Assembly Building at Fermilab	114

1	6.2 Schematic of the Materials Test System (MTS) cryostat at Fermilab	115
2	6.3 Electronics test TPC insertion into cryostat	117
3	6.4 Cosmic ray with a delta electron as seen in the Electronics Test Stand TPC	118
4	6.5 Liquid Argon Purity Demonstration filtration and tank at the PC-4 facility	119
5	6.6 Lifetime at different temperatures vs V_{DS}	122
6	6.7 Layout of 35-ton prototype at Fermilab's PC-4 facility	124
7	6.8 Membrane panel assembly and components	125
8	6.9 ArgoNeuT neutrino event with four photon conversions	128
9	6.10 Data from ArgoNeuT	128
10	6.11 ArgoNeuT: status of 3D reconstruction	129
11	6.12 ArgoNeuT: status of calorimetric reconstruction	130
12	7.1 Alternate cable routing from an APA to a cold feedthrough	138

1

xi

List of Tables

2	1.1	LBN Principal Parameters	4
3	1.2	LBNE CD-1 Documents	4
4	1.3	LAr-FD Principal Parameters for 10-kton Detector	20
5	3.1	Rates and data sizes/rates for various processes.	67
6	3.2	DAQ subsystem component counts	69
7	6.1	LBNE on-project development activities	113
8	6.2	LBNE off-project development activities	113

¹ Todo list

² | ²

¹ Chapter 1

² Introduction

³ 1.1 Introduction to the LBN Project

⁴ The The Neutrino Experiment (LBN) Project team has prepared this Conceptual
⁵ Design Report (CDR) which describes a world-class facility to enable a compelling
⁶ research program in neutrino physics. The ultimate goal in the operation of the
⁷ facility and experimental program is to measure fundamental physical parameters,
⁸ explore physics beyond the Standard Model and better elucidate the nature of matter
⁹ and antimatter.

¹⁰ Although the Standard Model of particle physics presents a remarkably accurate
¹¹ description of the elementary particles and their interactions, it is known that the
¹² current model is incomplete and that a more fundamental underlying theory must
¹³ exist. Results from the last decade, revealing that the three known types of neutrinos
¹⁴ have nonzero mass, mix with one another and oscillate between generations, point
¹⁵ to physics beyond the Standard Model. Measuring the mass and other properties
¹⁶ of neutrinos is fundamental to understanding the deeper, underlying theory and will
¹⁷ profoundly shape our understanding of the evolution of the universe.

¹⁸ 1.1.1 About this Conceptual Design Report

¹⁹ The LBN Conceptual Design Report is intended to describe, at a conceptual level,
²⁰ the scope and design of the experimental and conventional facilities that the LBN
²¹ Project plans to build to address a well-defined set of neutrino-physics measurement
²² objectives. At this Conceptual Design stage the LBN Project presents a *Reference*
²³ *Design* for all of the planned components and facilities, and alternative designs that
²⁴ are still under consideration for particular elements. The scope includes

- 1 • an intense neutrino beam aimed at a far site
 - 2 • detectors located at the near site just downstream of the neutrino source
 - 3 • a massive neutrino detector located at the far site
 - 4 • construction of conventional facilities at both the near and far sites
- 5 The selected near and far sites are Fermi National Accelerator Laboratory (Fermilab), in Batavia, IL and Sanford Underground Laboratory at Homestake (Sanford Laboratory), respectively. The latter is the site of the formerly proposed Deep Underground Science and Engineering Laboratory (DUSEL) in Lead, South Dakota.
- 6 This CDR is organized into six stand-alone volumes, one to describe the overall
7 LBN Project and one for each of its component subprojects:
- 8 • Volume 1: The LBN Project
 - 9 • Volume 2: The Beamline at the Near Site
 - 10 • Volume 3: Detectors at the Near Site
 - 11 • Volume 4: The Liquid Argon Detector at the Far Site
 - 12 • Volume 5: Cryogenic Systems
 - 13 • Volume 6: Conventional Facilities at the Near Site
 - 14 • Volume 7: Conventional Facilities at the Far Site
- 15 Volume 1 is intended to provide readers of varying backgrounds an introduction
16 to LBN and to the following volumes of this CDR. It contains high-level information
17 and refers the reader to topic-specific volumes and supporting documents, also listed
18 in Section 1.1.5. Each of the other volumes contains a common, brief introduction to
19 the overall LBN Project, an introduction to the individual subproject and a detailed
20 description of its conceptual design.

21 Volume 1 is intended to provide readers of varying backgrounds an introduction
22 to LBN and to the following volumes of this CDR. It contains high-level information
23 and refers the reader to topic-specific volumes and supporting documents, also listed
24 in Section 1.1.5. Each of the other volumes contains a common, brief introduction to
25 the overall LBN Project, an introduction to the individual subproject and a detailed
26 description of its conceptual design.

24 **1.1.2 LBN and the U.S. Neutrino-Physics Program**

25 Global?n its 2008 report, the Particle Physics Project Prioritization Panel (P5) rec-
26 ommended a world-class neutrino-physics program as a core component of the U.S.
27 particle physics program [?]. Included in the report is the long-term vision of a large
28 detector at the Sanford Laboratory and a high-intensity neutrino source at Fermilab.

1 On January 8, 2010, the Department of Energy (DOE) approved the Mission
2 Need for a new long-baseline neutrino experiment that would enable this world-class
3 program and firmly establish the U.S. as the leader in neutrino science. The LBN
4 Project is designed to meet this Mission Need.

5 With the facilities provided by the LBN Project, the LBN Science Collaboration
6 proposes to mount a broad attack on the science of neutrinos with sensitivity to
7 all known parameters in a single experiment. The focus of the program will be the
8 explicit demonstration of leptonic CP violation, if it exists, by precisely measuring
9 the asymmetric oscillations of muon-type neutrinos and antineutrinos into electron-
10 type neutrinos and antineutrinos.

11 The experiment will result in the most precise measurements of the three-flavor
12 neutrino-oscillation parameters over a very long baseline and a wide range of neutrino
13 energies, in particular, the CP- violating phase in the three-flavor framework. The
14 unique features of the experiment – the long baseline, the broad-band beam, and the
15 high resolution of the detector – will enable the search for new physics that manifests
16 itself as deviations from the expected three-flavor neutrino-oscillation model.

17 The configuration of the LBN facility, in which a large neutrino detector is lo-
18 cated deep underground, could also provide opportunities for research in other areas
19 of physics, such as nucleon decay and neutrino astrophysics, including studies of
20 neutrino bursts from supernovae occurring in our galaxy. The scientific goals and
21 capabilities of LBN are outlined in Volume 1 of this CDR and described fully in the
22 LBN Case Study Report (Liquid Argon TPC Far Detector) [?] and the 2010 Interim
23 Report of the The Neutrino Experiment Collaboration Physics Working Groups [?].

24 **1.1.3 LBN Project Organization**

25 The LBN Project Office at Fermilab is headed by the Project Manager and assisted
26 by the Project Engineer, Project Systems Engineer and Project Scientist. Project
27 Office support staff include a Project Controls Manager and supporting staff, a Finan-
28 cial Manager, an Environment, Safety and Health (ES&H) Manager, a Computing
29 Coordinator, Quality Assurance and Risk Managers, a documentation team and ad-
30 ministrative support. The Beamline, Liquid Argon Far Detector and Conventional
31 Facilities subprojects are managed by the Project Office at Fermilab, while the Near
32 Detector Complex subproject is managed by a Project Office at Los Alamos National
33 Laboratory (LANL).

34 More information on Project Organization can be found in Volume 1 of this CDR.
35 A full description of LBN Project management is contained in the LBN Project
36 Management Plan [?].

1.1.4 Principal Parameters of the LBN Project

¹ The principal parameters of the major Project elements are given in Table 1.1. ^{table: param-summ-fd}

Table 1.1: LBN Principal Parameters

Project Element Parameter	Value
Near- to Far-Site Baseline	1,300 km
Primary Proton Beam Power	708 kW, upgradable to 2.3 MW
Protons on Target per Year	6.5×10^{20}
Primary Beam Energy	60 – 120 GeV (tunable)
Neutrino Beam Type	Horn-focused with decay volume
Neutrino Beam Energy Range	0.5 – 5 GeV
Neutrino Beam Decay Pipe Diameter × Length	4 m × 200 m
Near Site Neutrino Detector Type	Liquid Argon Time Projection Chamber (LArTPC) Tracker
Near Site Neutrino Detector Active Mass	18 ton
Far Detector Type	LArTPC
Far Detector Active (Fiducial) Mass	54 (40) kton
Far Detector Depth	1480 m

1.1.5 Supporting Documents

³ ⁴ A host of information related to the CDR is available in a set of supporting documents. Detailed information on risk analysis and mitigation, value engineering, ⁵ ⁶ ES&H, costing, project management and other topics ⁷ ^{table: cd-1-doc-list} not directly in the design scope can be found in these documents, listed in Table 1.2. Each document is numbered and stored in LBNE’s document database, accessible via a username/password combination provided by the Project. Project documents stored in this database are made available to internal and external review committees through Web sites developed to support individual reviews.

Table 1.2: LBNE CD-1 Documents

Title	LBNE Doc Num-ber(s)
Acquisition Plan	5329

Alternatives Analysis	4382
Case Study Report; Liquid Argon TPC Detector	3600
Configuration Management Plan	5452
DOE Acquisition Strategy for LBNE	5442
Integrated Environment, Safety and Health Management Plan	4514
LAr-FD Preliminary ODH Analysis	2478
Global Science Objectives, Science Requirements and Traceback Reports	4772
Preliminary Hazard Analysis Report	4513
Preliminary Project Execution Plan	5443
Preliminary Security Vulnerability Assessment Report	4826
Project Management Plan	2453
Project Organization Chart	5449
Quality Assurance Plan	2449
Report on the Depth Requirements for a Massive Detector at Homestake	0034
Requirements, Beamline	4835
Requirements (Parameter Tables), Far Detector	3747 (3383)
Requirements, Far Site Conventional Facilities	4408
Requirements, Near Detectors	5579
Requirements, Near Site Conventional Facilities	5437
Risk Management Plan	5749
Value Engineering Report	3082
Work Breakdown Structure (WBS)	4219

¹

1.2 Introduction to the Liquid Argon Far Detector

²

1.2.1 Overview

³

- The reference design Far Detector for LBNE is a liquid argon time projection chamber (LArTPC). The basic components of this detector type are a cryostat to contain the liquid argon (LAr), a TPC detection mechanism immersed in the LAr, readout

1 electronics and a cryogenic system to keep the LAr temperature at 89 K and maintain
 2 the required purity.

3 As of 2014 the LBNE LArTPC, referred to as the LAr-FD, has been altered
 4 to consist of two massive detectors in separate, parallel caverns, oriented end-to-
 5 end along the beam direction (roughly east-to-west), and located at the 4850 level
 6 (4850L) of the Sanford Laboratory. The fiducial mass of first one to be built will
 7 be 10 ktons, the second, 30 ktons. Figure 1.1 shows the proposed layout of the
 8 Far Site, and Figure 1.2 shows the detector configuration. The cavern and related
 9 conventional facilities are described in Volume 6 of this CDR.

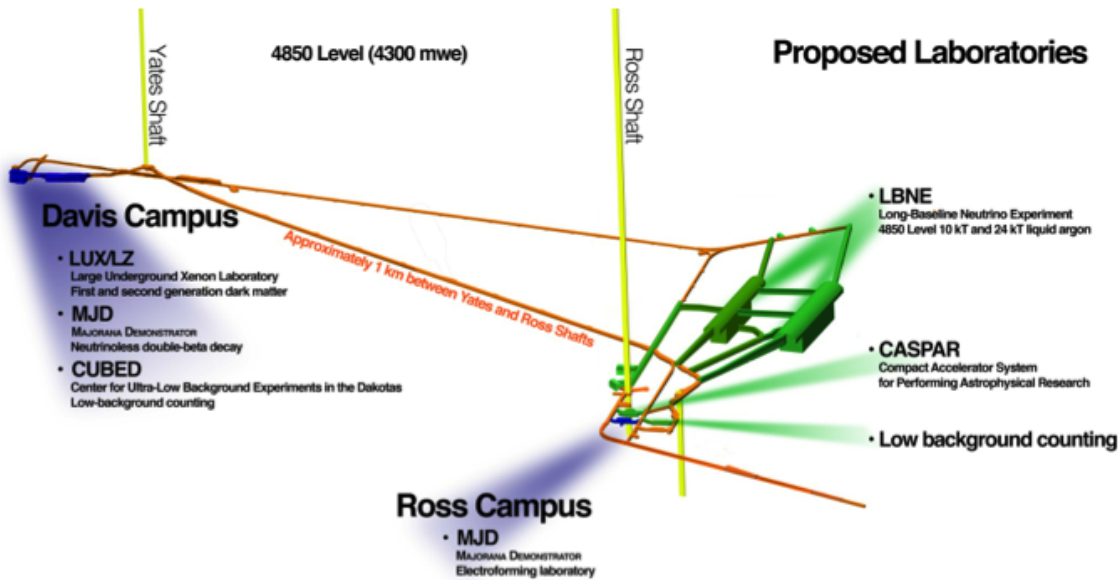


Figure 1.1: Location of LAr-FD caverns at the 4850L

fig:cavern-lay

10 The fiducial mass of the first is shown in Figure 1.3; a similar diagram for the
 11 second detector is not yet available.

12 In a LArTPC, a uniform electric field is created within the TPC volume between
 13 cathode planes and anode wire planes. Charged particles passing through the TPC
 14 release ionization electrons that drift to the anode wire planes. The bias voltage
 15 is set on the anode plane wires so that ionization electrons drift between the first
 16 several (induction) planes and are collected on the last (collection) plane. Readout
 17 electronics amplify and continuously digitize the induced waveforms on the sensing
 18 wires at several MHz, and transmit these data to the data acquisition (DAQ) sys-
 19 tem for processing. The wire planes are oriented at different angles allowing a 3D

fig:10kt-fiducial-mass

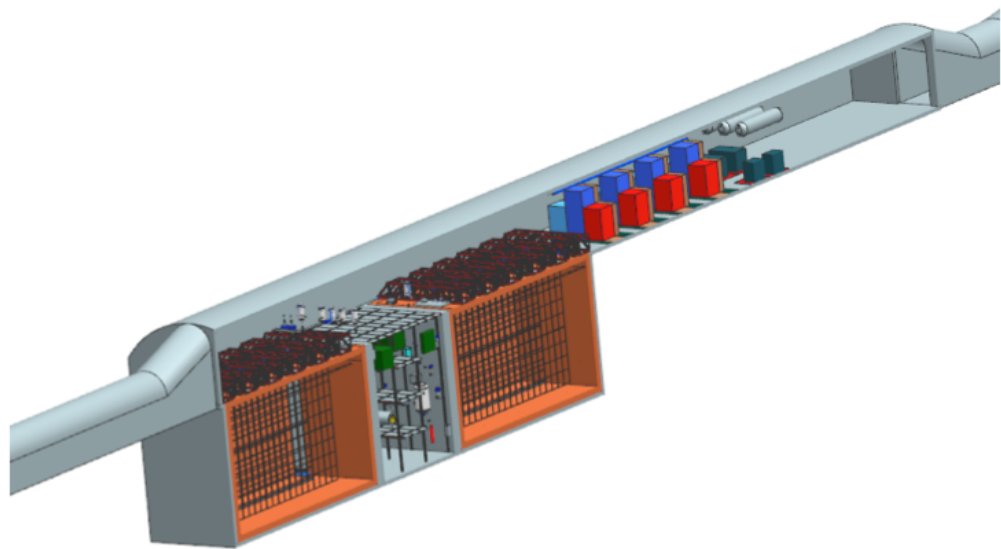


Figure 1.2: Detector configuration within the cavern. The TPC is located within a membrane cryostat, shown in orange. Cryogenic equipment is located at the far end of the upper cavern and the filtration equipment is in the septum area between the two cryostats.

fig:LAr-FD-con

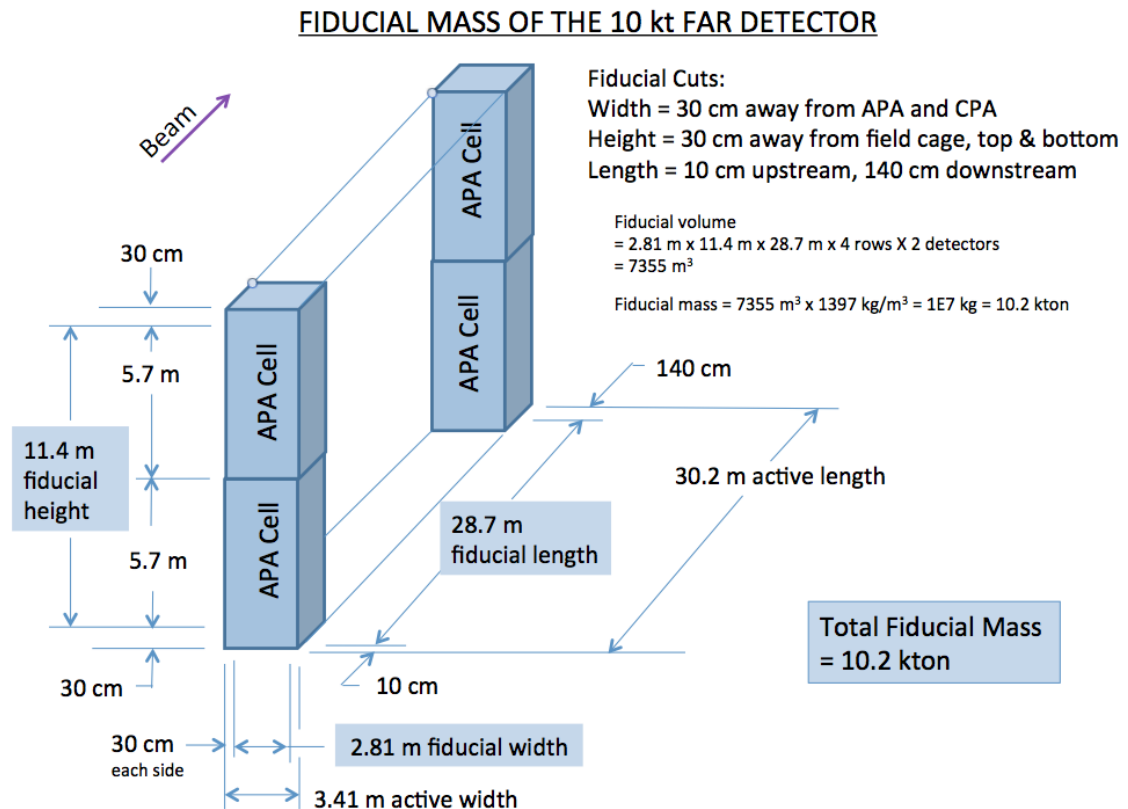


Figure 1.3: Fiducial mass of 10-kton detector

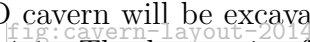
fig:10kt-fiducial

1 reconstruction of the particle trajectories. In addition to these basic components, a
2 photon-detection system provides a trigger for proton decay and galactic supernova
3 neutrino interactions.

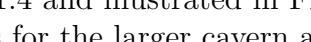
4 The design of the LAr-FD has been developed and refined over the past five
5 years. The starting point was the ICARUS T600 system [?], and the process was
6 informed and guided by the experience with small LArTPCs in the U.S., particu-
larly ArgoNeT [?], the development of designs for MicroBooNE [?]. The LAr-FD
7 concept is designed for assembly from small, independent elements which can be
8 repeated almost indefinitely in any dimension to form the entire assembly within a
9 large cryostat. Each of the elements provides an independent mechanical structure
10 to support the elements it contains. To a large extent, scaling from detector volumes
11 containing anywhere from a few to several hundred such elements is straightforward
12 with small and predictable risk. Scaling in other areas of LArTPC detector technol-
13 ogy, namely cryostat construction, LAr purification and electronics readout has been
14 incorporated into the design.

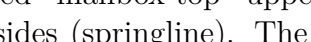
16 1.2.2 Cavern Layout

Editor’s Note: The current plan is to create space for a 40-kton detector in two separate, parallel caverns, one for 10 kton and one for 30 kton, instead of excavating a single cavern. The smaller cavern would be outfitted as soon as possible and the larger would be outfitted in a later phase of work.

17 The first (smaller) LAr-FD cavern will be excavated into a “mailbox” cross sec-
tion, as illustrated in Figure 1.1. The long axis of the cavern will point towards
18 Fermilab, parallel to and in line with the neutrino beamline. The pit, the below-
grade rectangular cavity inside of which the cryostats fit, will have dimensions as
19 detailed in Figure 1.4 and illustrated in Figure 1.6. 

20 The parameters for the larger cavern are given in Figure 1.5. 

21 The 10-kton detector pit will be segmented into three volumes: a space for each
22 cryostat plus a 15-m-wide clear space in the middle, called the septum, separated
23 from the cryostat areas by 1.5-m-thick walls. Equipment and vessels used for filtering
24 LAr to achieve high purity levels will be placed in the septum area. 

25 The cavern (highbay) roof, located above the pit, will be 17.7 m wide by 164.1 m
26 long, and its rounded “mailbox top” upper surface will arch to ~10 m in the center
27 and ~5 m on the sides (springline). The curved upper surface will extend beyond
28 

Cavern & Pit - Underground options only	
Configuration - End to End =1, Side by Side =2	1
Arrangement	End to End
Highbay length	164.1m
Highbay length allowance	75.0
Highbay width	17.7m
Highbay springline height	4.5m
Highbay height at center of cavern	9m
Crown area	55m ²
Primary access	Ross Shaft
Secondary access	Yates Shaft
Concrete pit thickness	0.5m
Excavated pit width	17.7m
Pit depth	15.6m
Excavated pit depth	16.1m
Pit Length per cryostat (inside)	35.0m
Septum length per cryostat	7.5m
Septum wall thickness	1.50m
Excavated pit length	89.1m

Figure 1.4: Parameters for 10-kton detector cavern and pit, 2014

fig:cavern-pit

Cavern & Pit - Underground options only	
Configuration - End to End =1, Side by Side =2	1
Arrangement	End to End
Highbay length	164.1m
Highbay length allowance	75.0
Highbay width	17.7m
Highbay springline height	4.5m
Highbay height at center of cavern	9m
Crown area	55m ²
Primary access	Ross Shaft
Secondary access	Yates Shaft
Concrete pit thickness	0.5m
Excavated pit width	17.7m
Pit depth	15.6m
Excavated pit depth	16.1m
Pit Length per cryostat (inside)	35.0m
Septum length per cryostat	7.5m
Septum wall thickness	1.50m
Excavated pit length	89.1m

Figure 1.5: Parameters for 30-kton detector cavern and pit, 2014

fig:cavern-pit

- 1 each end of the dual-cryostat detector along the long axis to provide additional space
2 for ancillary equipment as well as for installation and maintenance operations.

3 Space will be provided for the nitrogen refrigerators, nitrogen compressors and
4 necessary cryogen-storage vessels. Walkways will run the entire length of the cavern
5 through the roof truss of the detector to provide personnel access along the cryostat
6 roof. A separately ventilated emergency-egress passageway will be elevated over the
7 roof truss section and extend to the east and west ends of the cavern highbay.

Editor's Note: The illustration and dimensions in Figure 1.6 are for
a detector with APAs of dimensions 2.5 m × 7 m and a total of 10
adjoined end-to-end along the beamline. The current configuration
will use 2.3 m × 6 m APAs, in rows of 13 end-to-end, making the
detector slightly shallower and longer than shown in the figure.

fig:v5ch2-cavern-cryostat-section-2

1.2.3 Cryostat Construction

The 10-kton cryostat construction uses commercial stainless-steel membrane technology engineered and produced by industry. These vessels are widely deployed in liquefied natural gas (LNG) tanker ships and tanks, and are typically manufactured in sizes much larger than that of the LAr-FD. This is an inherently clean technology with passive insulation.

The LAr-FD cryostat reference design was selected on the recommendation of the experienced engineering consultants from ARUP USA, Inc. [?] after consideration of an alternative design that uses segmented, internally self-supporting, evacuable, modular cryostats. Evacuation, in particular, appears not to be necessary; in September 2011, the Fermilab Liquid Argon Purity Demonstrator (LAPD) achieved purity levels of less than 100 ppt oxygen-equivalent, using the method that is planned for use in the LAr-FD. This confirms that the method works, obviating the risk to LBNE that an evacuable vessel will be required. Operation of a 35-ton prototype using membrane-cryostat technology has provided a further demonstration.

The LAr-FD membrane cryostats are sealed containers supported by the surrounding rock. This “in-ground” configuration offers access only from the top and protects against possible cryogen leaks out of the tank. The side walls consist of a series of membranes, foam insulation and reinforced concrete poured against the shotcrete covered rock. The inner (primary) membrane liner, made of stainless steel, is corrugated to provide strain relief from temperature-related expansion and contraction.

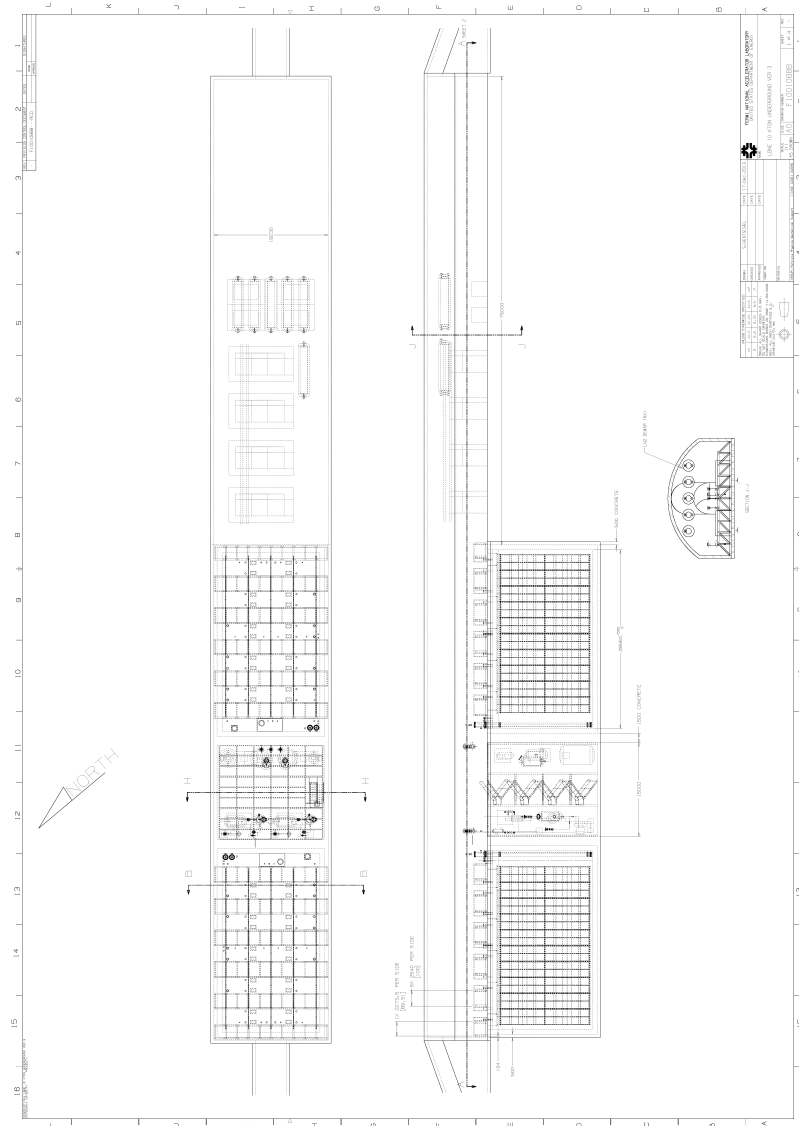


Figure 1.6: Dimensions for 10-kton detector cavern and cryostat, 2014. The left-hand figure is a top view of the cavern hall; on the right is an elevation view through the

fig:v5ch2-cave

1.2.4 Cryogenic Systems

Cryogenic systems are needed to manage the LAr, i.e., to keep it cold, pure and circulating smoothly during operations in order to maintain a sufficiently long drift lifetime for the ionization electrons. The major cryogenic systems used to perform these functions are the cryogen supply for cool-down and fill, gas filtration, argon condensing, liquid filtration and circulation and argon purity analysis.

The overall cryogenic system's layout and location is intended to optimize safety and efficiency. It is designed to minimize:

- the risk of personnel injury to any Oxygen Deficiency Hazard (ODH)
- heat ingress to the cryogenic system (by minimizing piping length and pump power)
- the volume of the argon system external to the cryostat and hence the potential for argon escape or contamination

It is also designed to provide safe access to refrigeration equipment that requires periodic maintenance.

Cryogenic systems are located on the surface and within the cavern. Figure ??
fig:eqp-at-surface
sec:cryosys-layout illustrates the cryogenic systems layout, which is described in Section ??.

The required flow rate of liquid argon to be sent for purification is expected to decrease over time. The initial maximum flow rate will be $51 \text{ m}^3/\text{hr}$ (224 gpm). The liquid-argon volume in one cryostat will turn over every five days at this rate. Longer term, the rate will decrease to $25 \text{ m}^3/\text{hr}$ with a turn-over rate of 11 days. As a point of comparison, ICARUS T600 has a maximum turn-over rate of eight to ten days.

1.2.5 LAr Purification

The purification of LAr is accomplished with standard industrial equipment, using molecular sieves and chemically reducing materials, which are scalable within the contemplated range to accommodate the estimated irreducible material-outgassing from warm materials in the vapor space above the liquid argon, called the ullage.

1.2.6 Time Projection Chamber

The Time Projection Chamber (TPC) is the active detection element of the LAr-FD. The construction concept is shown schematically in Figures 1.7 and 1.8. A TPC is located inside each cryostat vessel and is completely submerged in LAr at 89 K. Five

1 planes line up across the width: three Cathode Plane Assemblies (CPA) interleaved
2 with two Anode Plane Assemblies (APA). These planes are oriented vertically and
3 parallel to the beamline such that the electric fields applied between them are per-
4 perpendicular to the beamline. The TPC’s active volume within the cryostat is 12 m
5 high, 14 m wide and 30 m along the beam direction.

6 A “drift cell” is associated with one APA and the two CPAs on either side of it;
7 it is defined as the volume between the enclosed APA’s two surrounding CPAs, and
8 bordered by the CPAs’ edges. The maximum electron-drift distance between a CPA
9 and an adjacent APA (half of the drift cell) is 3.4 m. Both the CPAs and APAs
10 measure 2.3 m along beamline dimension and 6 m in height; they are each a few cm
11 wide.

12 Each row of CPAs and APAs is stacked two-high to instrument the 12-m active
13 depth. Each row contains 13 such stacks placed edge-to-edge along the beam direc-
14 tion, forming the 30-m active length of the cryostat’s TPC and resulting in a total
15 of 52 APAs and 78 CPAs per cryostat. A “field cage” surrounds the top and ends
16 of the cryostat to ensure uniformity of the electric field. The field cage is assembled
17 from panels of FR-4 sheets with parallel copper strips connected to resistive divider
18 networks.

19 Each APA has three wire planes that are connected to readout electronics; two
20 induction planes (labeled U and V in Figure 1.7) and one collection plane (X). A
21 fourth wire plane, grid plane (G), is held at a bias voltage but is not instrumented
22 with readout electronics. The grid plane improves the signal-to-noise ratio on the U
23 plane and provides electrostatic discharge protection for the readout electronics.

24 **1.2.7 Electronics, Readout and Data Acquisition**

et_electronics
25 Requirements for low noise and for extreme purity of the LAr motivate locating
26 the front-end electronics in the LAr (hence “cold electronics”) close to the anode
27 wires, which reduces the signal capacitance (thereby minimizing noise). The use
28 of CMOS electronics in this application is particularly attractive since the series
29 noise of this process has a noise minimum at 89 K. The large number of readout
30 channels required to instrument the LAr-FD TPCs motivates the use of CMOS
31 ASICs. Signal zero-suppression and multiplexing will be implemented in the ASIC,
32 minimizing the number of cables and feedthroughs in the ullage gas, and therefore
33 reducing contamination from cable outgassing. Figure 1.9 shows the conceptual
34 architecture of a front-end electronics design that meets the requirements for LAr-
35 FD. The entire electronics chain is immersed in the LAr.

36 All signal feedthroughs will be placed at the top of the cryostat, where they are

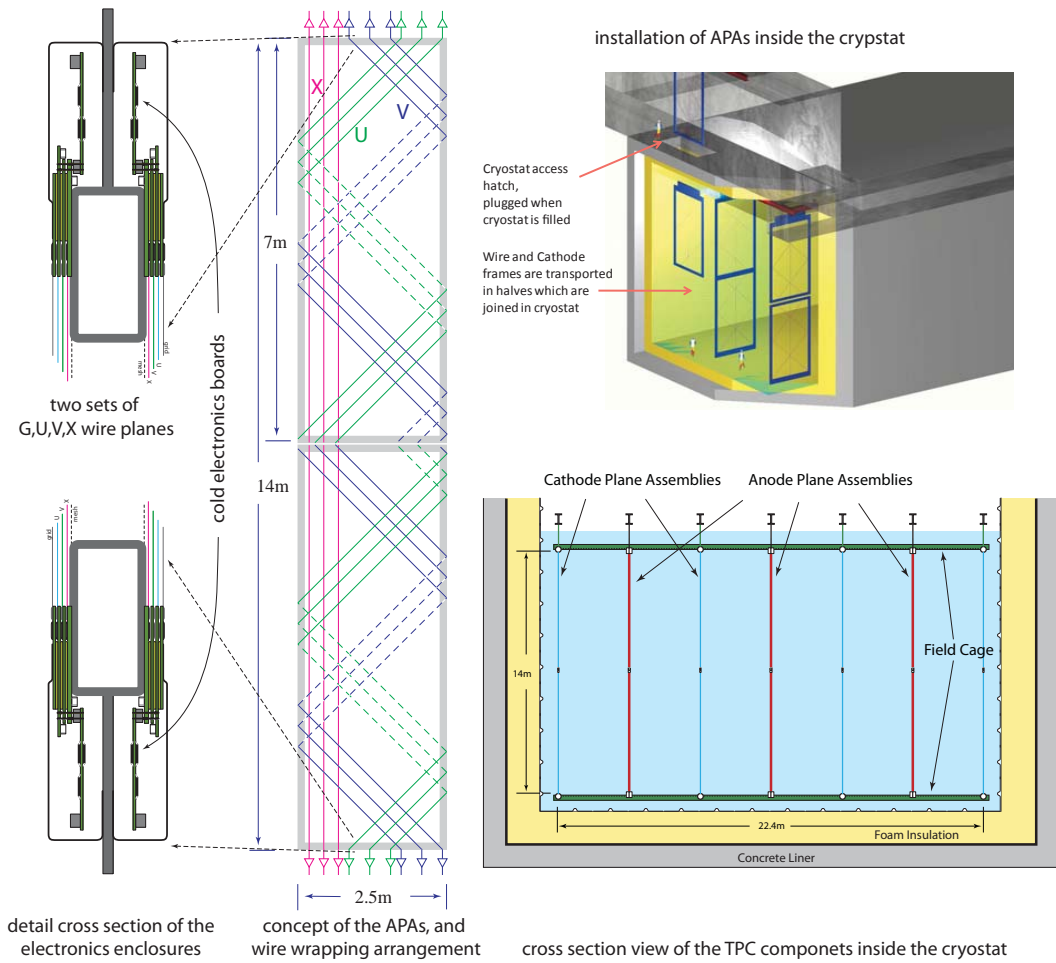


Figure 1.7: TPC modular construction concept; the APA and CPA arrangement has been changed to two APAs and three CPAs as of 2014, see Figure 1.8.

[fig:cpa-apa-arrangement-2014](#)

[fig:tpc-concept](#)

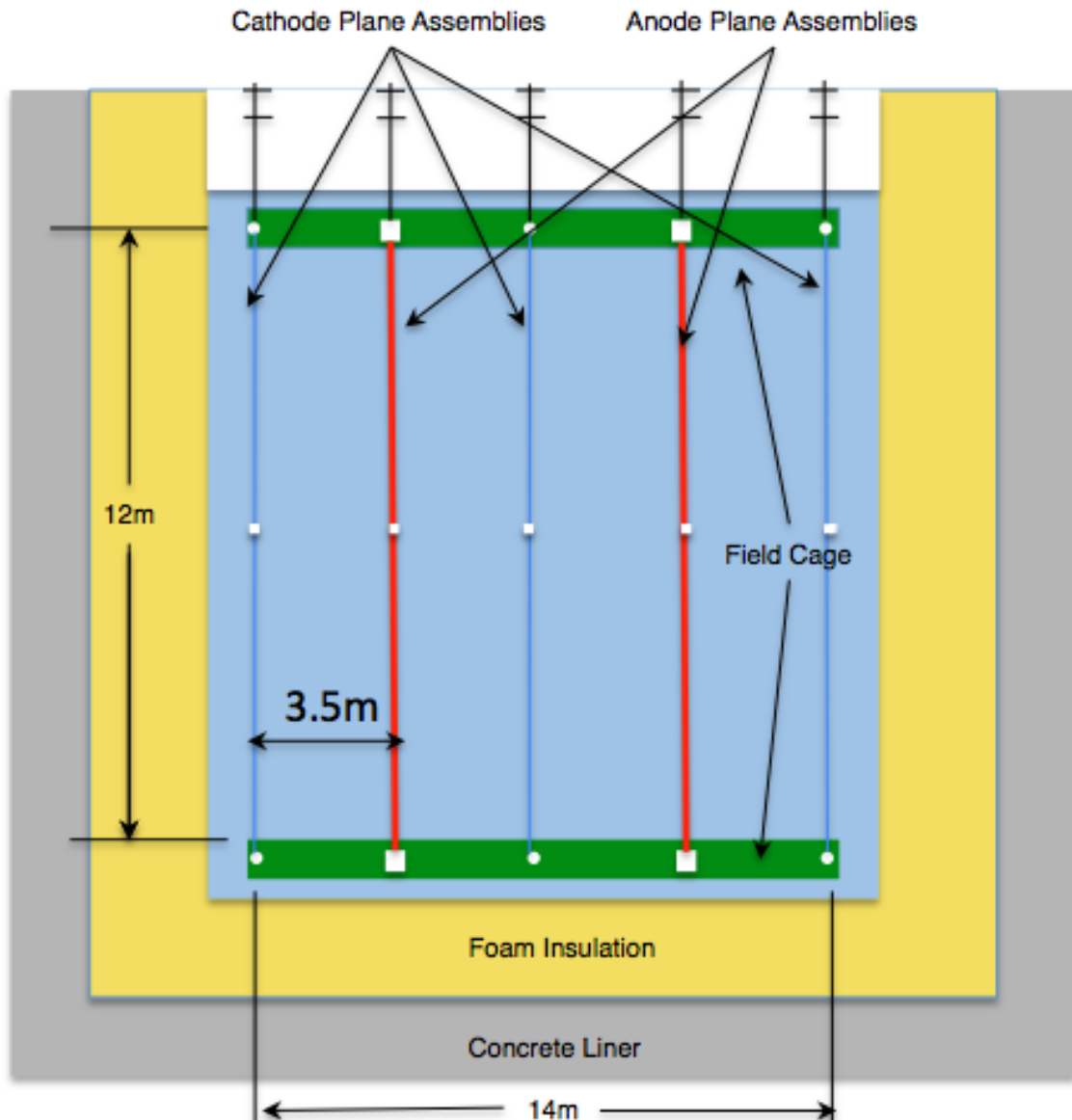


Figure 1.8: APA and CPA arrangement, 2014

fig:cpa-apa-ar

- 1 easily installed, are always accessible, are at low hydrostatic pressure and pose no risk
 2 of LAr leakage. The cold electronic system will include digitization, buffering, and
 3 a high level of digital output multiplexing (ranging from 1/128 to 1/1024). Output
 4 data links will include redundancy to eliminate the effect of any single-point failure.

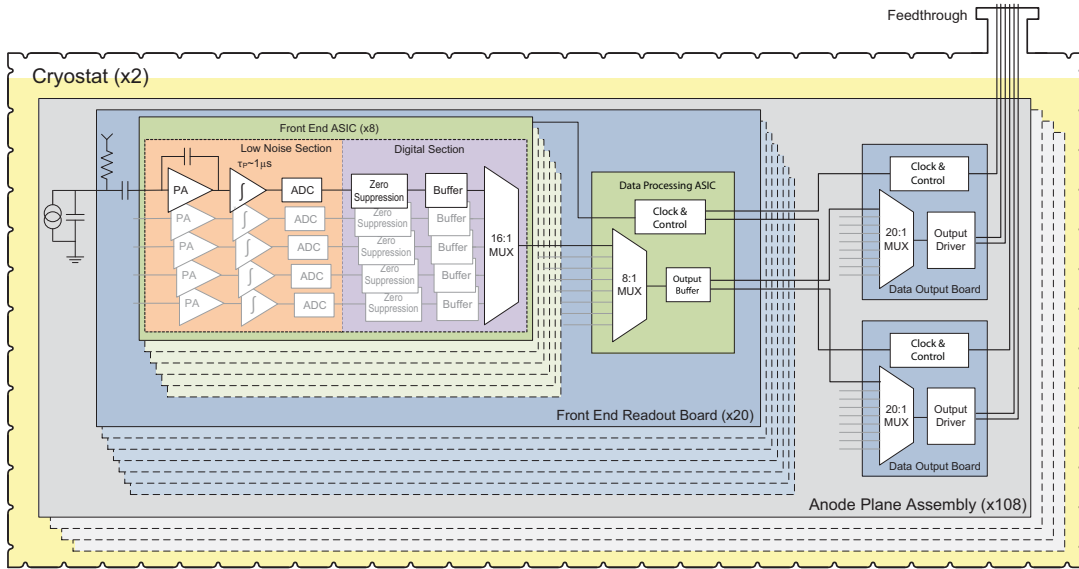


Figure 1.9: Conceptual front-end electronics architecture

fig:tpc-elec-s

1.2.8 Photon-Detection System

6 Identification of the different possible charged-particle types depends on accurate
 7 measurements of ionization along tracks. This requires accurate determination of
 8 the time of interaction, or event time, t_0 , which leads to the absolute location of the
 9 event along the drift axis, and allows the determination of Q_0 , the true ionization
 10 charge.

11 For non-accelerator physics events, t_0 is not known a priori. However, LAr is an
 12 excellent scintillator, generating of order 10^4 128-nm photons per MeV of deposited
 13 energy. Detection of scintillation photons provides a prompt signal that allows un-
 14 ambiguous location of particle positions along the drift axis.

15 The reference design for the photon detection system is based on acrylic bars,
 16 which are either coated in TPB or doped in bulk. The 128 nm photons interact with

- 1 the TPB on the surface and 430 nm light is re-emitted. The signals will be routed
2 out of the cryostat to standard readout electronics.

3 Twenty light-guide and SiPM assemblies, or “paddles”, will be installed within
4 each APA frame prior to wire winding. The SiPM signals will be used as a software
5 “trigger” in the DAQ to define the event time, t_0 , for non-accelerator events. This
6 system provides a t_0 signal throughout the entire detector in contrast to a system
7 similar to that used in MicroBooNE and ICARUS, where light is detected outside
8 the detector volume.

9 **1.2.9 Detector Installation and Operation**

10 Detector components will be shipped in sealed containers to the Far Site by truck
11 and lowered to the cavern. Shipping containers will be moved to a clean area over
12 the septum area between the cryostats. There the components will be unpacked from
13 the sealed container and lowered through an access hatch into the cryostat.

14 The construction of the two cryostats and the installation and commissioning
15 activities will be staged such that both TPCs can be tested cold while one cryostat
16 still remains available as a potential LAr storage vessel. The LAr in one cryostat can
17 be transferred to the other, and back again, if necessary, until all the tests complete
18 successfully. Once both TPCs are known to work properly at LAr temperature, the
19 second fill will take place.

20 To protect the membrane on the floor of the cryostat during TPC installation, a
21 temporary floor will be installed. After each pair of APAs is installed, they will be
22 connected to the DAQ system and the wire integrity tested. All wires on previously
23 installed APA pairs will also be tested. The wire integrity test will be performed
24 during cryostat cool-down as well. A relatively slow cool-down rate will ensure that
25 the temperature-induced stresses in the APA frames and wires are kept well below
26 the level experienced during testing.

27 An installation and integration detector mock-up will be constructed at Fermilab
28 to confirm that interfaces between detector systems are well defined and to refine
29 the installation procedures.

30 **1.3 Principal Parameters**

31 The principal parameters of the LAr-FD are given in Table [table:param-summ-larfd](#).

Table 1.3: LAr-FD Principal Parameters for 10-kton Detector

table:param-su

Parameter	Value
Active (Fiducial) Mass	13.8 (10.2) kton
Number of Detector Modules (Cryostats)	2
Drift Cell Configuration within Module	2 wide \times 2 high \times 13 long
Drift Cell Dimensions	2 \times 3.4 m wide (drift) \times 6 m high \times 2.3 m long
Detector Module Dimensions	14 m wide \times 12 m high \times 30 m long
Anode Wire Spacing	\sim 4.8 mm
Wire Planes (Orientation from vertical)	Grid (0°), Induction 1 (36°), Induction 2 (-36°), Collection (0°)
Drift Electric Field	500 V/cm
Maximum Drift Time	2.1 ms

¹ 1.3.1 Design Considerations

² TPCs operated to date have been constructed with an anode wire spacing in the
³ range of 3 mm (ICARUS) to 4.8 mm (Fermilab cosmic-ray stand). The amount of
⁴ ionization charge collected on the wires increases with larger wire spacing, resulting
⁵ in a better signal-to-noise ratio without serious consequences (the radiation length of
⁶ LAr is \sim 30 times larger than the typical wire spacing). The electron- π^0 separation
⁷ efficiency of a TPC with 5-mm wire spacing is only a few percent lower than one
⁸ with 3-mm wire spacing. It is also clear that a TPC with larger wire spacing requires
⁹ fewer wires and readout channels, resulting in lower cost.

¹⁰ Only two wire planes are required to reconstruct events in three dimensions,
¹¹ however three wire planes will be implemented to provide N+1 redundancy. The
¹² third will improve the pattern-recognition efficiency for a subset of multi-track events
¹³ in which trajectories can overlap in two views. The collection-plane wires are most
¹⁴ commonly used for calorimetric reconstruction and are oriented vertically (0°) to
¹⁵ minimize both the wire length and the electronics noise.

Editor's Note: The following paragraph refers to a wire orientation of 45 degrees. The chosen wire orientation has been changed to 35.7 degrees from vertical. The study and documentation justifying this choice is in LBNE-docdb-9374.

16

1 A study of wire orientation has shown that for a TPC with three instrumented
2 wire planes, the optimum orientation of the induction plane wires should be between
3 $\pm 40^\circ$ and $\pm 60^\circ$ when the collection plane wires are at 0° . The ideal orientation for the
4 more isotropic low-energy events, e.g., supernova-neutrino interactions, is $\pm 60^\circ$. The
5 selected induction-plane wire orientation of $\pm 45^\circ$ has better position resolution in
6 the vertical direction than $\pm 30^\circ$ and has shorter wires compared to a wire orientation
7 of $\pm 60^\circ$. The induction plane wires are wrapped around the APA frames so that the
8 readout electronics can be located on the top or bottom of the TPC. As a result, it
9 is natural to arrange the APAs vertically in a two-high configuration.

10 Access to the top of the cryostat is required to install and connect cabling. Therefore,
11 risk of personnel injury and detector damage, both of which increase with height,
12 form the primary considerations for the the detector height, 12 m. The The height
13 of the APA has been chosen, accordingly, to be 6 m, resulting in 6-m-long collection-
14 plane wires and 7.3-m-long induction plane wires.

15 The 2.3 m width of the APA was chosen to facilitate construction and to allow
16 standard, over-the-road transport.

17 The choice of cryostat width is based on the desired cryostat shape and cavern
18 span. From a cryogenics standpoint, the ideal cryostat for a modular TPC would be
19 a cube since membrane-cryostat capital and operating costs scale linearly with the
20 surface area. This shape is not ideal for cavern excavation, however. In the absence
21 of a geotechnical investigation for the cavern location, the cavern span has been
22 limited to ~ 30 m on the advice of rock engineers. A detector width of 14 m results
23 after making allowance for cryostat insulation, and personnel access both above and
24 within the cryostat.

25 A drift field of 500 V/cm was chosen based on experience from similar detectors
26 such as ICARUS, ArgoNeuT and the Fermilab cosmic-ray test stand. At this electric
27 field, $\sim 30\%$ of the ionization electrons produced by the passage of a minimum
28 ionizing particle (MIP) recombine and create scintillation light that provides a fast
29 trigger. The remaining ionization electrons drift to the APA and produce wire-plane
30 signals. The TPC could function at higher or lower drift fields but the relative yields
31 of scintillation light and ionization electrons would change. The use of a higher drift
32 field would require more care in the design of the high-voltage systems. The electron
33 drift velocity is 1.6 mm/ μ s at 500 V/cm.

34 The 14 m width of the the detector can be divided into four drift cells with a
35 maximum drift length of 3.41 m each. This drift cell length was chosen based on
36 experience from other detectors, the required minimum signal-to-noise ratio and high-
37 voltage considerations. The required minimum signal-to-noise ratio of 9:1 ensures
38 that the tracking efficiency will be 100% throughout the entire drift cell. The TPC

1 must be capable of detecting the smallest signal (1 MeV) produced in interactions
2 that LBNE will study. This situation occurs when a MIP travels parallel to a wire
3 plane and perpendicular to the orientation of the wires in the plane. A MIP loses
4 2.1 MeV of energy in each cm of travel, producing $\sim 40,000$ ionization electrons along
5 every 5 mm section of the track. About 28,000 electrons escape recombination and,
6 ignoring the effects of LAr purity and diffusion, would all drift to one collection plane
7 wire. The capacitance due to the maximum-length 7.3 m wire is 164 pF resulting
8 in an equivalent noise charge (ENC) of 500 electrons in the CMOS amplifiers. The
9 signal-to-noise ratio would therefore be 53:1 if all of the ionization electrons arrived
10 at the wire. For a maximum drift distance of 3.41 m and a drift field of 500 V/cm,
11 the required voltage on the cathode plane is 173 kV. This is within the range of
12 commercially available high-voltage cables and within the range of current designs
13 for cryogenic feedthroughs. Additional R&D would be needed for longer maximum
14 drift lengths.

15 Ionization electrons will be lost due to impurities in the LAr. The fraction that
16 survive passage to the anode planes is $e^{t/\tau}$, where t is the drift time and τ is the drift-
17 electron lifetime. The maximum drift time is the maximum drift length divided by
18 $1.6 \text{ mm}/\mu\text{s}$ which equals 2.3 ms for LBNE. The ICARUS detector has achieved a drift-
19 electron lifetime of 6 – 7 ms. The Materials Test Stand (described in Section 6.3.1)
20 regularly achieves a drift-electron lifetime of 8 – 10 ms. The Fermilab Liquid Argon
21 Purity Demonstrator achieved a lifetime of > 3 ms during initial tests. Based on this
22 experience, and by careful selection of materials in the ullage, a drift-electron lifetime
23 at least as good as ICARUS is expected. The signal-to-noise ratio would be 36:1 for
24 a drift electron lifetime of 6 ms. A minimum lifetime of 1.4 ms is required to meet
25 the 9:1 signal-to-noise ratio requirement.

26 The cloud of drifting ionization electrons will spread out in space due to the
27 effects of diffusion. The maximum transverse *RMS* width of the electron cloud is
28 2.4 mm for the chosen drift distance and drift field. This is well matched to the
29 5 mm wire spacing.

30 1.4 Detector Development Program

31 As mentioned above, the design of the LAr-FD has benefited greatly from other
32 experiments and related development activities. Development activities in the U.S.
33 are described in the *Integrated Plan for LArTPC Neutrino Detectors in the US* [?].
34 This program includes non-LBNE activities such as the Fermilab Materials Test
35 Stand, Fermilab electronics test stand, LAPD, photon detection, ArgoNeuT and
36 MicroBooNE as well as LBNE activities such as the 35-ton prototype and LAr1.

- ¹ The development plan is described in detail in Chapter 6.^{ch:randd}

Editor's Note: The far detector prototyping plan known as LAr1 has been replaced by a plan to build and test a prototype with full-size TPC components at CERN.

²

³ 1.5 Participants

⁴ The design for the LBNE Far Detector is being carried out by an LBNE subproject
⁵ team, headed at Fermilab but with participants also from Brookhaven National Laboratory,
⁶ Argonne National Laboratory and Indiana University, in conjunction with
⁷ an engineering design firm, Arup USA, Inc. This firm has assisted with cryostat
⁸ and cryogenic-plant design. The detector is planned for construction at the Sanford
⁹ Laboratory site, which is managed by the South Dakota Science and Technology
¹⁰ Authority (SDSTA).

¹¹ The LBNE Far Detector, called the LAr-FD, is managed by the Work Breakdown
¹² Structure (WBS) Level 2 Manager for the Far Detector subproject. The supporting
¹³ team includes a WBS Level 3 Manager for each of its component systems: Cryo-
¹⁴ genics & Cryostat, Time Projection Chamber (TPC), Trigger & Data Acquisition
¹⁵ (DAQ), Installation & Commissioning and Photon Detector. Figure 1.10 shows an
¹⁶ organization chart down to Level 3 (L3).

¹⁷ The Conventional Facilities Level 3 Far Site Manager is the LBNE Project liaison
¹⁸ with the LAr-FD subproject to ensure the detector requirements are met; this person
¹⁹ is responsible for all LBNE scope at the Far Site. [Management of the Sanford Lab
²⁰ and the organizational relationship between it and the LBNE Project and Fermilab
²¹ are in the process of being determined; this section will be updated when that is
²² known.]

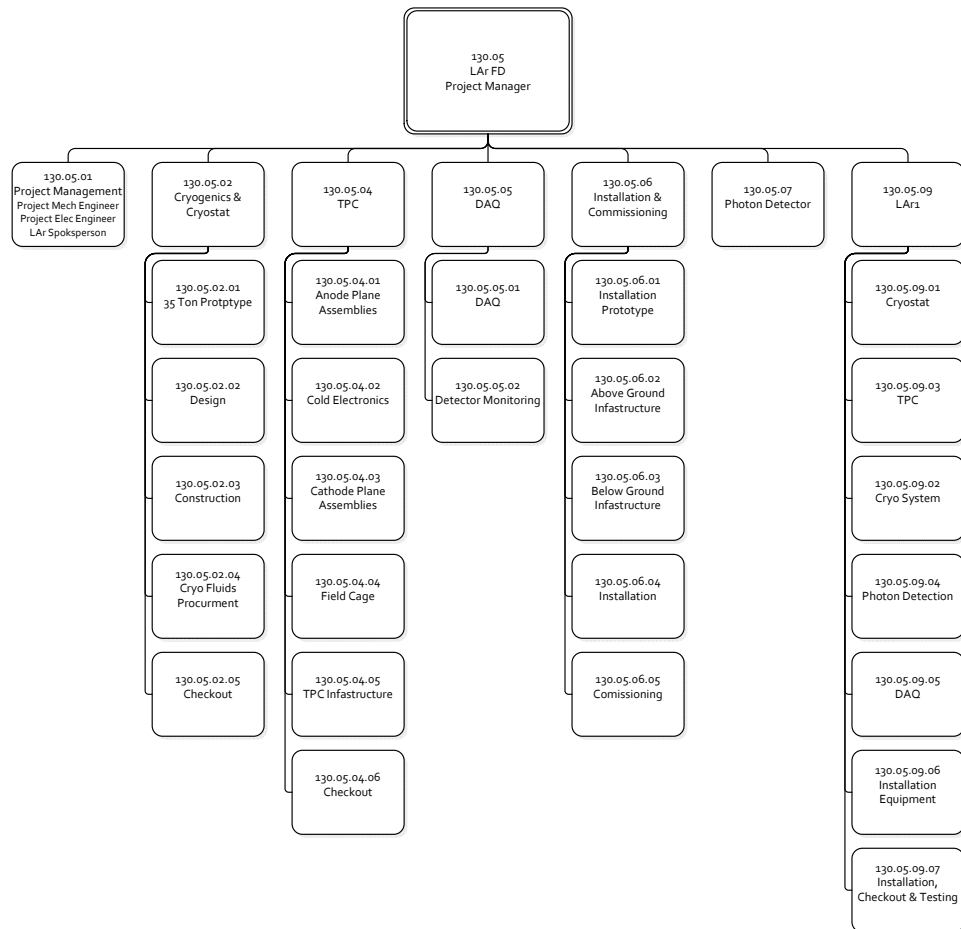


Figure 1.10: Organization chart for the Far Detector subproject (as of 2012)

¹ Chapter 2

² Time Projection Chamber and ³ Electronics

ch:tpc

- ⁴ The scope of the Time Projection Chamber (TPC) subsystem includes the design,
⁵ procurement, fabrication, testing, delivery and installation of the mechanical com-
⁶ ponents of the TPC:
- ⁷ • anode plane assemblies
- ⁸ • cathode plane assemblies
- ⁹ • field cage
- ¹⁰ and of all the in-vessel electronics, signal and power cables, their feedthroughs, as
¹¹ well as the low- and high-voltage power supplies feeding the electronics. This chapter
¹² describes the reference design for the TPC that meets the required performance for
¹³ charge collection in the LBNE liquid argon detector, LAr-FD.

¹⁴ 2.1 Introduction

- ¹⁵ The Time Projection Chamber (TPC) is the active detector element of LAr-FD. It
¹⁶ is located inside the cryostat vessel and is completely submerged in liquid argon at
¹⁷ 89 K. The TPC consists of alternating anode plane assemblies (APAs) and cathode
¹⁸ plane assemblies (CPAs), with field-cage panels enclosing the four open sides between
¹⁹ the anode and cathode planes. A uniform electric field is created in volume between
²⁰ the anode and cathode planes. A charged particle traversing this volume leaves a
²¹ trail of ionization. The electrons drift toward the anode wire planes, inducing electric
²² current signals in the front-end electronic circuits connected to the sensing wires.

1 TPC subsystem interfaces to the cryostat and cryogenic subsystem through the
2 TPC mounting fixtures, and it interfaces with the DAQ subsystem through the signal
3 feedthroughs.

4 The TPC's active volume (Figure 2.1) is 12 m high, 14 m wide and 30 m long in
5 the beam direction. Its three rows of CPA planes interleaved with two rows of APA
6 planes are oriented vertically, parallel to the beamline with the electric field applied
7 perpendicular to the planes. The maximum electron-drift distance between a cathode
8 and an adjacent anode is 3.4 m. Both the cathode and anode plane assemblies are
9 2.3 m wide and 6 m high. Two 6-m modules (either APA or CPA) stack vertically to
10 instrument the 12 m active depth. In each row, 13 such stacks are placed edge-to-
11 edge along the beam direction, forming the 30 m active length of the detector. Each
12 cryostat houses a total of 52 APAs and 78 CPAs. Each facing pair of cathode and
13 anode rows are surrounded by a “field cage,” assembled from panels of FR-4 sheets
14 with parallel copper strips connected to resistive divider networks.

15 On each APA, four planes of wires cover each side of a frame (the “wire frame”).
16 See Figure 2.2. The inner three planes of wires are oriented, going from the inside out:
17 vertically, and at $\sim \pm 36^\circ$ to the vertical, respectively. Each wire is connected to a
18 front-end readout channel. The wires on the outermost plane are oriented vertically,
19 and are not connected to the readout electronics. At a nominal wire pitch (center-
20 to-center separation) of 4.8 mm, the total number of readout channels in an APA is
21 2560, for a total of 133,120 in each cryostat.

22 The readout electronics are optimized for operation in the cryogenic environment.
23 The front-end ASIC chip utilizes a mixed-signal design. It has 16 channels
24 of preamp, a shaper and an analog-to-digital converter (ADC) in its analog section,
25 followed by a large, shared buffer and the digital IO interface. Eight such chips are
26 mounted on a single readout board, instrumenting 128 adjacent wires in one plane.
27 A digital-processing ASIC with an 8:1 multiplexer on this board further increases
28 the multiplexing factor to 128:1, resulting in a single output channel. Data from
29 this output channel will be transmitted through two redundant LVDS (low-voltage
30 differential signaling) output cables to two APA-level multiplexing boards. Each of
31 these boards connects to the 20 front-end readout boards on the APA, and provides
32 a further 20:1 multiplexing. The output from each of these APA-level multiplexing
33 boards are again duplicated for redundancy.

34 One cable bundle is planned for each APA to connect to the outside of the cryo-
35 stat. The bundle will consist of wires for low-voltage power, wire-bias voltages, data
36 out, clock in, digital control IO and an analog monitoring output. Redundant cables
37 will be provided for many of these functions. The 52 cable bundles will be con-
38 nected through 26 feedthroughs distributed on the roof of the cryostat. Additional

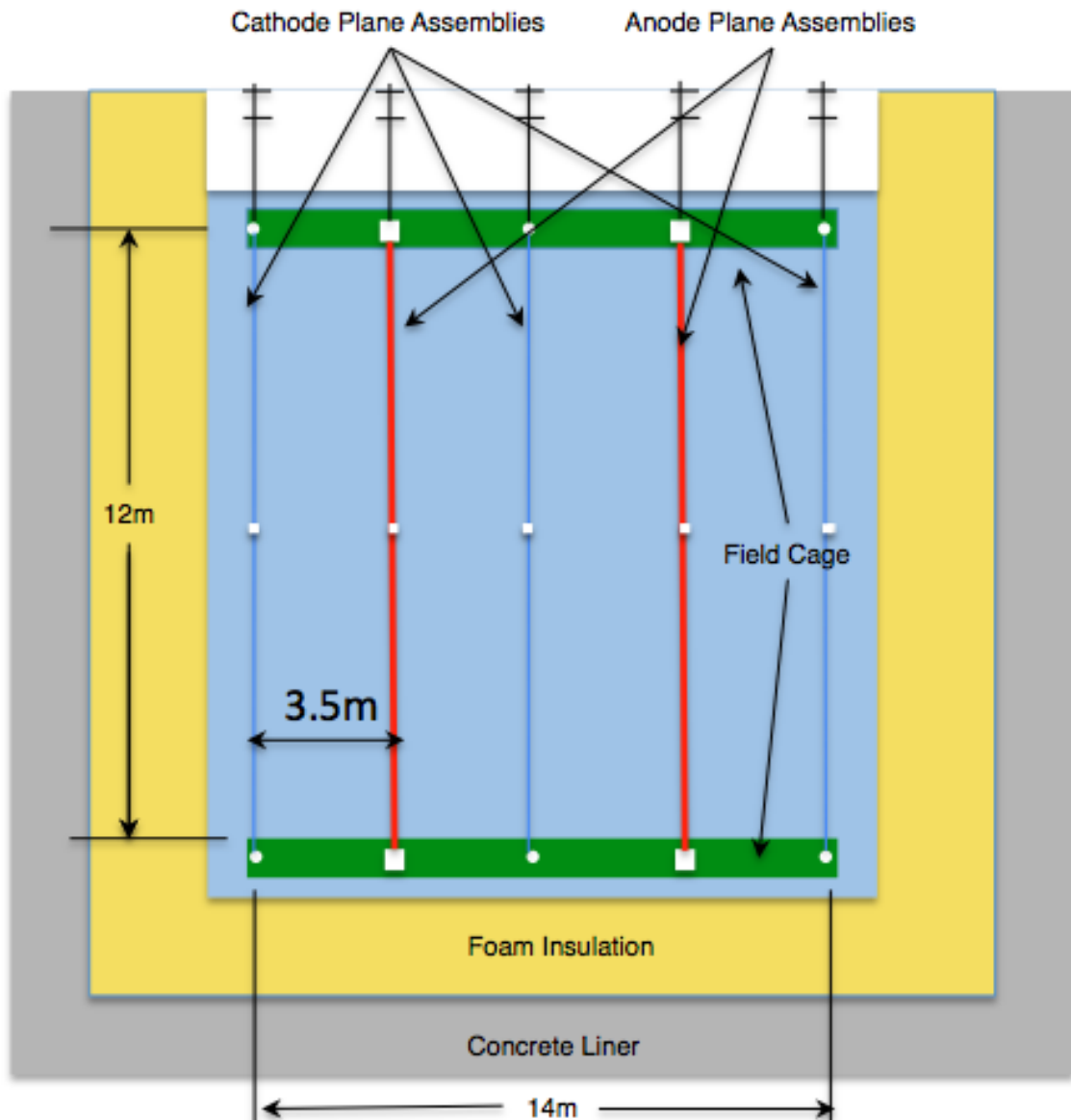
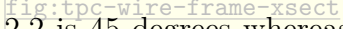


Figure 2.1: Cross section of the TPC inside the cryostat. The length of the TPC is 30 m along the direction of the neutrino beam (into the paper). (Updated 2014)

fig:tpc-xsect1

¹ feedthroughs will be required for redundant high-voltage connections to the CPAs.

² 
The wire angle shown in Figure 2.2 is 45 degrees whereas as of Jan. 2015 it will be 36 degrees.

³ 2.2 Design Considerations

⁴ The requirements for the TPC can be found in the requirements documentation ^{lar-fd-req} [?].
⁵ The most significant ones are the following:

- ⁶ • Provide the means to detect charged particles in the detector and transmit the
⁷ detector signals to the Data Acquisition System (DAQ)
- ⁸ • Meet the physics requirement for electron/photon discrimination; the TPC wire
⁹ spacing will be < 5 mm
- ¹⁰ • Limit variation in the wire sag to < 0.5 mm such that it does not significantly
¹¹ impact the position and energy resolution of the detector
- ¹² • Provide redundancy in the discrimination of electrons from photon conversions
¹³ and ensure long-term reliability over the life of the experiment; configuration
¹⁴ will use three instrumented wire planes
- ¹⁵ • Optimize the measurement of high-energy and low-energy tracks from accelerator-
¹⁶ neutrino interactions; the wire-plane orientation is optimized for neutrinos in
¹⁷ the LBNE energy range
- ¹⁸ • Enable the detector to distinguish a Minimum Ionizing Particle (MIP) from
¹⁹ noise with a signal-to-noise ratio > 9:1
- ²⁰ • Enable the detector to measure the ionization up to 15 times that of a MIP
²¹ particle; this is necessary to perform particle identification of stopping kaons
²² from proton decay
- ²³ • Enable the in-vessel electronics to operate for the life of the facility
- ²⁴ • Record the wire-signal waveforms continuously without dead time
- ²⁵ • Use only materials that are compatible with high-purity liquid argon

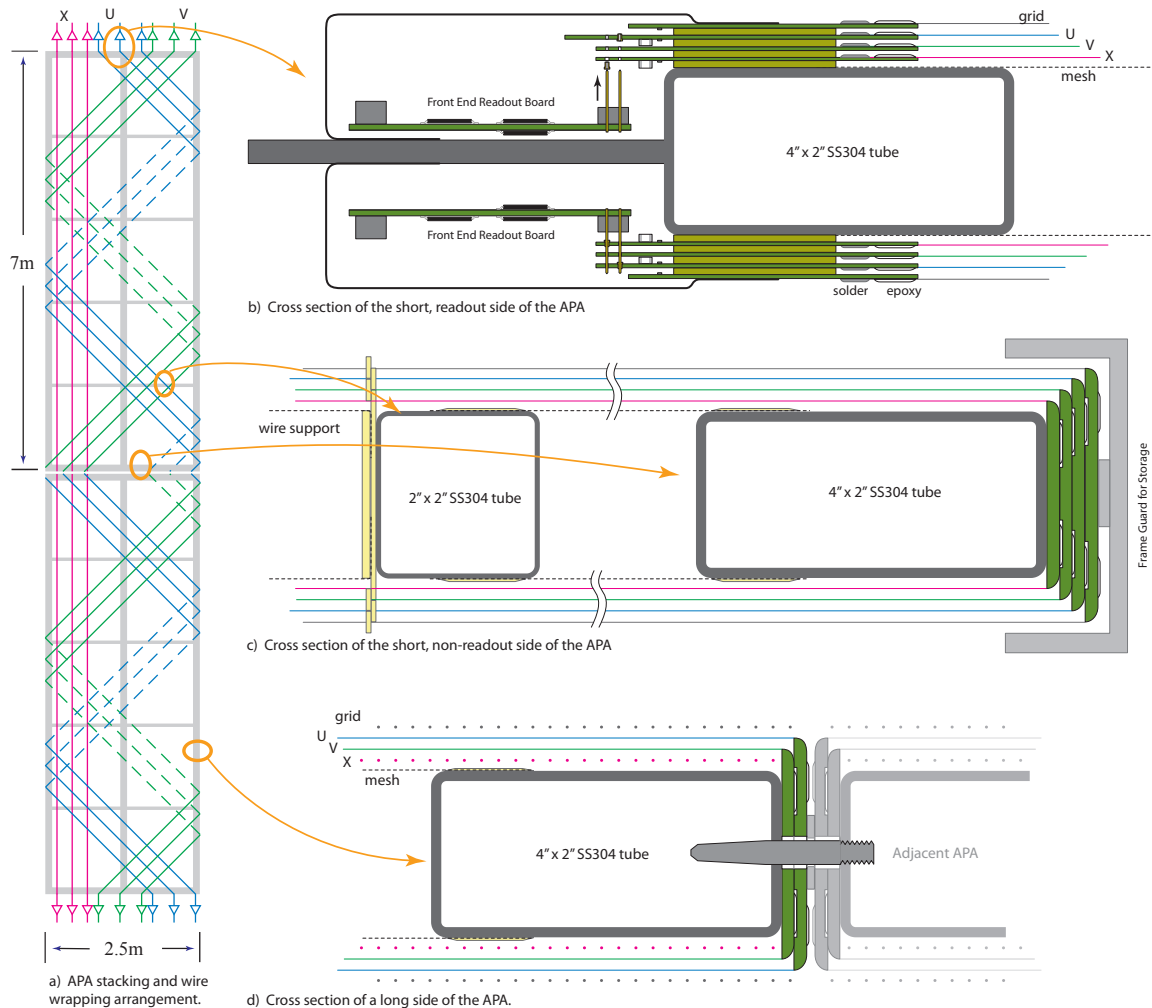


Figure 2.2: Illustration of the APA wire wrapping scheme, and three cross sectional views. (The wire angle shown in this figure is 45 degrees whereas as of Jan. 2015 it will be 36 degrees.)

fig:tpc-wire-f

2.3 Anode Plane Assemblies

The APAs are 2.3 m wide, 6 m long, and \sim 9 cm thick. The 6-m length is chosen for fabrication purposes and will limit the maximum wire length to 7.3 m (which caps the input capacitance to the preamps to \sim 165 pF) at a 36° wire angle, and the 2.3-m width is set to fit in a standard HiCube container for storage and transport. Each APA is constructed from a framework of light-weight, stainless-steel rectangular tubing, with four layers of wires wrapped over both sides of the frame. The front-end electronics boards are mounted on one end of the wire frame and protected by a metal enclosure.

2.3.1 Wires

The wires used in the TPC must provide:

- High break load to withstand the applied tension
- Good conductivity to minimize noise contribution to the front-end electronics
- Comparable thermal-expansion coefficient to that of the stainless-steel frame to avoid tension change after cool-down

Both stainless-steel and copper-beryllium (CuBe) wires are potential candidates. Stainless steel was the choice of ICARUS, while a copper-plated stainless-steel wire was chosen by MicroBooNE (to reduce resistance). Both experiments use a wire-termination technique that is labor-intensive and impractical for LAr-FD. Previous experience from FNAL [?] has shown that a CuBe wire under tension can be reliably bonded to a copper-clad G10/FR4 (glass epoxy material) surface by a combination of epoxy (mechanical bonding) and solder (electrical connection). This bonding technique greatly simplifies the electrical connection to the readout electronics and it can be easily automated with commercial equipment. Therefore CuBe wire is selected as the reference design wire of choice.

At 150 μm diameter, the breaking tension of a hardened CuBe wire is \sim 30 N. To ensure no wire breakage in the TPC, e.g. during cryostat cool-down, the nominal operating tension of the wire will be set at 5 N. Periodic support structures on the wire frame will limit the unsupported wire length to less than 2 m, resulting in less than 0.2 mm deflection due to gravitational or electrostatic forces. Wire ends will be glued and soldered (if electrical connection is needed) onto printed circuit boards attached to the wire frame.

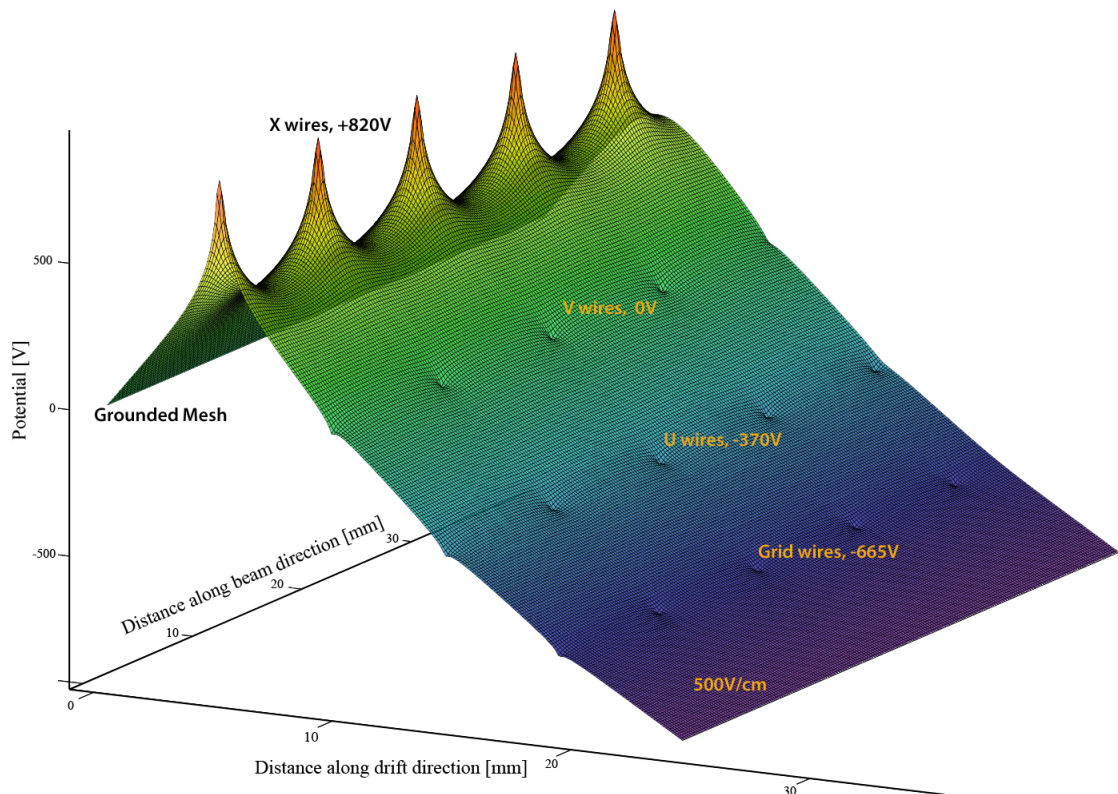


Figure 2.3: A surface plot of the electric potential distribution near the wire planes. The voltages on the wire planes are biased to provide complete electron transparency through the first three planes, and complete collection on the fourth plane.

fig:tpc-bias-v

¹ 2.3.2 Wire Planes

Editor's Note: This section needs to be revised based on the 36-degree wire angle.

²

³ Four planes of wires are installed on each side of an APA as shown in Figure 2.2. ^{fig:tpc-wire-frame-xs}
⁴ A nominal wire pitch of 4.5 mm is selected to meet the position resolution and
⁵ signal-to-noise ratio requirement. The distance between wire planes is set to 4.8 mm
⁶ (3/16 in) to use standard printed circuit board thickness, while maintaining optimal
⁷ signal formation. These four planes (along the direction of electron drift) are labeled
⁸ as: the *grid plane*, the *first induction plane* (U), the *second induction plane* (V), and
⁹ the *collection plane* (X). The wires on the grid and the collection planes are vertically
¹⁰ oriented, while the two induction planes are oriented at $\sim \pm 45^\circ$ to the vertical. This
¹¹ wire layout is shown to be the best for reconstructing beam-neutrino events [?]. The
¹² wires on the grid plane are not connected to the readout electronics; they shield
¹³ the first induction wire plane from being influenced by distant ionizations. The
¹⁴ four wire planes will be electrically biased so that electrons from an ionizing-particle
¹⁵ track completely drift past the first three planes and are collected by the fourth plane.
¹⁶ Calculations show that the minimum bias voltages needed to achieve this goal are
¹⁷ $V_G = -665\text{V}$, $V_U = -370\text{V}$, $V_V = 0\text{V}$ and $V_X = 820\text{V}$ respectively. A grounded mesh
¹⁸ plane, located 4.8 mm behind the collection plane, prevents the electric field around
¹⁹ this set of wires from being distorted by the metal frame structure and the wires
²⁰ on the opposite side of the frame. It also shields the sensing wires from potential
²¹ EM interferences from the silicon photomultipliers (SiPMs), discussed in Chapter 4,
²² mounted within the frame. The mesh should have a wire pitch less than 2 mm to
²³ ensure a uniform electric field and a high optical transparency. Figure 2.3 shows the
²⁴ electric potential distribution near the APA frame with the wire planes biased with
²⁵ the appropriate voltages. ^{ch:photon} ^{fig:tpc-bias-voltages}

²⁶ The V wire plane is directly connected to the front-end electronics, i.e. $V_V = 0\text{V}$,
²⁷ to simplify the coupling and reduce the maximum bias voltages on the other planes.
²⁸ The wires on the two induction planes (U & V) are wrapped in a helical pattern
²⁹ around the long edges of the wire frame (Fig.2.2a). This technique makes it possible
³⁰ to place readout electronics only at one short edge of a wire frame, enabling joining
³¹ the APAs on the other three sides with minimal dead space. It slightly complicates
³² the track reconstruction because the U & V wires are sensitive to tracks on both
³³ sides of the APA. The upper APAs in the cryostat will have their readouts at the top
³⁴ edge of the frame (as shown in Figure 2.2), while the lower APAs will mount their
³⁵ electronics at the bottom edge. ^{fig:tpc-wire-frame-xsect} ^{fig:tpc-wire-frame-xsect}

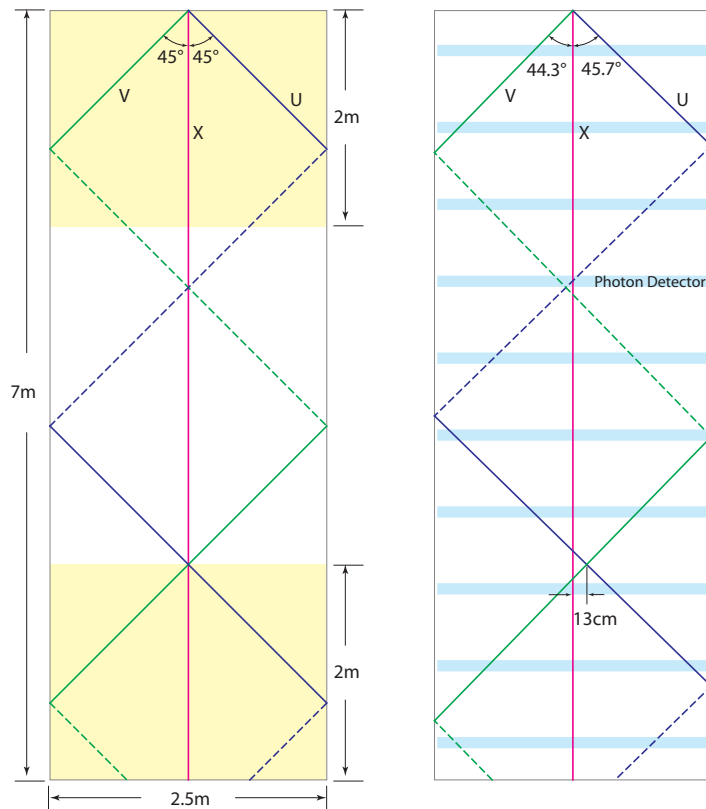


Figure 2.4: Left: illustration of the ambiguity problem if the U & V wire angles are equal;
Right: slightly changing the wire angles and photo detectors help to resolve the problem.

`fig:tpc-wire-a`

If the wire angles of the U & V planes are equal to 45° , both wires wrap around the frame one complete cycle, covering a 5-m height, then repeat the same pattern for another 2 m. An ambiguity problem arises when wire pattern of all three sensing planes in the top 2-m section is identical to that in the bottom 2-m section. The detector will not be able to tell if a track is in the top or the bottom section of an APA (see Figure 2.4). To resolve this ambiguity, the wire angles of U & V planes are set slightly differently: $45^\circ \pm \delta$, such that the same three wires do not cross again. In addition, the multiple photon detectors embedded in the APA frame will help to identify the vertical location of an ionizing track.

The angles and pitches of the U & V wires are chosen such that (1) a modularity of 128 channels form at the readout end of the APA, with the X wire pitch at 4.5mm; (2) a modularity on the side wrapping boards form with a module length similar to that of the readout board. The current configuration has the U wires at 45.7° from vertical, at a 4.9-mm pitch, while the V wires at 44.3° from vertical, and 5.0-mm pitch.

The APA readout electronics are divided into 20 identical modules. Each module covers 128 readout wires, consisting of 56 X, 36 U and 36 V wires. These 128 readout wires span a width of 252 mm. Using this modularity, the APA's active width is set to 2520 mm. There are 1120 X wires, 720 U wires, 720 V wires, and 1120 grid wires for each APA. The total number of readout channels is 2560 per APA. The total number of wires per APA is 3680.

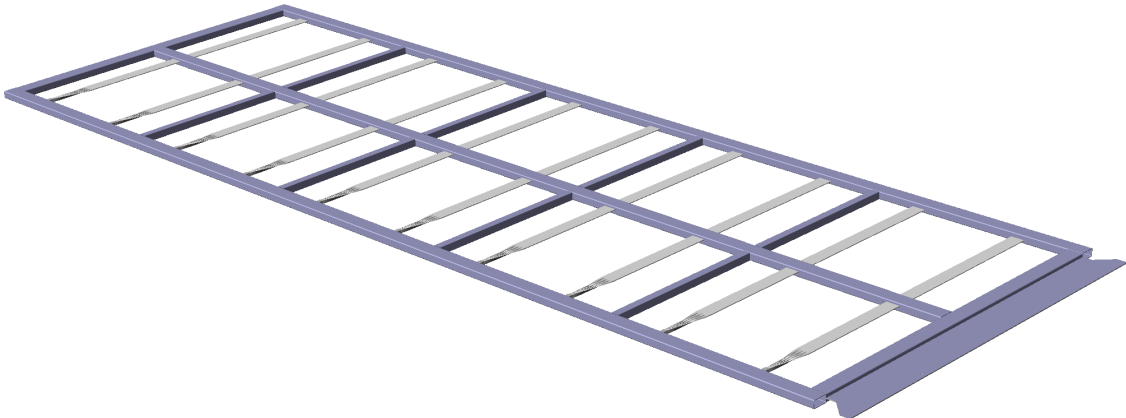


Figure 2.5: Conceptual design of a wire frame (shown without wires). The photon detectors are shown installed on the APA frame.

`fig:tpc-wire-frame`

2.3.3 APA Frame

At a nominal wire tension of 5 N, the 3680 wires exert a force of ~ 6.4 kN/m on the short edges of the APA, and a ~ 2 kN/m force on the long edges. The wire frame must be able to withstand the wire tension with a minimal distortion, while minimizing the thickness of the frame to reduce the resulting dead space. A conceptual design of the wire frame is shown in Figure 2.5. It is constructed from all stainless-steel tubes welded in a jig. Finite element analysis has shown that the maximum distortion of the frame due to wire tension is under 0.5 mm. The total mass of a frame is ~ 250 kg. All hollow members of the frame are vented to prevent the creation of trapped volumes. The two long outer members of the frame are open-ended, so that signal and power cables can be threaded through them to reach the readout end of the lower APA.

2.3.4 Wire Wrapping Around an APA

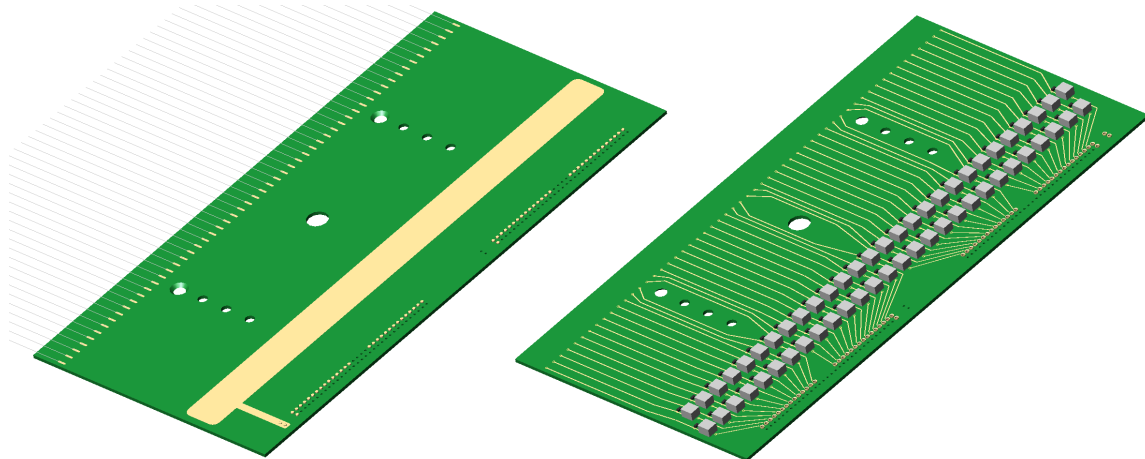


Figure 2.6: Conceptual design of a wire bonding board for the x wires. Left: An array of wires are glued on the leading edge of the top surface, and then soldered onto the soldering pads; Right: the bottom side of the board has the RC network for the bias voltage.

Figure 2.2b-d shows three major cross sections of an APA. The top figure is the cross section of the readout end of an APA. The four planes of wires are attached to their respective wire-bonding boards through a combination of epoxy and solder. Figure 2.6 shows both sides of the board for the x wires. The wires are wound on the

fig:tpc-wire-b

1 top surface of the board (left) using a winding machine. The wires are then glued
2 down with a bead of epoxy at the leading edge of the board. After the epoxy has
3 cured, the wires are soldered onto the copper pads under each wire, and the wires
4 are cut beyond the pads. On the bottom of this board, the copper traces connect
5 the wires to the bias voltage supply through an RC network. The resistors in this
6 network have values about $20\text{ M}\Omega$, such that in the event that a wire from a different
7 plane breaks and is shorted to these wires, the bias voltages on the rest of the wires
8 will not be affected. The AC-coupled signals from the wires are connected to sockets
9 that will mate with the front-end readout boards.

10 Similar boards for the U & V planes are aligned and stacked above the X boards.
11 An array of pins on the front-end readout boards is pushed through the stack of wire
12 bonding boards, making electrical connection between the readout electronics and the
13 matching wires. These readout boards, as described in Section 2.7, process the analog
14 signals from the wires and transmit the digital information through feedthroughs to
15 the DAQ system outside the cryostat. The electronics on the readout boards dissipate
16 an estimated $\sim 60\text{ W}$ of heat per APA and may generate a small quantity of argon
17 bubbles. Two stainless-steel covers are placed over the readout boards to contain the
18 bubbles and direct them to the gas volume of the cryostat. In the case of the lower
19 APAs, the bubbles, if not already recondensed, will be funneled through the vertical
20 hollow frame members to the top of the cryostat.

21 Figure 2.2c shows the cross section of the short, non-readout end of an APA. All
22 wires are mechanically terminated on this end on the four layers of wire-wrapping
23 boards. No electrical connections are needed.

24 Figure 2.2d shows the cross section of a long edge of an APA. Only two layers (U
25 & V) of wire wrapping boards are needed here. The wire-wrapping boards are made
26 from printed circuit boards, shown in Figure 2.7. The boards are attached to the
27 APA frame, and then a winding machine wraps a wire around the APA in a helical
28 fashion, placing the wire into the grooves on the edges of each board. After winding,
29 the wires are glued down to the wire-wrapping boards near the grooved edges. To
30 clear the mounting holes on the board, a few wires are soldered onto the copper pads,
31 and cut, leaving the copper traces to bridge the connection.

32 Figure 2.8 is a closeup view of a corner of an APA frame with some wires and
33 various wire bonding boards to demonstrate the assembly.

34 After the grid plane wires are placed on the APA, metal guards are placed along
35 the three wrapped edges of an APA. These guards protect the fragile wires during
36 APA handling, storage and transport.

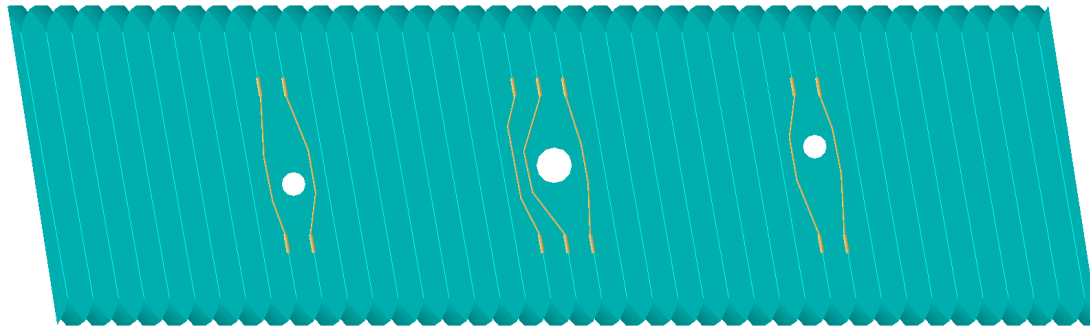


Figure 2.7: Conceptual design of a wire wrapping board for the U wires on a long edge of an APA. The light cyan colored lines represent the wires wrapped over the board surface. Some wires near the mounting holes must be soldered to the copper traces and then cut.

fig:tpc-wire-b

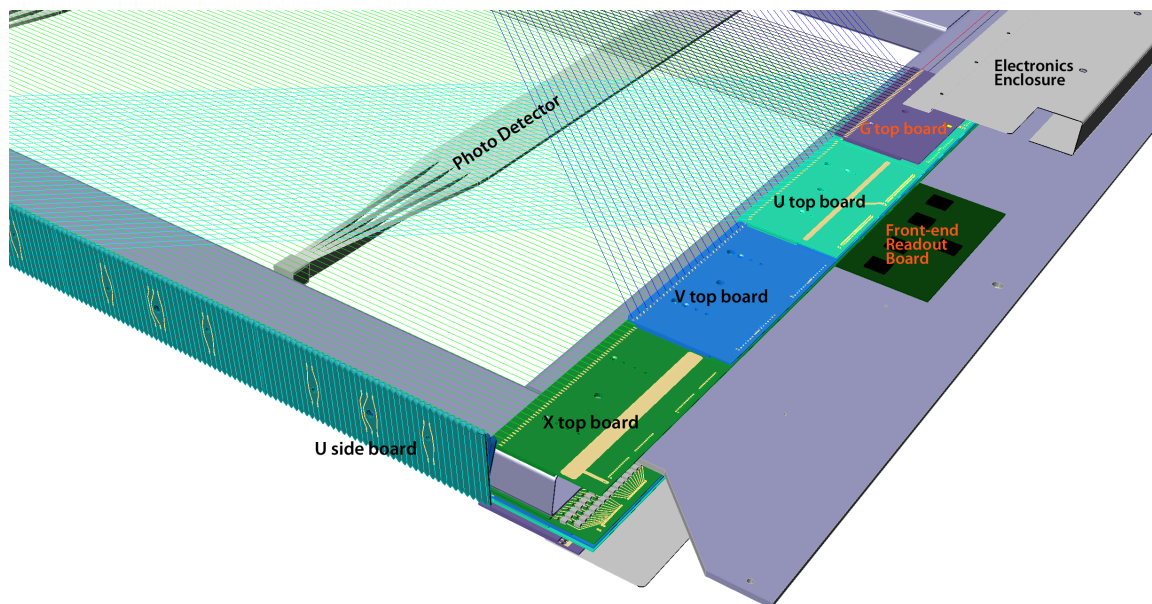


Figure 2.8: A closeup view of a partially assembled corner of an APA. For clarity, only every other wire is shown in this illustration.

fig:tpc-APA-cc

2.3.5 Wire Supports on Inner Frame Members

The left of Figure 2.2b also shows the wire-support structure mounted on one of the inner horizontal frame members. A detailed rendering of this concept is illustrated in Figure 2.9. The support structure is composed of strips of thin fiberglass boards, with notches machined at specific intervals. The support strips for X plane is directly mounted on the inner frame members. After all X wires have been placed into the slits, the V support strip (shown in green) is glued onto the tips of the X strips, trapping the X wires in position. After the V wire are placed into the slits, the U support strip (identical to the V strip) is glued to the V strip, trapping the V wires. These structures are repeated four times along the 7-m length of an APA, limiting the unsupported wire length on any wire plane to < 2 m, while introducing only millimeter-scale dead regions. These wire supports play a key role in minimizing wire deflection due to gravity and electrostatic force, enabling the use of a moderate wire tension and reducing the risk of wire breakage.

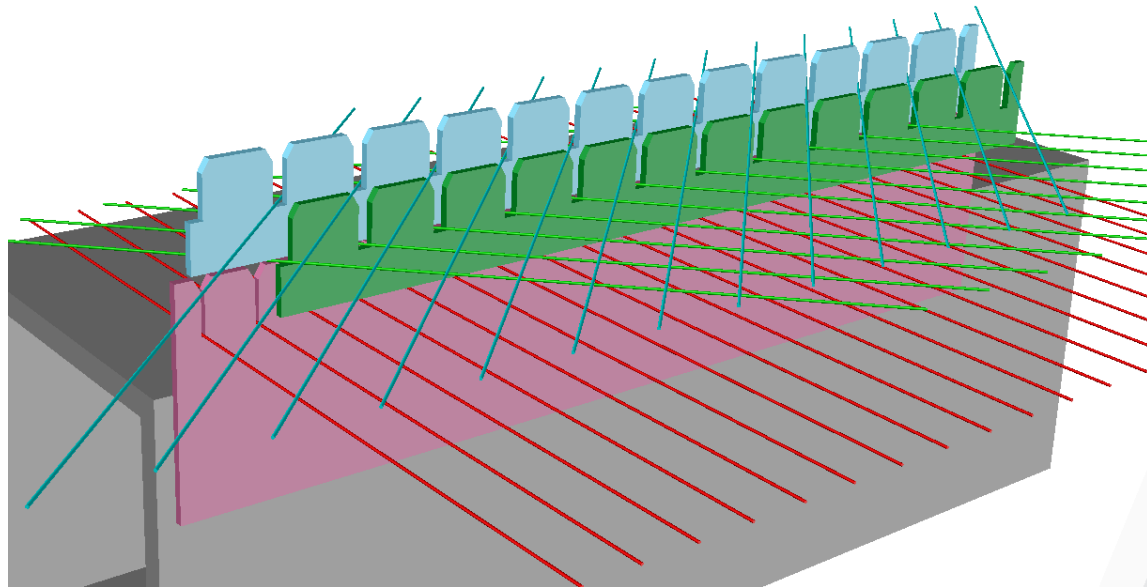


Figure 2.9: Conceptual design of the wire support for the U, V & X wires. Similar structures will be used to support the grid wire plane.

fig:tpc-wire-s

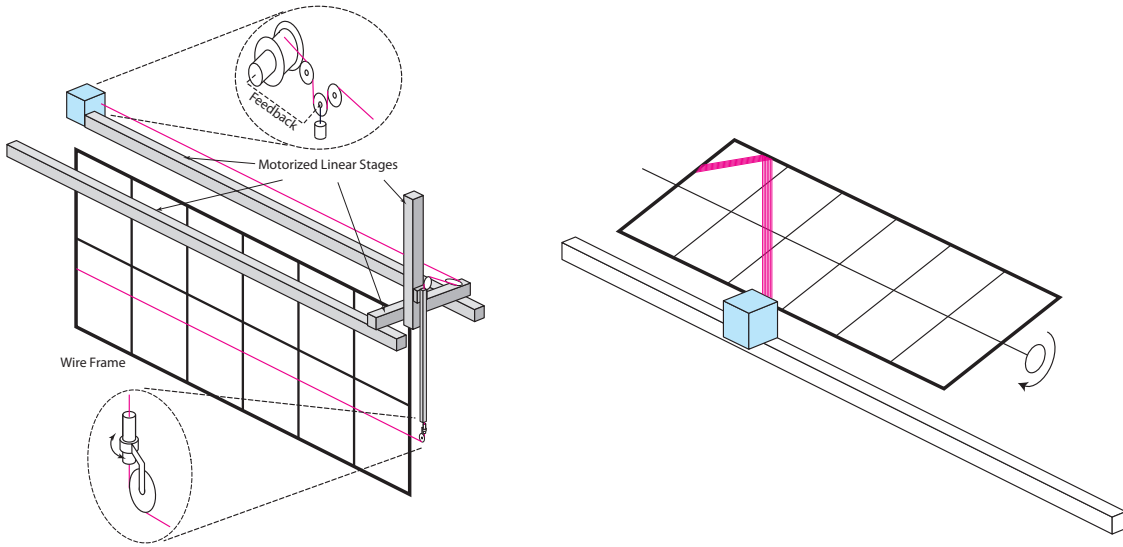


Figure 2.10: Two winding machine concepts. The left figure is for the X and grid wires. The right figure is for the U & V wires. The 'blue boxes' are wire spools with automatic tension control.

[fig:tpc-winding-machine](#)

2.3.6 Wire-Winding Machines

Two winding machines will be constructed to lay the 3680 wires on each APA. Their working concepts are illustrated in Figure 2.10. For the X and the grid wire planes, (left figure), the wire frame will be standing on one of its long edges, while a wire is wrapped around the frame using a commercial 3-axis gantry robot. A wire-tension controller maintains the wire tension and feed rate of the wire off the spool. Although the entire plane of wires can be wound in one pass, a more fault-tolerant procedure is to pause the winding machine periodically and solder the last wire onto the frame. This intermediate soldering step will prevent the unraveling of a large section due to an accidental broken wire. The winding machine for the U & V planes will wrap a group of wires (~ 10) as a band in each pass. An automatic soldering robot will solder the wire ends after the group of wires has been laid down on one side of the frame. A wire-tension measuring device will scan the newly placed wires and record the wire tension of each wire. Any wires with abnormal tension will be replaced manually.

2.3.7 Alternative APA Construction

Editor's Note: The APA size described in this section does not reflect the change from $2.5\text{ m} \times 7\text{ m}$ to $2.3\text{ m} \times 6\text{ m}$.

1

2 The APA design described above requires two customized machines capable of
3 placing wires directly on the $2.5\text{ m} \times 7\text{ m}$ APA frame with a precision of the order of
4 1 mm. Cleaning the solder flux off the APA after wire bonding also poses a challenge
5 on an object this size. An alternate APA design is under development to alleviate
6 these difficulties. In this design, the APA frame dimensions and the wire geometry
7 remain approximately the same, but the wires are attached to the APA frame in a
8 two-step process.

9 The first step is to bond a group of wires (~ 64) with epoxy and solder on two
10 FR-4 boards to form a wire module. The second step is to mount all the assembled
11 wire modules onto an APA frame using a stretching table. The wire lengths in each
12 wire module are determined in such a way that when a module is mounted on the
13 frame, all wires will reach a uniform tension of 5 N. Jumper cables interconnect the
14 corresponding U or V wire modules along the two long edges of an APA to complete
15 the helical wire wrapping pattern electrically. The assembly of an APA frame using
16 prefabricated modules will be easier and faster than direct winding on the big frame.
17 If a wire is broken while being attached to the frame, it is relatively straightforward
18 to replace the affected wire module. The details of APA assembly are shown in
19 Figure 2.11.

20 One major drawback of this alternative design is a relatively large dead space
21 between any APA joints ($\sim 2 \times 35\text{ mm}$) due to the FR-4 board size. The electric
22 field in the drift region directly above the FR4 boards will have some irregularities,
23 causing minor distortion to the track trajectories. To eliminate these problems,
24 additional special wire modules could be placed over the dead region at the APA
25 edges. For example, a module with two layers of 18 wires ($\sim 90\text{ mm}$ wide) would
26 completely cover the FR-4 boards between two APA frames. The upper layer wires
27 maintain the uniform drift field, collect the electrons, and provide the X position
28 information, just like the regular X readout wires. The obtained X coordinates and
29 charge information partially restore the detector sensitivity at the APA joints. The
30 scheme with additional wire modules is shown in Figure 2.12.

31 Using the wire geometry shown in Figure 2.12 the bias voltages for wire planes
32 have been defined and electric field strength calculated in 2D. The calculation con-
33 firmed that the drift field above the FR-4 boards is uniform, and full collection of
34 electrons can be achieved on the additional wire modules. From past experience, the
35 electric field is not expected to change very much in a 3D simulation. Nevertheless,

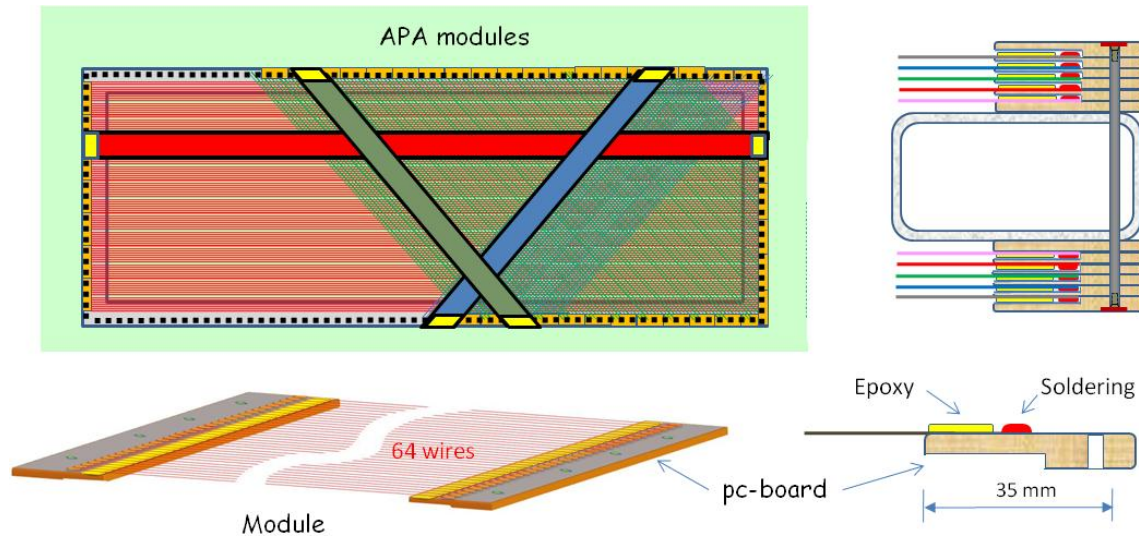


Figure 2.11: Concept of the alternative APA wiring scheme using pre-assembled wire modules

fig:tpc-APA-AD

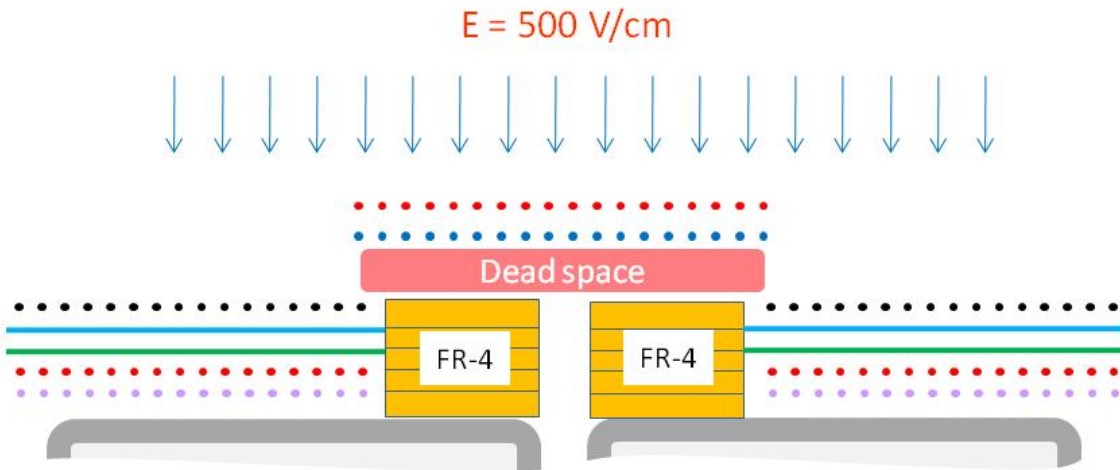


Figure 2.12: Illustration of dead space above FR-4 boards and possible solution with installation of two additional wire planes above.

fig:tpc-APA-AD

- ¹ it is necessary to develop a full 3D model for more accurate field calculations and
² simulation of electron drift in real APA geometry.

³ One of the advantages of this alternative design is the modularity of wire planes
⁴ that will simplify the wire placement and APA assembly. The winding procedure
⁵ becomes simple and reliable and a simple winding machine with replaceable wheels
⁶ is required. The module production could be done at several sites to accelerate the
⁷ APA assembly schedule. The completed modules will be cleaned in an ultrasonic
⁸ bath, dried in a vacuum oven and stored in dry air. A set of tests will be performed
⁹ to ensure that modules meet the technical specifications. The winding scheme for
¹⁰ module fabrication is presented in Figure 2.13. fig:tpc-APA-AD4

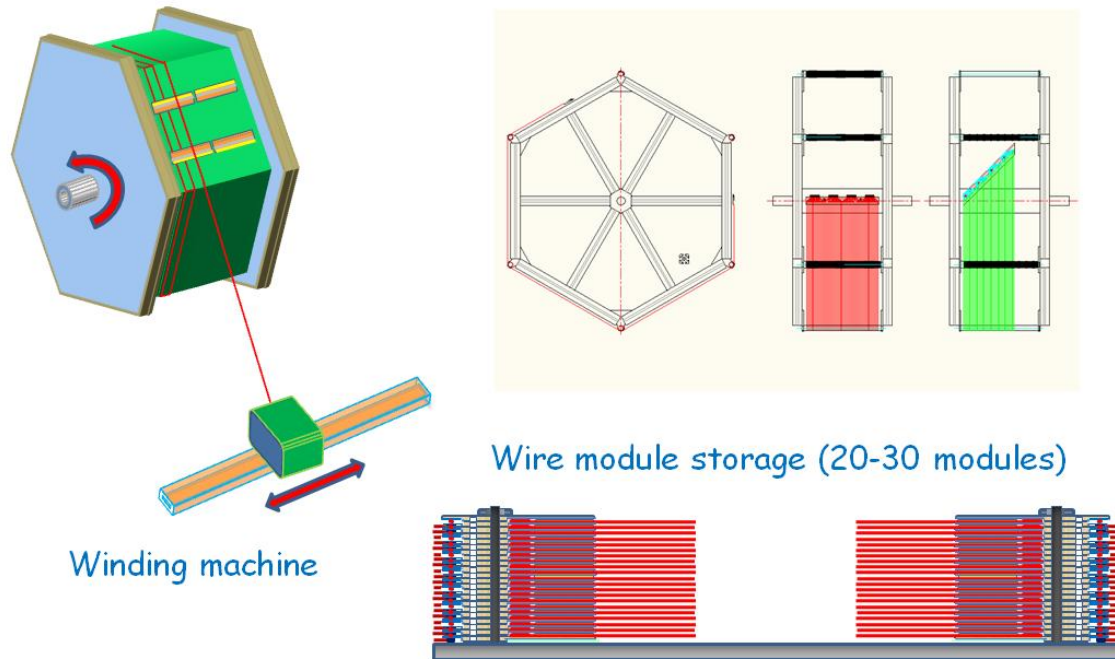


Figure 2.13: Conceptual designs of the wire winding machine and wire module storage fixture. Upper left: the fabrication of the wire modules are accomplished by attaching the wire module boards on to a large drum with specific circumference, and laying the wires over the boards at a constant pitch. Upper right: placement of the wire module boards for the X and grid wires (red), and U, V wires (green). Bottom: completed wire modules are stacked on a storage fixture. fig:tpc-APA-AD4

- ¹¹ For the assembly of the wire modules onto APA frames, a special assembly table
¹² will be used. The table will allow frame rotation in order to allow access to both

1 sides of an APA frame. A special movable, stretching mechanism will be mounted on
2 the table edge for installation of wire modules. After assembly of each plane the final
3 wire tension and wire spacing will be measured. If some wires' tension or spacing are
4 out of specifications, their corresponding wire modules will be replaced. A schematic
5 design of a wire-stretching table is shown in Figure 2.14.

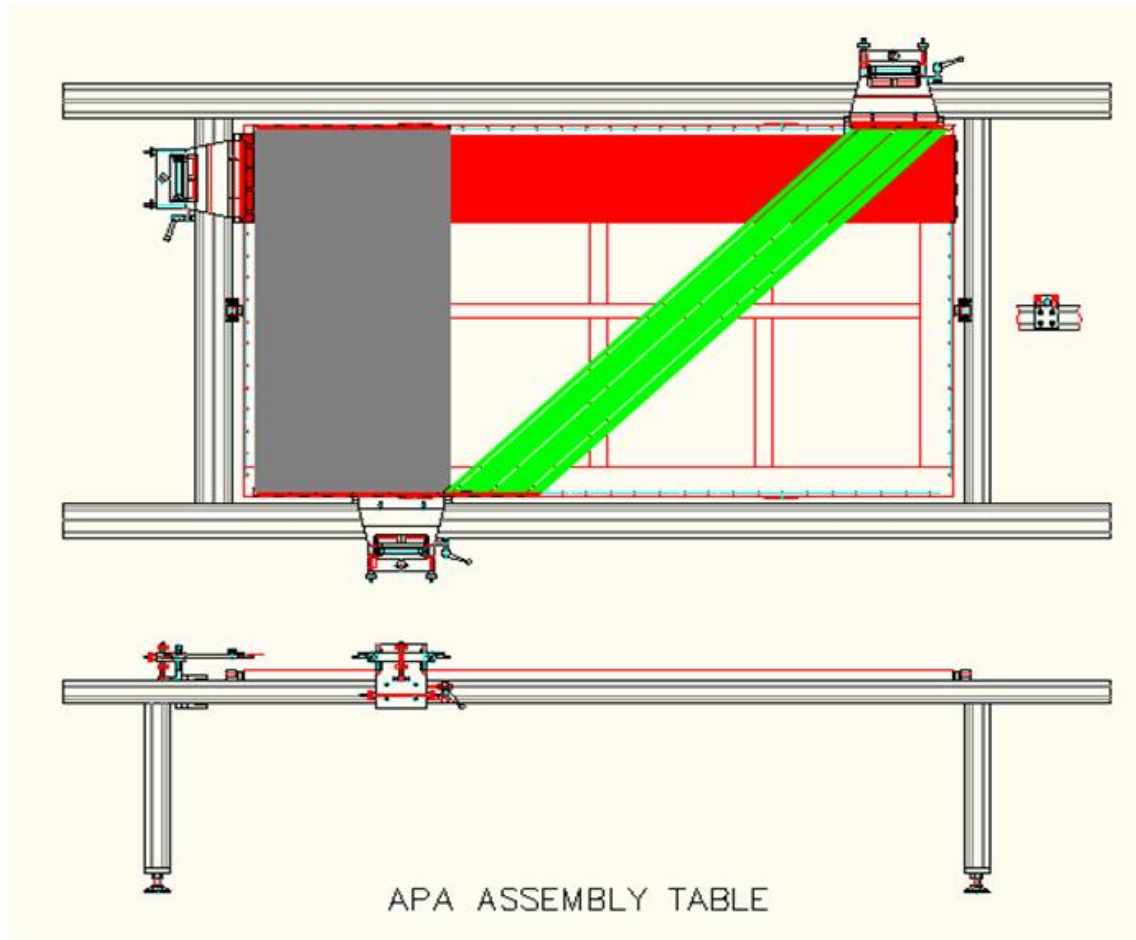


Figure 2.14: Assembly table with equipment for stretching wires.

fig:tpc-APA-ADS

6 Demonstration modules of both APA designs are being constructed. They will
7 be evaluated to determine which design will be used in the final APA construction.

2.4 Cathode Plane Assemblies

The cathode plane assemblies (CPAs) have similar dimensions to the APAs, 2.3 m wide and 6 m high. Each CPA is made of a stainless-steel framework, with a layer of stainless-steel wire mesh stretched over one side of the frame. To reduce drift-field distortion, all surfaces that rise significantly above the mesh, including the stainless-steel frame structure on the other side of the mesh, are covered with field-shaping electrodes biased at appropriate voltages. Figure 2.15 illustrates the concept of the CPA.

Editor's Note: Figure 2.15 shows the 2012 design. The design has evolved to a tubular member with stainless steel sheet.

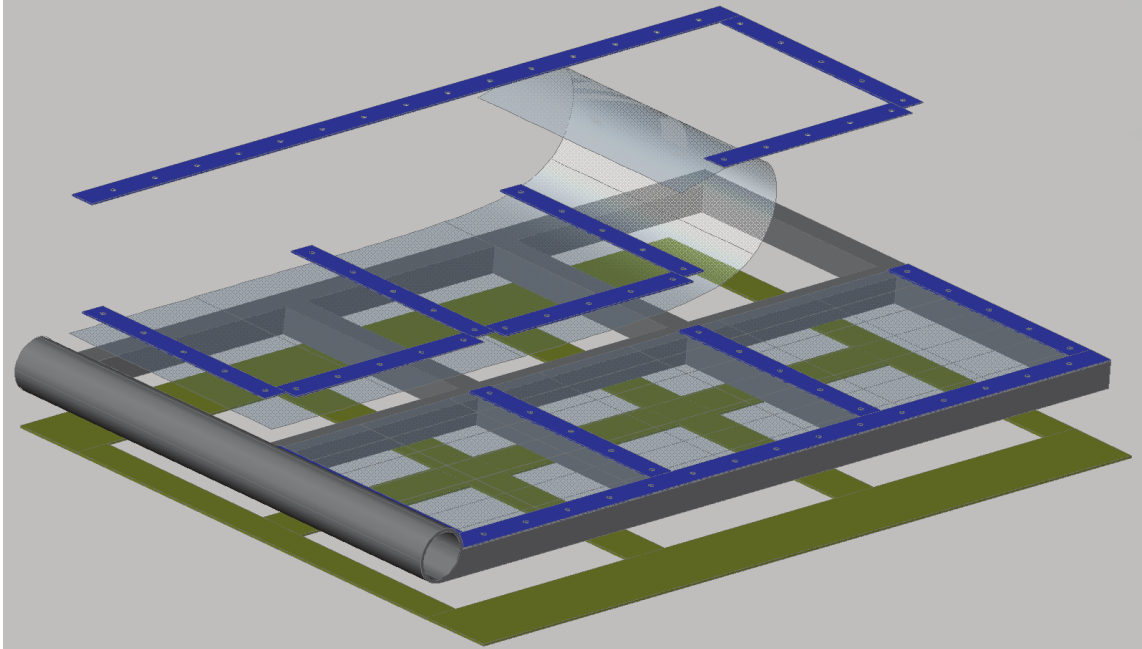


Figure 2.15: Conceptual design of a cathode plane assembly (not to scale). The assembly is 2.3 m wide and 6 m tall, similar to the APAs. As of December 2014 the design has evolved to a tubular member with stainless steel sheet.

To achieve a 500 V/cm drift field over a 3.4 m distance, the bias voltage on the cathode plane must reach -170 kV. The minimal high-voltage bias system requires

1 three high-voltage (HV) power supplies, one for each CPA row in the cryostat. Further
 2 partitioning of the CPA row and the field cages is being considered to reduce
 3 the loss of active volume in the event of HV failure inside the cryostat. For example,
 4 a six-zone configuration will require that a gap of several centimeters be maintained
 5 in the middle of each CPA row and field cage. Failure to maintain HV in one zone
 6 will result in the loss of no more than 20% of the active volume.

7 **2.5 Field Cage**

8 Each pair of facing cathode and anode rows forms an electron-drift region. A field
 9 cage completely surrounds the four open sides of this region to provide the necessary
 10 boundary conditions to ensure a uniform electric field within, unaffected by the
 11 presence of the cryostat walls.

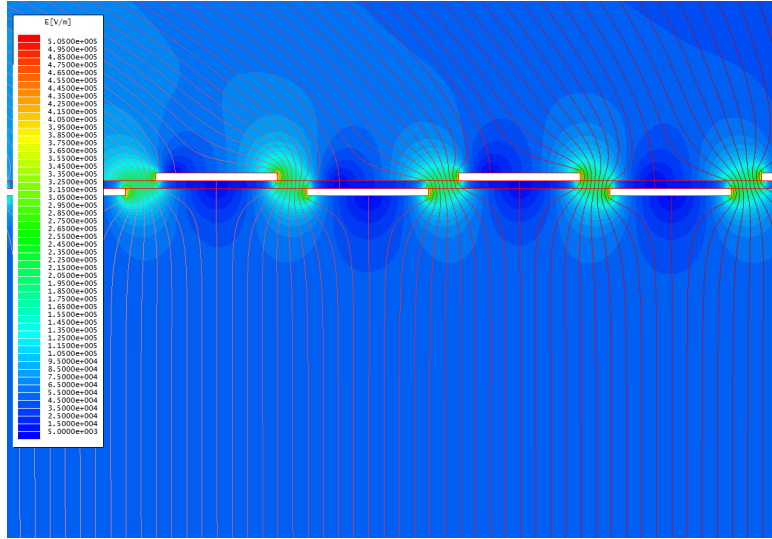


Figure 2.16: Electrostatic simulation of the electric field near a section of the field cage. The filled color contours represent the electric field strength. The line contours represent the electric potential at 500 V intervals. The pitch of the electrodes is 5 cm in this model.

fig:tpc-field-

12 The entire TPC requires $\sim 1100\text{m}^2$ of field cage material per 5-kton detector.
 13 The field cages are constructed using copper-clad FR4 sheets reinforced with fiber
 14 glass I-beams to form panels of $2.5\text{ m} \times 3.7\text{ m}$ in size. Parallel copper strips are
 15 etched/machined on the FR4 sheets. Strips are biased at appropriate voltages pro-
 16 vided by a resistive-divider network. These strips will create a linear electric-potential

¹ gradient in the LAr, ensuring a uniform drift field in the TPC's active volume. Figure 2.16 shows the results from an electrostatic simulation of a particular strip pattern. The drift-field non-uniformity quickly drops below 1%, roughly a strip pitch away from the field-cage surface. Since the field cage completely encloses the TPC drift region on four (of six) sides, the FR4 sheets must be frequently perforated to allow natural convection of the liquid argon. The “transparency” of the perforation will be determined by a detailed LAr computerized fluid dynamic (CFD) study.

⁸ The resistor-divider network will be soldered directly onto the field-cage panels. ⁹ Multiple resistors will be connected in parallel between any two taps of the divider, in ¹⁰ order to provide fault tolerance. One end of the divider chain is connected directly ¹¹ to the cathode, while the other end is connected to ground at the APA through ¹² resistors of the appropriate value.

¹³ 2.6 TPC Assembly in the Cryostat

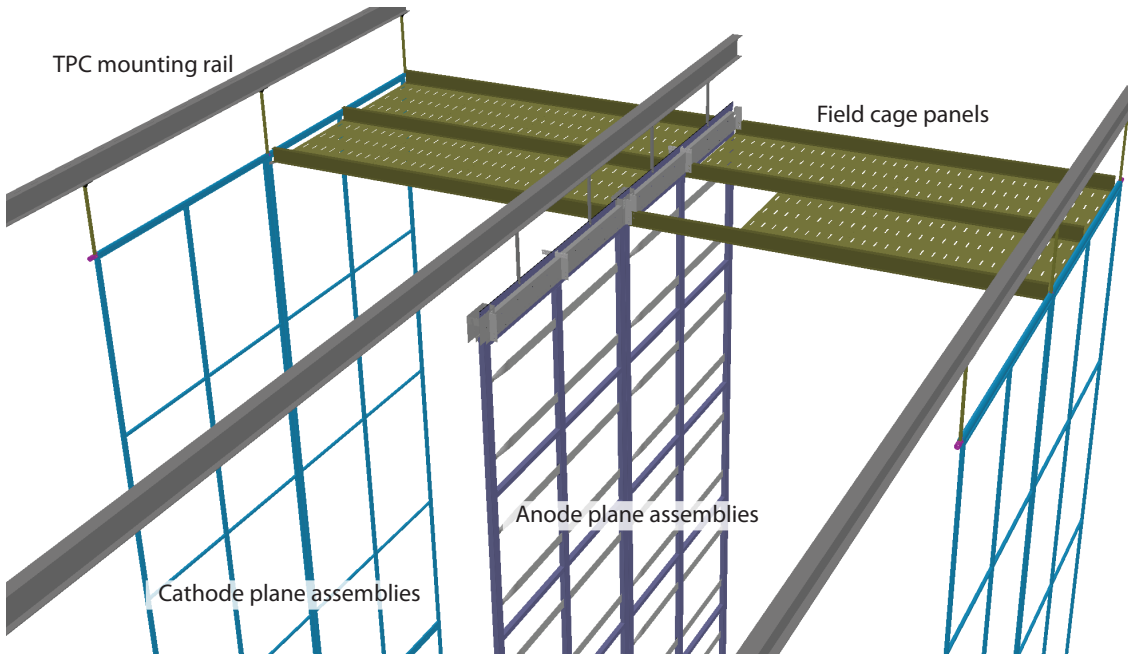


Figure 2.17: A partial assembly of the TPC showing all major components

¹⁴ Figure 2.17 shows a partial assembly of a section of the TPC. The finished cryostat ¹⁵ has five rows of anchor points distributed along the ceiling (not shown in the figure).

- 1 A mounting rail is suspended through stainless-steel rods to each row of the anchor
2 points. Under these five mounting rails, rows of CPAs and APAs are suspended in
3 an interleaved fashion. Because the cathodes are at a high voltage, the CPAs are
4 attached to their mounting rails through G10 rods. The distance between the facing
5 anode and cathode is maintained by the pultruded fiberglass I-beams holding the
6 FR4 sheets forming the field cage. The TPC installation procedure is discussed in
7 Chapter 5.
ch:install

8 **2.7 In-Vessel Front-End Electronics**

ec:v5-tpc-elec
Editor's Note: This section has not been updated for the increased number of APAs or APA size change. Therefore some values reported here will be incorrect for the design as of January 2015.

9
10 The front-end electronics will operate at cryogenic temperatures. The system
11 must provide amplification, shaping, zero suppression, digitization, buffering and multiplexing of the signals. All functions of the readout chain will be programmable via
12 a register on the ASICs. The APAs will need to be self-triggering since, unlike
13 neutrino-oscillation measurements for which the pulsed beam can provide a trigger
14 for readout, most other measurements, such as proton decay and supernova bursts,
15 will have no trigger.

17 **2.7.1 Architecture**

18 The large number of readout channels (276,480) required to instrument each cryostat
19 of the LAr-FD TPC dictates the use of CMOS ASICs for the electronics. Requirements
20 of low noise (less than 1000 rms electrons for a wire capacitance of 220 pF)
21 and for achieving extreme purity of the LAr dictate that the front-end electronics be
22 located at the signal wires in the LAr. This reduces the signal capacitance and hence
23 the noise. Significant levels of signal multiplexing can then also be used, minimizing
24 the number of cables in the ullage gas and the attendant outgassing of electronegative
25 impurities. This electronics architecture, combined with the modular TPC elements,
26 also leads to a TPC implementation that can be readily scaled to any detector size
27 or geometry.
fig:tpc-elec-schematic

28 Figure 2.18 shows the architecture of a front-end electronics design that meets
29 the requirements for the LAr-FD TPC. The entire electronics chain is immersed in

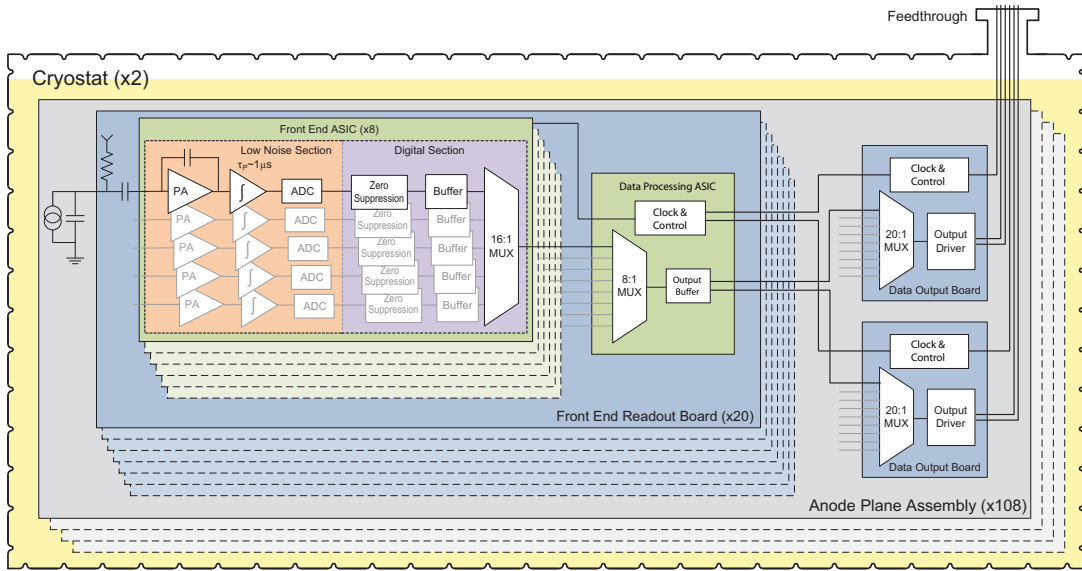


Figure 2.18: Conceptual architecture of the front-end electronics operating in LAr

fig:tpc-elec-s

the LAr and operates at 89 K. It is composed of a 16-channel front end implemented as a mixed-signal ASIC providing amplification, shaping, digitization, buffering, a 16:1 multiplexing stage, a driver and voltage regulators. Eight front-end ASICs plus a single digital ASIC implementing an 8:1 multiplexer, clock and control circuitry comprise a single 128-channel front-end readout board. A third digital ASIC containing a multiplexing stage (20:1) and driver is used for each APA module to serialize all of the data from the 20 readout boards on a single APA (for a total of 2,560 channels per APA) and transmit it out of the cryostat on either a twisted copper pair or an optical fiber. The choice between twisted-pair copper and optical fiber will be postponed until further work is completed to evaluate the long-term reliability of optical drivers at LAr temperature. The data rates per APA are not expected to be high enough to require the use of optical fibers. For either choice, a two-fold redundancy per APA will be implemented to minimize the probability of the loss of an entire APA.

Figure 2.19 shows a block diagram of the proposed 16-channel front-end ASIC. Each channel includes a charge amplifier with a selectable gain of 4.7, 7.8, 14 and 25 mV/fC (full scale charge of 55, 100, 180 and 300 fC), a high-order anti-aliasing filter with adjustable time constant (peaking time 0.5, 1, 2, and 3 μ s), an option to enable an AC coupling, baseline adjustment for operation with either the collecting

or the non-collecting wires, a 12-bit 2 MS/s ADC and a zero-suppression/data compression stage. Shared among the 16 channels are the bias circuits, programming registers, a temperature monitor, the digital multiplexer (16:1), an analog buffer for signal monitoring, and the digital interface. A 600-kb buffer will be included in this design, capable of storing a 1.5-ms event sampled at 2 MS/s in each channel assuming no compression. Two or more events can be stored with compression. The layout size is on the order of 10×5 mm², which would provide a yield in excess of 90%. The estimated power dissipation is below 15 mW per channel at 1.8 V supply.

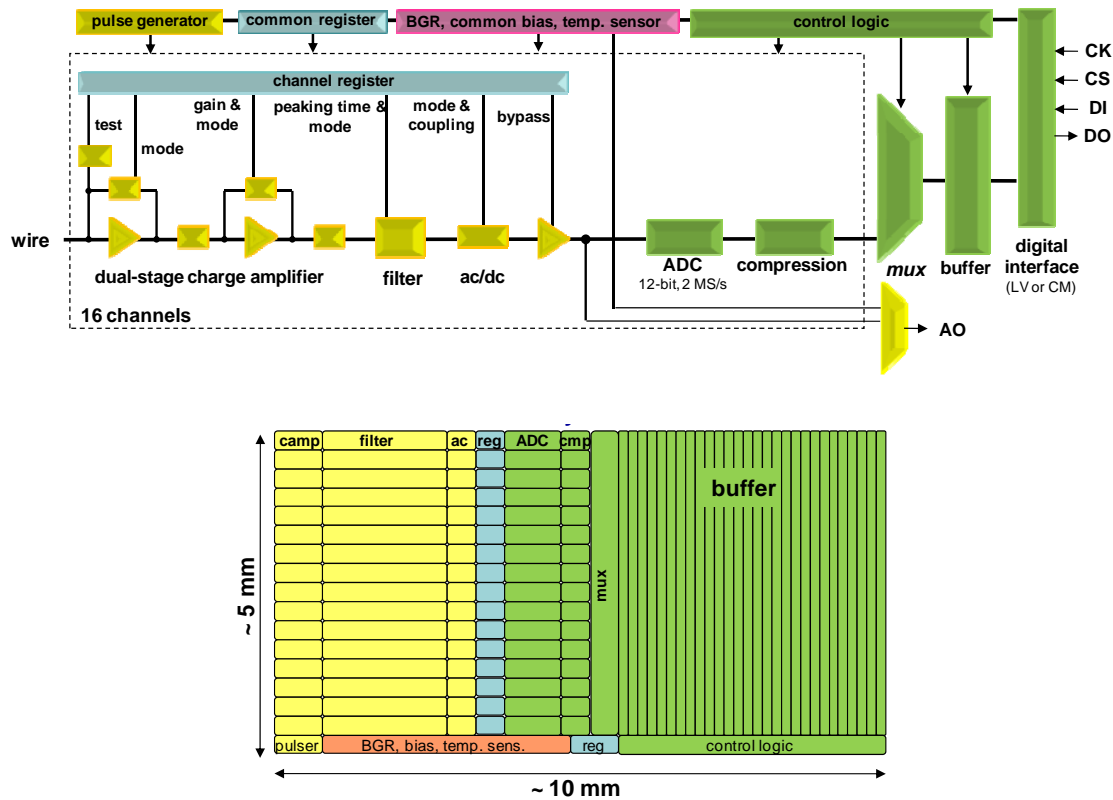


Figure 2.19: Architecture and layout of the 16-channel front-end mixed-signal ASIC

fig:tpc-elec-a

2.7.2 Data Rates

For neutrino-oscillation measurements the pulsed beam can provide a trigger for readout, but for most other measurements, such as proton decay and supernova

1 bursts, there will be no trigger. Therefore the APAs will be self triggering.

2 Data rates will then be dependent on the event rates for background processes.
3 Dominant backgrounds are decays of radionuclides in the LAr, predominantly the
4 naturally occurring Ar³⁹. The cosmic-muon rate at the 4850 Level is approximately
5 2.3 mHz per APA. Reading an APA (2,560 wires) for one drift time (4,625 samples)
6 gives 142 Mb of data. At the cosmic-event rate, the net data rate is 0.3 Mb/s
7 per APA. For radioactive decay of Ar³⁹ the rates are much higher: the specific
8 activity is 1 Bq/kg which results in 183 kHz/APA. At this rate, the APA will be
9 continuously read out, at a prohibitive data rate of 61 Gb/s; of course, since the
10 ionization produced by these events is highly localized, most of the drift “frame” is
11 empty.

12 The mean range of the beta from Ar³⁹ decay is only 0.3 mm, so all of the signal is
13 contained in a single over threshold sample of a single wire, for a true “information”
14 rate of 0.6 Mb/s. In order to reduce the rate (and volume) of recorded data to
15 tolerable values, zero suppression and data buffering must be provided. The simplest
16 scheme is to do this at the APA level, deriving a write-enable from the logic OR of
17 discriminators on all the charge collecting (Y) wires in an APA, and then writing all
18 data to a buffer while the write-enable is true. Baseline samples could be recorded
19 with reduced range (4 bits) and compacted into full words. This mode would still
20 record large volumes of data without useful information, particularly for simple event
21 topologies and from low-energy events (radioactive decays) and noise.

22 A more effective zero-suppression can be implemented at the chip level with
23 a dedicated buffer for each channel having a write-enable consisting of the OR of
24 that channel and its two nearest neighbors. A few samples before and after the
25 write-enable will also be recorded to capture the below-threshold leading and trailing
26 edges of the signal waveform. This mode provides maximal zero-suppression that is
27 insensitive to localized low-energy events and noise. This scheme would reduce the
28 data rate per APA for Ar³⁹ decays to 18 Mb/s. The rate for Kr⁸⁵ decays would be
29 about four times lower.

30 A conceptual diagram of this zero-suppression implementation is shown in Fig-
31 ure 2.20. The write-enable for each channel is derived from a separate shaping
32 amplifier with AC coupling to remove low-frequency, baseline fluctuations. Multiple
33 programmable discriminators in the “write-enable” logic are needed to sense both
34 unipolar (collection wire) and bipolar (induction wire) waveforms. The write-enable
35 gate passes to, and is OR-ed with, channels of adjacent wires to record the below-
36 threshold portion of charge shared with these wires. As individual channel buffers
37 fill, they are transferred to a large output buffer shared with all 16 channels for
38 transmission off the chip.

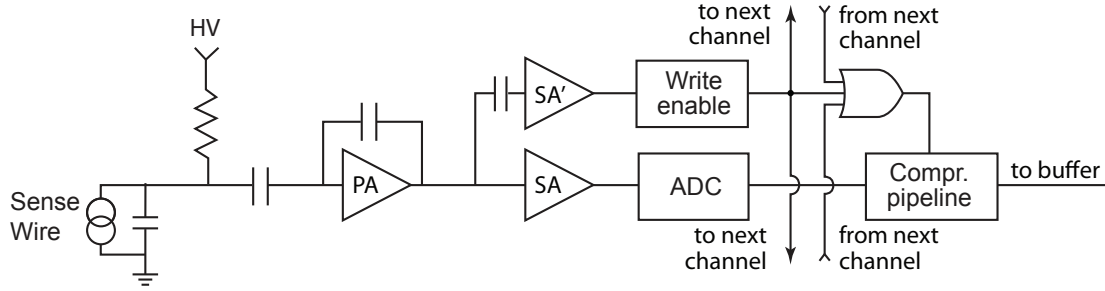


Figure 2.20: Conceptual architecture of zero-suppression using a write enable using separate analog shaping

fig:tpc-elec-w

2.7.3 CMOS Circuit Design

To successfully design CMOS circuits that will operate at cryogenic temperatures, two critical issues must be addressed and resolved. The first is the requirement for realistic models at the operating temperature of active devices, interconnects and passive components (resistors and capacitors) in order to reliably predict operating points, signal response and noise during the design process. The second critical requirement is that the design must ensure a long operational lifetime, since once the TPC is filled with LAr the detector must operate for about 15 years without any access to the electronics for repair or replacement. Concerning the availability of realistic models, our preliminary results from the cryogenic characterization (down to 40 K) of a complete mixed-signal ASIC [?] in a commercial CMOS 0.25 μm technology, originally developed for room-temperature applications, indicates that the models are useful to first order. To refine these models, several single-transistor test structures were fabricated on the first prototype of the 0.18 μm device. Measurements of the properties of these structures at cryogenic temperatures have been used to refine the device models at 89 K.

The lifetime of CMOS circuits is limited by several mechanisms which degrade the performance over time, eventually causing the circuit to fail to perform as specified. The rates of most degradation mechanisms in CMOS, such as electro-migration (EM), stress migration (SM), time-dependent dielectric breakdown (TDDB), thermal cycling (TC), and negative bias-temperature instability (NBTI), all scale with temperature such that cryogenic operation is favored [?][?]. The only mechanism that could affect the lifetime at cryogenic temperature is the degradation due to impact ionization, which causes charge trapping in the MOSFET gate oxide at large drain-current densities (the “Hot Carrier” effect). Results from a CMOS reliability

1 study [?] provide general design guidelines (for device geometry, bias and current
2 density) that should guarantee a lifetime well in excess of 15 years for continuous
3 cryogenic operation. These design guidelines also provide information for design-
4 ing test conditions to observe the deterioration mechanism and to extrapolate from
5 accelerated deterioration rates, measured under stressed conditions within practical
6 times, to the ultimate lifetime under normal operation.

7 A monitor of the impact ionization is the bulk current, which reaches a maximum
8 at $V_D S = V_D D$ and at $V_G S = 0.5V_D D$. When operating constantly in this condition
9 at room temperature, a properly designed device will typically have a lifetime (defined
10 as a 10% degradation in g_m) of about 10 years. The bulk current (i.e., the impact
11 ionization) increases by roughly a factor of four from 300 K to 77 K [?] and a circuit
12 designed for operation at room temperature would have a proportionately shorter
13 useful life at cryogenic temperature. As stated above, in order to guarantee the
14 required lifetime at cryogenic temperatures, design guidelines must be modified for
15 both analog and digital circuits. For analog circuits, this is done by operating the
16 devices at moderate-to-low drain current densities, where impact ionization becomes
17 negligible. For digital circuits, operating the devices with reduced $V_D D$ (about 20%)
18 and using non-minimum channel length L, which is easily accommodated since at
19 cryogenic temperature the speed of the digital circuit increases, compensating for
20 the increased L. These guidelines will be verified with accelerated aging tests, at
21 increasing values of $V_D D$, on dedicated structures. Such tests also will be conducted
22 on prototype samples throughout the development process to verify the long-term
23 reliability of the final ASICs.

24 The development of the readout ASIC has begun by designing and fabricating in a
25 commercial CMOS process ($0.18 \mu\text{m}$ and 1.8V) a 16-channel ASIC implementing the
26 complete analog front-end section of the scheme shown in Figure 2.19. This process
27 is expected to be available for at least another 10 years. The charge amplifier input
28 MOSFET is a p-channel biased at 2 mA with a L/W (channel length/width) ratio
29 of $0.27 \mu\text{m} / 10 \text{ mm}$, followed by dual cascade stages. The charge amplification and
30 shaping filter have digitally programmable gain and peaking time as described above.
31 Each channel also implements a high-performance output driver which, in the final
32 version, will be replaced with a sample-and-hold stage preceding the ADC. The ASIC
33 integrates a band-gap reference (BGR) to generate all the internal bias voltages and
34 currents. This guarantees a high stability of the operating point over a wide range
35 of temperatures, including cryogenic. The ASIC is packaged in a commercial, fully
36 encapsulated plastic QFP 80 package.

37 This ASIC has now been through three design/fabrication/testing revision cy-
38 cles. Prototypes from each cycle have been evaluated and characterized at room

(300 K) and liquid nitrogen (77 K) temperatures. During these tests the circuits have been cycled multiple times between the two temperatures and operated without any change in performance. Figure 2.21 shows the measured pulse response, along with details on the adjustability of the gain, peaking time and baseline. These results are in close agreement with the simulations and indicate that both the analog and the digital circuits and interface operate as expected in a cryogenic environment. Simulations and experimental results show that the pole-zero cancellation needs to be optimized, which will be done in the next revision of the design. Also reported in Figure 2.21 are the outputs of the BGR and temperature sensor, which are in close agreement with the simulations as well.

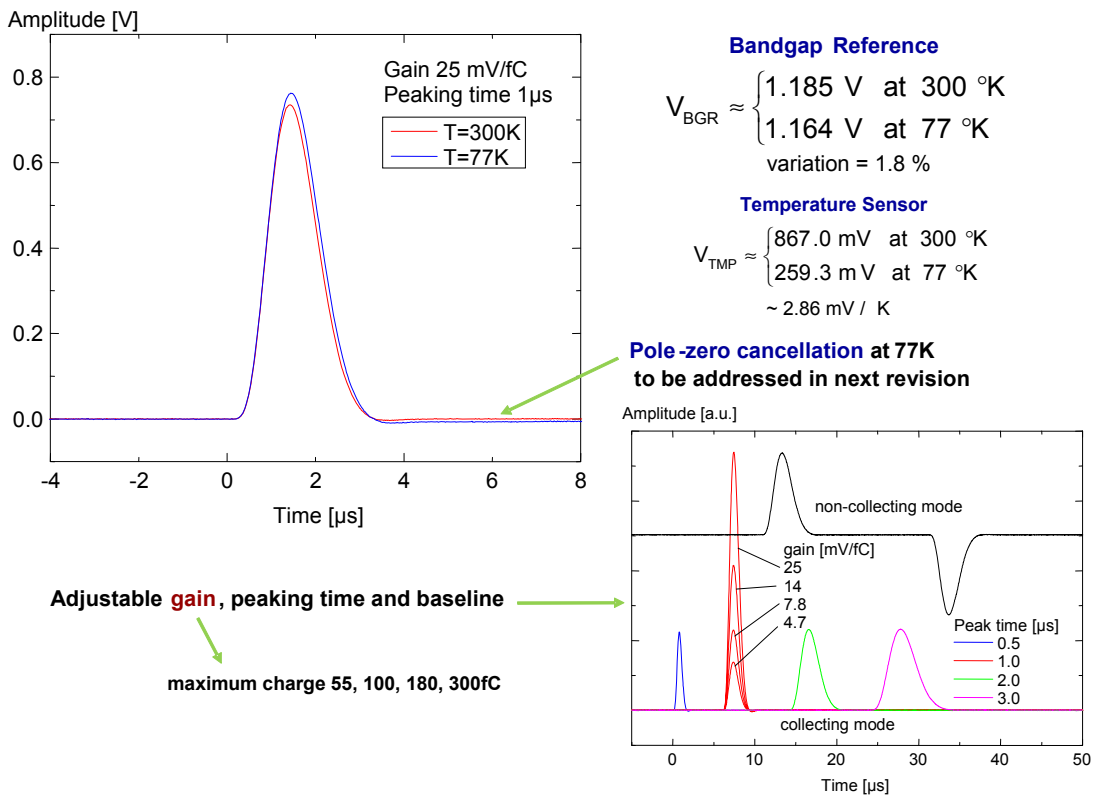


Figure 2.21: Measured pulse response with details on gain, peaking time and baseline adjustments

Figure 2.22 shows the measured ENC versus filter-time constant (peaking time). At 1 μ s about 650 e⁻ was measured, to be compared to the simulated value of 500

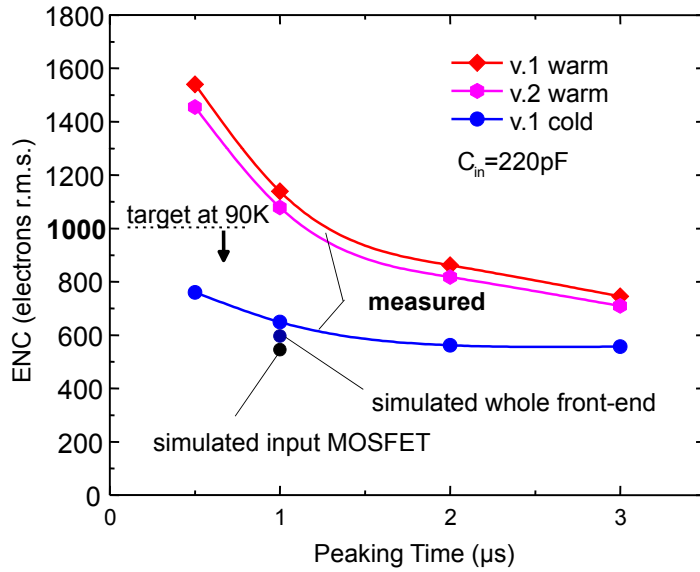


Figure 2.22: Measured ENC vs filter time constant from the first two versions of the analog front end ASICs

`fig:tpc-elec-enc`

¹ e^- . The difference is mainly due to the thermal noise from a $\sim 11\text{-ohm}$ parasitic ² resistance of the input line (shown in the detail of Figure 2.22), which contributes ³ about 350 electrons at 77 K. The width of the line will be increased in a revision in ⁴ order to make this contribution negligible. A second contribution, on the order of ⁵ 100 e^- , was due to the dielectric loss from the capacitor (220 pF) used to simulate ⁶ the wire (the cases of MICA and NPO ceramic were compared). This contribution ⁷ would not be present with the input connected to a sense wire in the TPC.

⁸ Each channel is equipped with an injection capacitor which can be used for test ⁹ and calibration and can be enabled or disabled through a dedicated register. The ¹⁰ injection capacitance has been measured using a calibrated external capacitor. The ¹¹ measurements show that the calibration capacitance is extremely stable, changing ¹² from 184 fF at room temperature to 183 fF at 77 K. This result and the measured ¹³ stability of the peaking time demonstrate the high stability of the passive compo- ¹⁴ nents with the temperature. Channel-to-channel and chip-to-chip variation in the ¹⁵ calibration capacitor are typically less than 1%. Measurements are being carried out ¹⁶ on the individual test structures fabricated on this ASIC to confirm device models ¹⁷ and design guidelines.

¹⁸ All data, control, bias and power supply lines will be duplicated to provide re-

1 dundancy to avoid the loss on an entire APA. Four APAs will be cabled to warm
2 feedthroughs in “chimneys” in the roof of the cryostat that contain the support rods
3 for the TPC planes.

4 **2.8 TPC Infrastructure**

5 The TPC infrastructure includes low-voltage and high-voltage supplies, all power
6 cables and cable routing to the supplies, signal cables and cable routing to the DAQ,
7 and all cryogenic feedthroughs.

8 **2.8.1 Design Considerations**

- 9 • All power supplies must be able to be monitored and controlled both locally
10 and remotely through the DAQ system. They must have over-current and
11 over-voltage protection circuits.
- 12 • The power supplies for the TPC cathode planes must be able to provide –200
13 kV at 1 mA current. The output voltage ripple must not introduce more
14 than 10% of the equivalent thermal noise from the front-end electronics. The
15 power supplies must be programmable to trip (shutdown) their output at a
16 certain current limit. During power on and off, including output loss (for
17 any reason), the voltage ramp rate at the feedthrough must be controllable to
18 prevent damage to the in-vessel electronics through excess charge injection.
- 19 • The power supplies for the wire-plane bias voltages must provide sufficient
20 current. The output-voltage ripple must not introduce more than 10% of the
21 equivalent thermal noise from the front-end electronics.
- 22 • High-voltage feedthroughs must be able to withstand –250 kV at their center
23 conductors in 1 atm air or argon gas environment when terminated in liquid
24 argon.
- 25 • Medium-voltage feedthroughs must be able to withstand twice their nominal
26 operating voltages with a maximum specified leakage current in 1-atm argon
27 gas.
- 28 • Low-voltage power feedthroughs must be able to deliver sufficient DC current.

2.8.2 Reference Design

There are three types of power supplies and matching feedthroughs in the cryostat: TPC high voltage, wire-bias voltages and low-voltage DC power to the readout electronics. There are two additional types of feedthroughs carrying digital signal: LVDS and optical fiber.

With the exception of the TPC high-voltage connections, all other cables inside the cryostat will be attached to their corresponding feedthroughs distributed throughout the cryostat roof. The other ends of the cables will be connected to the matching connectors on the APAs in the cryostat. The cables for the lower APAs must be carefully threaded through the hollow frames of the APA stacks. The cables will be strain-relieved on the mounting rails above the APAs.

Measurements in the Materials Test Stand at Fermilab (described in Section 6.3.1) have shown that impurities (principally O₂ and H₂O) embedded in objects submerged in the liquid argon do not result in a decrease in electron-drift lifetime, whereas impurities in objects located in the warmer gas phase do. This indicates the importance of minimizing the amount of material in the gas ullage at the top of the cryostat. Therefore it may be desirable to connect all cables to feedthroughs below the liquid surface, and then pass the cables out of the cryostat, through an evacuated volume that traverses the gas and cryostat insulation, to a matching set of feedthroughs to the outside.

2.8.3 TPC High Voltage

The cathode planes are biased at -170 kV to provide the required 500 V/cm drift field. At a minimum, three high-voltage power supplies, each connecting through their own feedthroughs, will be used. Each supply will provide high voltage to one of the three rows of the cathode plane assemblies.

The current candidate for the high-voltage power supplies is the Heinzinger PNChp series, which is used by the ICARUS experiment. Additional filtering of the voltage ripples is done through the intrinsic HV cable capacitance and series resistors. Established techniques and practices will be implemented to eliminate micro-discharges and minimize unwanted energy transfer in case of an HV breakdown.

To ensure safe and reliable operation, the feedthroughs will be tested at a much higher voltage than expected in routine operation (~ 250 kV) in liquid argon. The feedthroughs will be mounted on the ceiling of the cryostat, their cold ends reaching through the gas ullage space and submerging into the liquid argon. The center conductor on the cold side of a feedthrough will be insulated and shielded by a

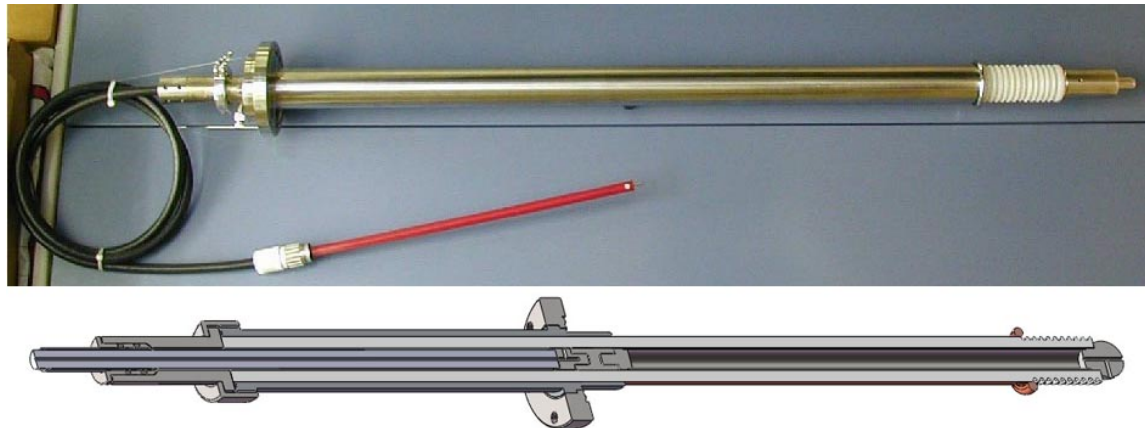


Figure 2.23: Top: A high voltage feedthrough developed by the UCLA group for the Icarus experiment. It was tested up to 150 kV. Bottom: a conceptual design of a new feedthrough for the LAr-FD TPCs.

`fig:tpc-UCLA-feedthrough`

1 grounded shroud at least 50 cm below the surface of the liquid. Connections between
 2 the feedthroughs and the CPA rows are made through stainless-steel pipes in the
 3 liquid argon. Figure 2.23 shows an example of a feedthrough made by the UCLA
 4 group for the ICARUS experiment, as well as the conceptual design of a feedthrough
 5 suitable for the LAr-FD TPCs.

2.8.4 Wire-Bias Voltages

6
 7 Each anode plane assembly requires three bias voltage connections at +820V, -370V,
 8 and -665V. The current on each of these supplies is expected to be zero at normal
 9 operation. However the ripple voltage on the supply must be carefully controlled to
 10 avoid noise injection into the front-end electronics.

11 The power supplies for the wire bias will be similar to those used for conventional
 12 multi-wire proportional chambers. Additional filtering networks will be needed to
 13 further reduce voltage ripples. The default feedthroughs are the commercial SHV
 14 type. However, other, higher-density multi-channel feedthroughs capable of with-
 15 standing the maximum voltage are under investigation.

2.8.5 Power for the Cold Electronics

16
 17 The power-per-channel for the front-end ASIC is designed to be about 15 mW and
 18 the total power requirement for each APA is expected to be about 65 W. Power will

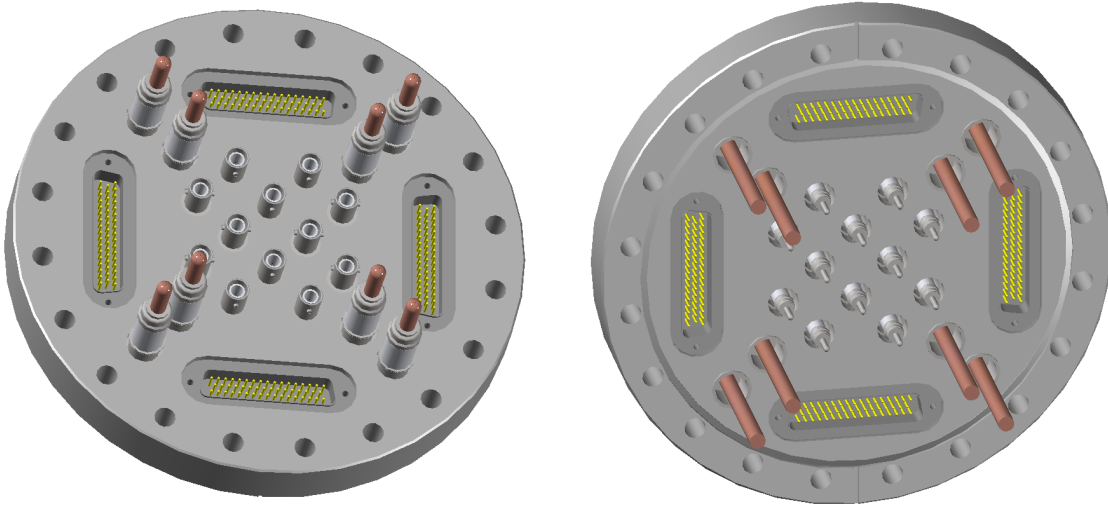


Figure 2.24: A conceptual design of a signal/power feedthrough using all off-the-shelf commercial components

fig:tpc-signal

¹ be supplied to the electronics on each APA separately by low-noise power supplies
² outside the cryostat, either directly by low-voltage (1.8 V), high-current (36 A) con-
³ ductors or by high-voltage (48 V) low-current (2 A) conductors to DC-DC converters
⁴ placed locally in the LAr. The use of DC-DC converters requires conductors with
⁵ smaller cross section, minimizing heat input to the cryostat (and ice formation of the
⁶ feedthroughs). However, the power dissipated by the (somewhat inefficient) convert-
⁷ ers in the LAr will create boiling which may introduce contamination directly into
⁸ the high-purity LAr, and if enough LAr is vaporized, may also produce strong mixing
⁹ of the ullage gas, driving more impurities into the liquid. These effects of boiling
¹⁰ LAr, unless they can be demonstrated to be harmless, will drive a preference for
¹¹ eliminating DC-DC converters, and directly powering the front-end readout boards.

¹² Heat conduction through the high-current feedthroughs and the self-heating ($I \cdot R$)
¹³ of the wires are the factors contributing to additional heat load on the cryogenic
¹⁴ system. The sum of the these two factors as a function of the wire gauge, however, has
¹⁵ a minimum due to the two opposing dependencies on the copper-wire cross section.
¹⁶ An optimum wire gauge can be chosen to minimize heat input to the cryostat.

¹⁷ 2.8.6 Digital Data IO Feedthroughs

¹⁸ The TPC data rate per APA, using the zero-suppression and full event-buffer scheme
¹⁹ described earlier, appears sufficiently low that it is within the capability of a single

1 LVDS channel on copper. Optical fiber will be used if data must be transmitted at a
2 much higher rate. In this case, the number of optical fibers will be two per APA for
3 redundancy, or 102 for each five-kton module. Commercial optical-fiber feedthroughs
4 are available to meet this demand.

5 In addition to the high-speed data-output channels, LVDS connections will be
6 made to each APA to distribute a clock signal and control information. These data
7 can be transmitted at a lower bit rate, clearly within the capabilities of LVDS. The
8 number of channels for these signals are on the order of thousands in the entire
9 detector, easily covered by commercial multichannel feedthroughs.

10 A conceptual design of an APA signal/power feedthrough flange is shown in
11 ^{fig:tpc-signal-feedthrough} Figure 2.24. Based on a standard 8-in conflat flange with all commercial off-the-shelf
12 components, each of these feedthroughs will serve the bias/power/digital IO needs
13 of four APAs.

14 **2.9 TPC Prototyping, Test and Checkout**

15 **2.9.1 TPC Prototyping**

16 Several prototype TPC modules will be constructed during the design phase. The
17 initial prototypes will be fraction scale or partial models of the APA and CPA. The
18 CPA prototype will be used to evaluate the wire-mesh tension and field-shaping
19 electrode attachment techniques. The APA prototype will be used to study the
20 placement of the wire-wrapping boards and wire-support structures. It will also
21 be used to develop the prototype winding machines. The prototypes will undergo
22 numerous thermal cycles down to liquid-nitrogen temperature to test the integrity
23 of the wire-to-board and board-to-frame bonds.

24 The second set of prototypes will be scale models of the APA and CPA. They will
25 be used to validate the designs and to evaluate production procedures. Prototype
26 front-end electronics boards are expected to be available at this stage. This TPC
27 will be assembled in the 35-t prototype cryostat, expected to be operational in 2015.

28 A prototype that is proposed to go into the CERN neutrino beamline requires
29 three full-size APAs with fully instrumented readout electronics, six full-size CPAs,
30 and complete field-cage coverage. The TPC will be constructed using identical APAs,
31 CPAs and field-cage panels as designed for the LAr-FD. Additional features will be
32 installed to ensure proper TPC operation given the half-height cryostat configuration.
33 The construction and assembly of all TPC mechanical components will use the same
34 materials and techniques as designed for LAr-FD, with the exception of a reduced
35 degree of automation that will be used to wire APAs for the LAr-FD.

1 A complete set of cold electronics will be installed on the APAs. The electronics
2 components will closely resemble those designed for the LAr-FD. All key features
3 of the LAr-FD electronics chain, including preamp, shaper, ADC, digital buffer,
4 zero suppression and multiplexing will be implemented. Some electronics may be in
5 prototype or functional-equivalent form.

2.9.2 Assembly Testing

6
7 The front-end readout boards will be thoroughly tested.

- 8 • A small number of the ASICs will undergo a complete suite of tests, including
9 thermal cycling to determine the batch yield.
- 10 • If the yield is high ($> 95\%$), all ASICs will be mounted on the front-end boards.
11 Tests will be performed on each board and bad chips replaced as needed.
- 12 • If the yield is not high, an automated test fixture will be fabricated to validate
13 every ASIC chip before mounting on the readout boards. Board-level tests
14 after mounting the ASICs will be conducted.
- 15 • The fully assembled front-end boards will be thermally cycled multiple times
16 while connected to a simple DAQ system to ensure reliable operation.
- 17 • The wire-carrier boards will be thermally cycled and HV stressed.

18 The APAs will also undergo testing.

- 19 • The tension and electrical continuity of each wire will be measured after the
20 plane of wires is bonded to the frame.
- 21 • After the front-end electronics boards have been installed on the APA, an initial
22 calibration of all electronic channels will be performed. The electronic gains
23 and noise levels of all channels will be recorded in a database.
- 24 • A cool-down stress test will be performed on each completed APA in a liquid-
25 nitrogen environment. Electronic calibration on all channels will be performed
26 while the APA is cold and again after it is warmed up. Significant differences
27 in the cold and warm calibration results will be investigated and remediated.

28 For the CPAs, a cool-down stress test will be performed on each completed CPA
29 in a LN₂ environment. After warming up, the tension of the wire mesh will be
30 checked.

1 For the field cages, the resistance will be measured along each copper strip, and
2 between strip pairs. The resistance between two strips should exceed $1\text{ G}\Omega$, without
3 the resistive divider.

4 **2.9.3 Checkout**

5 After passing the tests at the assembly level, the APAs will be put into storage,
6 and later transported to the LBNE Far Site. Prior to installation, another round
7 of electronic calibration will be performed on the APAs to validate their acceptable
8 status.

9 During installation, the DAQ system will be running continuously. As soon as
10 each stack of APAs is connected to the pre-routed cables, a suite of calibration runs
11 will be performed to validate that all connections have been made properly. Repair
12 or replacement at this stage will still be straightforward.

13 After the entire TPC is assembled, a system-wide calibration will be performed
14 at room temperature and again at cryogenic temperature in argon gas. Repair or
15 replacement would require partial disassembly of the TPC and should be avoided
16 unless absolutely necessary.

17 The responsibility and authority for the design, installation and use of the detector
18 quiet-power distribution and detector-grounding system is held by the subproject
19 electrical engineer. This engineer has oversight responsibility for all electrical and
20 electronics design and installation tasks, including all attachments to the detector
21 that create an electrical connection.

¹ Chapter 3

² Data Acquisition

ch:trig

- ³ The scope of the data acquisition (DAQ) subsystem includes the design, procurement, fabrication, testing, delivery and installation of a combination of custom and commercial electronics modules, (including commodity computing and networking hardware), as well as both commercial and internally developed software.

Editor’s Note: This chapter has not been updated since 2012, with the exception of this note. Most of the text from 2012 is no longer valid.

The data acquisition system has been evolving since the 2012 design. The design for the 35-ton prototype, the most recent, is based on artdaq, a toolkit for building DAQ systems that provides core DAQ functions. Experimenters leverage the infrastructure it provides and are able to focus on developing artdaq-compatible software modules to perform functions specific to the experiment.

Artdaq has been developed at Fermilab and is in use in several other experiments. It has been the default choice for the DAQ framework for the full LBNE detector for some time.

LBNE collaborators have so far developed modules that configure and read out the RCE and SSP boards that are connected to the TPC and photon system detectors, respectively, for the 35-ton detector. They are also developing reconstruction and filtering software modules that will analyze the data as it is acquired.

This artdaq-based DAQ system has been successfully used to acquire data in electronics and detector integration tests for the 35-ton prototype. As part of this, a preliminary design has been developed for the full detector. The design uses a two-stage artdaq system to stream zero-suppressed data into a farm of processes, run software modules to find events of interest, and use the results of this software trigger to initiate the readout of all of the data produced for the events of interest.

Since artdaq uses art, the same event analysis framework can be used online and offline. This allows experimenters to develop and substantially test their software in an offline environment and only include the full DAQ infrastructure for final testing.

¹

3.1 Introduction

2 The DAQ subsystem will perform the primary functions of:

- 3 • Configuration, online calibration/checkout, and control of operations of detector subsystems, including the generation and distribution of timing and control signals,
- 6 • Readout of raw data from the TPC and other detector subsystems,
- 7 • Filtering the data and constructing event records to be logged to persistent storage media,
- 9 • Control of, and readout of data from, devices providing real-time information on detector, subsystem and environmental conditions,
- 11 • Providing user/operator interfaces for these functions via a run control system, and
- 13 • Receiving and handling the LBNE beam-spill signal.

14 In this chapter, a reference design for the DAQ subsystem is presented. The development of this design is guided by recent experience gained in the development of relevant systems for the NO ν A [?] and MicroBooNE [?] experiments, as well as from running experiments with comparable channel counts and/or experimental conditions, such as D-Zero, CDF, MINOS and ICARUS.

19 The DAQ subsystem is to be located external to the cryostat vessel, with components in the detector hall and in an on-site control room. The primary interface is with the TPC front-end electronics. Additional interfaces are with the front-end electronics systems for the photon-detector subsystem, with the Fermilab Accelerator complex (the beam-spill signal), and with the cryogenics subsystem (for logging of conditions).

25 The DAQ subsystem reference design described in this chapter consists of the following components:

- 27 • custom ‘Data Concentrator’ modules located in the detector hall to receive data from the TPC (transmitted via redundant LVDS lines) and to carry out low-level data processing operations (these connect to the network, listed next)
- 30 • a network consisting of commercial ethernet switches located in the detector hall and a commercial router located in the counting house/control room, (for the transmission of data to the farm, listed next)

- 1 • a local farm of commodity computers that provide trigger event-building and
 - 2 real-time processing/event reconstruction functions
 - 3 • a custom timing system consisting of a master unit that locks onto a GPS clock
 - 4 and distributes timing signals to the data concentrator modules via slave units
 - 5 • dedicated computer nodes that host run control, routing control, node super-
 - 6 visor and slow controls processes
- 7 The DAQ subsystem does not include power-supply hardware for the TPC or front-
- 8 end electronics, nor does it include the cryogenics subsystem process-control and
- 9 monitoring functions.

10 **3.2 Design Considerations**

11 **3.2.1 Physics Considerations**

12 Physics considerations determine the scale of the primary tasks of digitized TPC
13 data readout, event building and online processing. In addition to rates for pro-
14 cesses of interest, the DAQ subsystem design depends critically on the specifications
15 for the TPC and front-end electronics systems, chosen to satisfy the LBNE physics
16 requirements. As described in Chapter 2, obtaining sensitivity to signals that oc-
17 cur independently of the LBNE beam spill, such as those from nucleon decay or
18 supernova-neutrino bursts, requires a free-running transmission of data from the
19 TPC front-end electronics. The sampling rate of 2 MHz has been chosen so as to
20 achieve the required position resolution along the ionization drift direction. The task
21 of data transfer is facilitated by multiplexing and data compression/zero-suppression
22 in front-end ASICs in the LAr, and by redundant data lines that provide connection
23 to data-acquisition hardware located outside the cryostat. With these specifications,
24 event building and triggering/filtering can be accomplished outside the cryostat. The
25 LBNE beam-spill signal and data from the photon-detection system are considered
26 part of the data stream, and can be used at this stage to select events for processing
27 and storage through physics-specific data streams, as desired.

28 **3.2.2 Technical Considerations**

29 In addition to physics considerations, DAQ design goals include minimizing the im-
30 pact of single-point failures and maximizing the use of commercial components. For
31 the reference design described here, sited at the 4850L of the Sanford Laboratory,

the atmospheric-muon rate is small enough – 0.1 Hz within the full LAr-FD active volume – to contribute only negligibly to the DAQ bandwidth requirement. For reference, the rate at the alternate 800L site is estimated to be 500 Hz within the active volume. This and other assumptions are discussed below in Section 3.2.3. The requirements on the DAQ system are listed in the requirements documentation [?].

3.2.3 Event Rates and Timing

Signals associated with beam events will be localized within the TPC and synchronous with discrete ($\mathcal{O}(1\text{ s})$ rep rate) beam-spill intervals spanning approximately $10\,\mu\text{s}$. However other physics events of interest will occur at random times, and can be dispersed throughout the TPC volume as in the case of neutrino bursts from supernovae. Other specific signatures, such as very slow-moving magnetic monopoles ($\beta < 10^{-3}$) may involve signals spanning sample times exceeding the 2.3-ms maximum ionization-drift time.

Cosmic-ray muons dominate the physics rate, even at the proposed 4850L site. However, this rate is negligible with respect to noise sources. This is not the case at other possible detector depths: at the alternate site identified at 800L, the total rate in the detector is estimated to be approximately 500 Hz, accounting for variations in overburden due to topography at the prospective cavern site, while the rate at the 300L is expected to be higher than this by a factor of 10. For shallow depths, the frequency of muon incidence is comparable to the maximum duration (2.3 ms) of the signal from an event, and hence cosmic-ray muons would have an impact on the required bandwidth of the DAQ system: while the system described here has sufficient bandwidth to operate at depths as shallow as the identified 800L site, going shallower still would impact the design.

As described earlier in this report (see Figure 2.18), the cold electronics for a single Anode Plane Assembly will consist of twenty 128-channel Front-End Readout Boards, each providing a single digital input to a 20-channel Data Output Board, which includes a $20 \times$ MUX stage into a driver for a redundant pair of LVDS outputs.

The Front-End Boards will generate zero-suppressed data: worst-case scenarios (i.e., $> 10\,\text{GeV}$ EM showers contained within a single APA) indicate roughly a factor of ten reduction in the number of samples read out with respect to the maximum ($2304\,\text{wires} \times 4625\,0.5\text{-}\mu\text{s samples per wire}$). For cosmic-ray muons, the rejection factor is estimated to be ~ 200 . The rejection factor is of course much higher in APAs not containing any portion of a physics event. Radioactive decay from ^{39}Ar and ^{85}Kr in the LAr, and to a lesser extent from detector materials (U/Th/Co/K), is estimated to provide a 65-kHz/APA rate of activity of energy above about 300 keV

¹ (0.3 MIPs) but less than ~ 5 MeV, while electronics noise (assuming 10:1 S/N for 1
² MIP, and a threshold of 0.3 MIPs) will contribute a relatively low rate per APA of
³ singles. Table ^{tbl:daq-signal-rates} provides a summary of these rate estimates. Work is ongoing to further refine them.

Table 3.1: Per-APA estimates of rates and data sizes/rates for various processes. Unless otherwise stated, estimated numbers of samples and data rates assume suppression of signals below 0.3 MIP. ‘Inst. Data Rate’ refers to the number of bits in a 2.3-ms long data block divided by this time interval, while ‘Avg. Data Rate’ factors in the process rate. A 12-bit ADC is assumed, and no allowance is made for data items such as time-stamp, channel identifier, etc.

Process	Rate (kHz/APA)	Samples (per APA)	Inst. Data Rate (Mbps)	Avg. Data Rate (Mbps)
Generic 2.3 ms interval (not zero-suppressed)	0.43	1.06×10^7	55,000	55,000
Cosmic ray muons (4850L)	6×10^{-7}	5×10^4	260	1×10^{-4}
Cosmic ray muons (800L)	0.0034	5×10^4	260	2.0
10 GeV EM shower	—	1×10^6	5,200	—
Radioactivity: U/Th (γ 's) $^{39}\text{Ar}/^{85}\text{Kr}$ (β 's)	~ 1 63	40 24	0.48 18	0.48 18
Electronics noise (not common mode)	~ 1	15	0.2	0.2

⁴
⁵ It can be concluded from the table that the average data rates out of the front-end electronics system are manageable: about 20 Mbps of ‘salt and pepper’ per APA
⁶ due to radionuclides in the Ar and TPC materials. Large beam- or atmospheric-neutrino interactions or showering ultra-high-energy cosmic-ray muons will result in
⁷ high (Gbps-level) instantaneous rates on the scale of the maximum ionization drift
⁸ period, but contribute negligibly to the average rate. With sufficient buffering in
⁹ front-end ASICs, as described in Chapter 2, the plan of having a single LVDS output
¹⁰ line per APA (plus a second one for redundancy) is easily realizable. However, to
¹¹ be conservative, and to provide opportunities for collecting data with relaxed zero-

- ¹ suppression, the DAQ reference design described below allows for as many as 20
² output lines per APA (one per front-end board), each operating below 24 Mbps.
³ This leads to a capacity for APA output rates up to 480 Mbps, well above the ~ 20
⁴ Mbps expected.

⁵ 3.3 Architecture Summary

- ⁶ The reference design of the DAQ system is summarized in block diagram form in
⁷ Figure 3.1. Component counts are given in Table 3.2. The main elements of the
 design are described in the following sections.

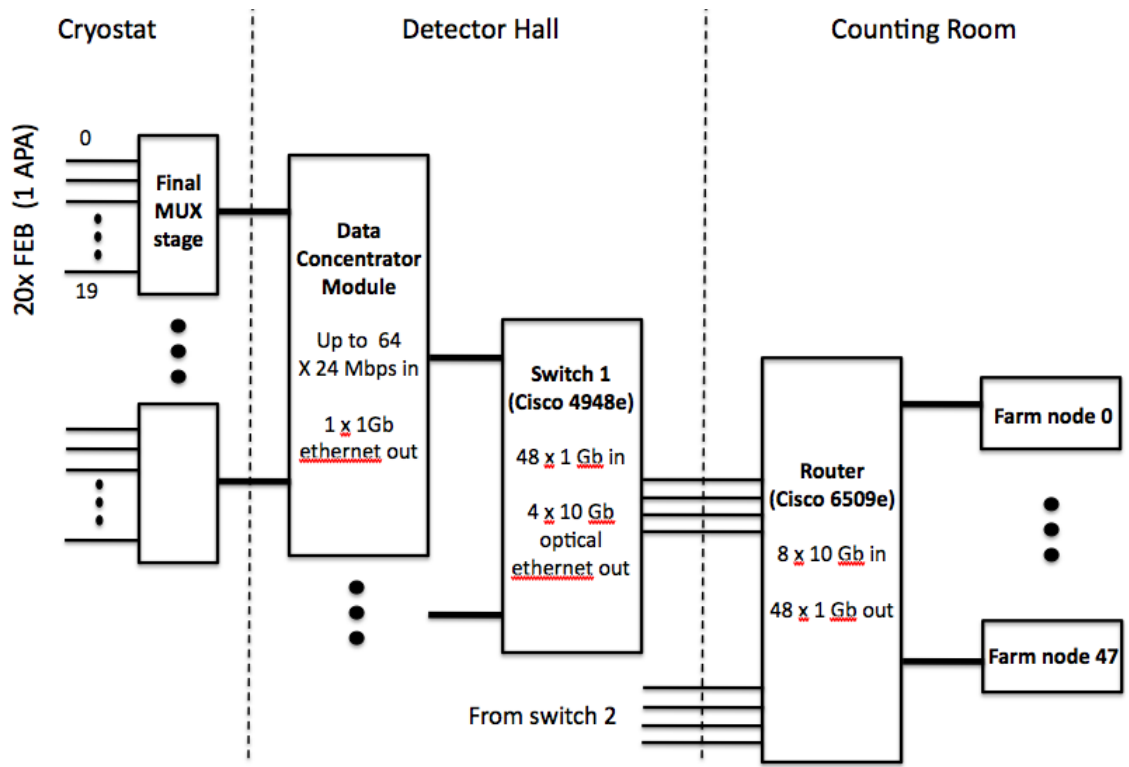


Figure 3.1: Block diagram depicting the DAQ reference-design architecture

[fig:daq-block-diagram](#)

Table 3.2: DAQ subsystem component counts for one 20-kton module/cryostat. The total component count for the two-cryostat LAr-FD will be twice what is shown.

Quantity	Description
54	Data Concentrator Modules
2	Ethernet Switches (Cisco 4948E or similar)
1	Ethernet Switch Chassis (Cisco 6509E or similar), with
1	8-port input optical 10-GB ethernet interface module, and
1	48-port output 1-GB ethernet interface module
48	Data Farm compute nodes
1	Readout Supervisor compute node (not shown in Figure)
1	Routing Master compute node (not shown in Figure)
1	Master timing unit + GPS receiver (not shown in Figure)
9	Slave timing units (not shown in Figure)
1	Run Control compute node (not shown in Figure)
1	Slow Controls compute node (not shown in Figure)

3.4 Data Concentrator Module

The LBNE/LArTPC Data Concentrator Module (DCM) serves as the primary interface between the cold TPC electronics and the DAQ subsystem, with the main task of receiving serial data pushed out of the front end. It also packetizes and transmits the data to ‘data farm’ computers for event building via an ethernet switch array, described in Section 3.5. Finally, it will provide the interface for transmitting timing and control signals to the cold electronics. As such, it is envisioned to provide the functionality of NO ν A’s custom electronics module of the same name, and similarly, the digital portion of MicroBooNE’s “Front End Module” (FEM) cards.

For the purposes of this conceptual design, the NO ν A DCM is considered as is. Several NO ν A prototype modules are shown in Figure 3.2. The NO ν A DCM consists of 64 input ports (RJ45 sockets), and a single 1 GB output line. A large FPGA provides preliminary data processing capability. A processor (running Linux) provides local control for configuration, buffering and routing functions.

Assuming the Data Output Board is implemented in the cold volume with $20 \times$ muxing to provide a single output line per APA, only a handful of NO ν A-style DCMs would be required to read out the entire detector. Considering typical data rates of order 20 Mbps per APA (see Table 3.1), the 1 Gb (80 MB/s) DCM output bandwidth could comfortably accommodate more than a few APA’s. More likely,



Figure 3.2: Photograph of several prototype NO ν A Data Concentrator Modules.

fig:daq-dcm-ph

- 1 the LBNE DCMs would be designed for fewer input lines in this case, in order to
2 distribute them rationally.
3 On the other hand, allowing for the possibility of 20 output lines per APA, the
4 NO ν A DCM footprint is well matched to the LBNE APA granularity. In this case,
5 a single DCM could serve two or three APAs. Outputs from auxiliary detector
6 elements could make use of the otherwise unused DCM input channels. To obtain a
7 conservative estimate of costs, this configuration is considered with two APA's per
8 DCM.

9 **3.4.1 Data Processing/Handling**

- 10 As currently imagined, buffers in the front-end electronics will constitute a source
11 of variable-length (i.e., zero-suppressed) time-ordered sequence of samples for each
12 channel (wire) registering activity, along with a channel address and time stamp.
13 Although this format is likely to be suitable for transmission to the data farm, the
14 DCM's task of generating ethernet packets also provides an opportunity for addi-
15 tional data processing. If re-formatting or additional zero suppression is desired, it
16 could be done here.

3.4.2 Timing, Control and Configuration Signals

The DCM will provide the interface for the transmission of timing, control and configuration signals to the TPC/front-end electronics. More detail on these signals is given in following sections.

3.5 Ethernet Switch Network

The network accomplishing transmission of data from DCMs to the data farm will consist of two layers of ethernet switch arrays. The first level will reside in the detector hall, and is imagined to be able to operate with little external control. Commercial switch modules such as the Cisco 4948E are well suited for this application. The 4948E has 48 1-GB input ports and four 10-GB optical output ports, as well as 175 MB of buffer memory. Two modules will support the required data throughput for the entire detector.

The second level will be deployed in the counting room and will serve as a router to the data farm nodes located there. For this application the Cisco 6509E switch chassis provides a possible implementation. This would be loaded with a single 8-port 10 GB blade for input data from the 4948E's, and a single 48-port 10/100/1000 MB blade for 1-GB output to farm nodes.

Routing information will be provided to DCMs by a Routing Master. This task will run on a computer located in the counting room. It will monitor the state of data farm nodes, and provide routing information to DCMs.

3.6 Event Building and Triggering

The event building and triggering function of the LAr-FD DAQ system will be performed by the data-farm computers. Event data will be staged locally before being transmitted in quasi real-time (nominally to Fermilab) for archival to persistent storage.

3.6.1 Event Building

At present it is imagined that an event will consist of raw data from the entire detector, spanning a time interval yet to be determined. To construct such an event, DCM packets corresponding to data with a common (range of) timestamp value(s) will be routed to a particular data-farm node.

An alternate scenario considers events as being localized to individual APAs, or possibly small APA clusters. Individual farm nodes would work only on the corresponding data to generate event records. This concept is attractive in that (1) the routing of data to farm nodes is simplified, and (2) event record sizes are kept as small as possible. The main drawbacks are that (1) offline processing/analysis of these event records for physics events with activity spanning geographical boundaries would become more cumbersome; (2) certain physics studies, such as proton-decay searches, might benefit from simple access to data-registering activity in remote sections of the detector ; and (3) auxiliary data would either be unnecessarily duplicated or would have to be stored in its own event record, again adding complexity to the data-analysis process. Evaluation of this alternative is ongoing.

3.6.2 Event Data Model

We will need to develop an Event Data Model (EDM). It may be advantageous to implement the raw data EDM in a custom format, as opposed to one based on ROOT. Experience with MicroBooNE will be helpful in optimizing the design for this.

3.6.3 Triggering and Selection for Output Streams

Significant work remains to understand how data-farm nodes will carry out event filtering and creation of separated physics/task-specific data streams. Use of the LBNE beam-spill signal to identify events recording beam-induced activity is expected to be straightforward. However, identifying events of interest that lack such a signal requires study. Is it sufficient to find a suitable way to generically veto events based on lack of coherent detector activity, or must ‘positive’ signatures for each of the physics processes of interest be identified for triggering? To indicate the range of signatures, these processes of interest include, for example, (1) beam-induced events for which the corresponding beam-spill signal is missing due to network failure or other malfunction, (2) atmospheric-neutrino interactions, (3) supernova-neutrino bursts, (4) proton decay, and (5) magnetic-monopole incidence.

Rejection of Event Records

Since the dominant rate is due to dispersed low-energy activity associated with radionuclide decays, simple trigger primitives can be generated and combined so as to reject event records failing well-defined (and easy-to-model) criteria. For example,

- ¹ event records in which no APAs register energy deposition in excess of some threshold
² (say 5 MeV) will be sufficient to reject most background events.

³ **Event selection for Physics-Specific Streams**

⁴ Even given the above statements about event rejection, it is desired to perform some
⁵ type of high-level event reconstruction to identify candidates compatible with spe-
⁶ cific physics signatures. This level of analyses is essential both for online detector
⁷ performance diagnostics as well as for the case where candidate event records of
⁸ particular types are to be written to parallel output streams. For the former appli-
⁹ cation, an unanticipated shortfall in the DAQ data farm computing capacity could
¹⁰ be easily addressed through establishment of a separate computer farm for online
¹¹ analysis. For the latter application, it would be necessary to adjust the size of the
¹² data farm depending on the processing requirements. These are not known at this
¹³ time. However, with anticipated costs for commodity computing systems, it is not
¹⁴ expected that the overall cost of the DAQ/online computing systems would increase
¹⁵ significantly relative to the currently budgeted system.

¹⁶ **3.7 Timing System**

¹⁷ Comparable requirements and conditions suggest a timing system similar to that
¹⁸ being implemented for NO ν A. That system meets the requirements of deterministic
¹⁹ timing and coherence of signals distributed across the entire detector. It consists of
²⁰ a Master Timing Unit (MTU) whose main task is generation of GPS-based timing
²¹ packets, and an array of Timing Distribution Units (TDUs). The TDUs are geo-
²² graphically distributed: they compensate for propagation delays before transmitting
²³ timestamp packets to the front ends via DCMs. Such a system could work well for
²⁴ LBNE and may be able to be adapted with only minor design modifications. For
²⁵ NO ν A, each TDU is associated with 12 DCMs; for LBNE a reasonable distribution
²⁶ could be achieved with 9 TDUs, one for every 6 DCMs (i.e., spaced at intervals of
²⁷ 5 m along the length of the detector).

²⁸ **3.8 Run Control**

²⁹ The scope of functionality of the Run Control system includes operation of DAQ
³⁰ subsystem components, configuration of front-end electronics, control of power sup-
³¹ plies and other auxiliary equipment, and control of data collection. Development

1 of a user interface for experimenters during data-taking and for technical person-
2 nel to assist with commissioning and debugging activities is key. To date, limited
3 effort has been put forth in the design of the Run Control system. To the extent
4 that the challenges faced are similar to those that have been addressed at MINOS
5 and ICARUS, no technical obstacles are foreseen. As the designs of the DAQ and
6 other subsystems continue to develop, specifications of the Run Control system will
7 become more concrete.

8 **3.9 Slow Control Systems**

9 The Slow Control system is a critical element of the DAQ, providing the main inter-
10 face to power supplies for the detector and electronics as well as to equipment used
11 to monitor the operational status of the detector and supporting systems. As in the
12 case of the Run Control system, the development of the conceptual design for the
13 Slow Control system is in its early stages. Again, based on experience from other
14 experiments, no obstacles are foreseen with regard to the development of a robust
15 system.

16 **3.10 DAQ Infrastructure**

17 **3.10.1 Wide Area Network**

18 As in the case of MINOS and NO ν A, it is expected that event data can be transmitted
19 over the network to Fermilab. Although rates for events of interest are comparable,
20 data throughput for the LBNE LArTPC is expected to be at least an order of mag-
21 nitude higher. A detailed analysis of the requirements of Sanford Laboratory for the
22 appropriate level of connectivity within and off the lab site will need to be carried
23 out.

24 **3.10.2 Online Data Storage**

25 To protect against significant periods of absent network connectivity, it is desired to
26 store a significant amount of the data emerging from the DAQ to local storage. A
27 local data storage facility of ~ 100 TB is expected to be more than adequate for five
28 days worth of detector data, even without prescaling cosmic-ray muon events.

3.10.3 Power and Cooling

² Power and cooling requirements for the DAQ system described here are modest.
³ DCMs operate at below 50 Watts each, while the maximum power consumed by
⁴ each of the two Cisco 4948Es is 275 Watts. Assuming power supplies that operate
⁵ at 75% efficiency, and accounting for other components, the total DAQ subsystem
⁶ budget for power in each 20-kton detector/cryostat hall is likely to be below 15 kW.

¹ Chapter 4

² Photon Detector

ch:photon

³ 4.1 Introduction

⁴ Liquid argon is an excellent scintillating medium. With an average energy needed
⁵ to produce a photon of 19.5 eV (at zero field) a typical 1 MeV particle will generate
⁶ 51,000 photons with 128 nm wavelength. At higher fields this will be reduced but at
⁷ 500 V/cm the yield is still \sim 40,000? photons per MeV. Roughly 1/3 of the photons
⁸ are prompt 2-6 ns and 2/3 are generated with a delay of 1100-1600 ns. LAr is
⁹ highly transparent to the 128 VUV photons with a Rayleigh scattering length and
¹⁰ absorption length of 95 cm and >200 cm respectively. The relatively large light
¹¹ yield makes the scintillation process an excellent candidate for determination of t_0
¹² for non-beam related events. Detection of the scintillation light may also be helpful
¹³ in background rejection.

¹⁴ 4.2 Requirements and Goals

¹⁵ 4.2.1 Beam-based physics

¹⁶ There are no requirements for the beam-based physics program, as the machine clock
¹⁷ will provide a t_0 with roughly 10 μ s resolution. Given that the electron drift is 1.6
¹⁸ mm/ μ s the uncertainty to the electron lifetime correction is small is the beam timing
¹⁹ is used. The photon system can be useful in determining the t_0 of cosmic ray events
²⁰ and events from radiological decays. The impact of this on the detector performance
²¹ needs to be determined, but it is not expected that the reduction in backgrounds for
²² the oscillation program will introduce additional requirements to the photon system
²³ design.

4.2.2 Proton decay and atmospheric physics

The photon detector system must provide the t_0 for non-beam related physics channels if a correction for electron recombination during drift is to be applied. The requirements for electronics and hadronic energy resolution for the proton decay and the atmospheric neutrino program are $1\%/\sqrt{E(\text{GeV})} \oplus 1\%$ and $30\%/\sqrt{E(\text{GeV})}$ respectively. With these resolutions the collected charge must be accurately corrected for recombination. Therefore the photon system must provide a t_0 for particles with >100 MeV with $>95\%$ efficiency in the fiducial volume of the detector.

4.2.3 Low-energy physics

Supernova events will produce neutrinos down to about ~ 5 MeV. Studies have estimated the momentum resolution for 5 MeV electrons to be 20% using only TPC information and assuming a highly efficient trigger and an electron lifetime of 5 ms. The impact of various detector resolutions on the physics potential of LBNE has not been studied in detail. At present there is no strong requirement that the energy resolution must be better than 20% so no requirement on the photon system trigger efficiency is set at this time. However it is clear that if a detector design can be found the energy resolution would greatly improve. A goal of the photon detection R&D is to develop a system with the lowest possible threshold for a reasonable cost. At time of the start of final design a final decision as to the configuration will need to be made based on cost and added physics capability.

4.2.4 General Considerations

In the event that larger photon collection efficiencies can be achieved then it is possible to improve the energy resolution of the detector by adding the photon yield to the electron yield information. However this requires several orders of improvement in light collection efficiency so it is beyond the scope of present designed.

4.3 Cast or Bulk doped acrylic bars

The reference design for the photon detection system is based on acrylic bars, which are either coated in TPB or doped in bulk. The 128 nm photons interact with the TPB on the surface and 430 nm light is re-emitted.

A PD module is made up of 4 light guides that capture, waveshift, and channel VUV photons to silicon photomultipliers (SiPMs) at one end. A schematic drawing

¹ of a cast acrylic light guide with its photosensors is shown in Figure 4.1.

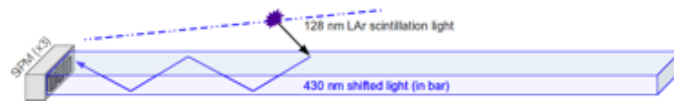


Figure 4.1: Schematic drawing of cast acrylic light guide with associated photo-sensors

² The light guides are made from cast acrylic bars that have wavelength shifter embedded in them. The wavelength shifter converts VUV scintillation photons striking it to 430 nm photons inside the bar, with an efficiency of 50% of converting a VUV to an optical photon. A fraction of the waveshifted optical photons are internally reflected to the bar's end where they are detected by SiPMs whose QE is well matched to the 430 nm waveshifted photons. The light guides were made with one of two wavelength shifters: the conventional TPB (1,1,4,4-tetraphenyl-1,3-butadiene) and the less expensive alternative bis-MSB (1,4-bis-(o-methyl-styryl)-benzene). Preliminary studies with a VUV monochromator show that the two wavelength shifters compare favorably in their waveshifting efficiency. Several technologies have been investigated at Indiana University for incorporating the waveshifter into the acrylic (or in one case, polystyrene), including:

¹⁴ 1. Flash heated bars

¹⁵ These light guides were made with TPB and bis-MSB using commercially available Lucite-UTRAN cast UVT acrylic sheet that was laser-cut into bars of the proper size. Lucite-UTRAN has an attenuation length of 2.5 m. To embed the WLS in the acrylic, the bars coated with waveshifter are flash heated to rapidly melt the WLS into a thin outer layer of the bar.

²⁰ 2. Hand-dipped bars

²¹ These light guides were made by dip-coating acrylic bars in a WLS solution, a process that was pioneered at MIT. This process improves the clarity and uniformity of the coating, as well as its scalability to the manufacture of the large number of light guides needed for LBNE. In this process, a solution is mixed with 2 parts TPB/bis-MSB to 100 parts DCM (dichloromethane, CH_2Cl_2). Each acrylic bar is submerged in this solution, removed, and then left to air dry.

²⁷ 3. Doped, cast acrylic bars

²⁸ These light guides were cut from a sheet of acrylic cast with TPB or bis-MSB mixed into the plastic. This sheet was manufactured commercially by Astra Products, Baldwin, NY. The sheet had 1% TPB or bis-MSB by mass added during their proprietary casting process, which distributes WLS throughout the volume. Experiments show that 1% WLS is the maximum that can be cast into the plastic without

1 particles settling out. Since VUV photons have a very short penetration depth in
2 acrylic, this manufacturing method uses more WLS than necessary. On the other
3 hand, light guides function more efficiently when their surfaces are flat and the cast-
4 ing process results in very flat surfaces. This is a strong mitigating factor when the
5 prime consideration is efficiency for the detection of VUV photons.

6 4. Doped, cast polystyrene

7 These light guides are made commercially by Eljen Technologies, a “world leader
8 in the development and manufacturer of organic plastic scintillation material.” These
9 light guides were cut from a sheet of polystyrene cast with TPB or bis-MSB mixed
10 into the plastic by a proprietary process. The sheet had 1% TPB or bis-MSB by mass
11 added during their proprietary casting process, which distributes WLS throughout
12 the volume.

13 In addition to these designs a thin bar (or fiber) with dimensions 3 mm by 3 mm
14 was developed by the CSU group. The square profile fiber-based prototype design
15 was motivated by the fact that 4 fibers would exactly couple to the 6 mm by 6 mm
16 active area of the SiPM currently under consideration for the photon detector system.
17 The fiber size allowed 100% areal acceptance to SiPM mapping, within efficiencies
18 associated with photon conversion and transport. The fibers used in the prototype
19 were custom fibers made by St. Gobain with a concentration of 1%, by weight, of
20 TPB mixed into the bulk during manufacture.

21 **4.3.1 Current status of design**

22 The designs have been tested at two facilities, the local LAr at Indiana University
23 and at the TallBo dewar in lab PAB at Fermilab. The light guide designs are tested
24 in a PD paddle frame designed and built at Colorado State U that holds 4 light
25 guides.

26 Selected Results from IU dewar facility

27 The IU dewar shown in Figure 4.2 below can hold 1 paddle. The IU dewar tests
28 can be used for both studying cosmic muons and attenuation length measurements
29 with a ^{241}Am α source. For the setup shown in Fig. 2, the ^{241}Am α source is moved up
30 the light guide and a set of waveforms are collected every 2 inches. The distribution
31 of the waveforms collected at each of the 10 positions for a hand-dipped bar with
32 TPB is shown in the left side of Figure 4.3. The individual photoelectron peaks are
33 clearly visible. The peak of the distribution nearest the SiPM is approximately 30
34 pe’s. At the farthest point, the peak is approximately 15 pe’s. The distributions
35 have all been normalized to have the same area. Since the standard deviation of the
36 waveform distribution nearest to the SiPM are larger than those farther away, the

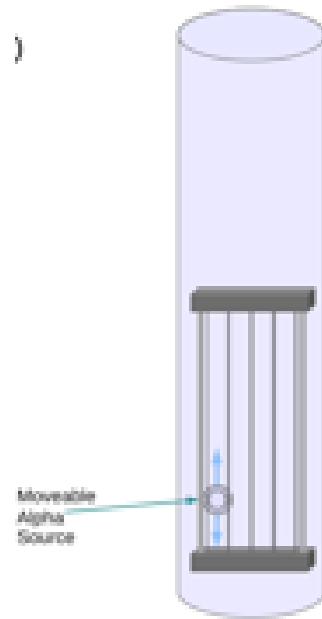


Figure 4.2: IU dewar paddle frame showing movable alpha source

fig:iu-dewar-p

1 near distributions are less peaked and wider.
2 The distribution of waveforms at each position along the bar is shown in the right
3 side of Figure 4.3. Superposed is an exponential fit to the peak of these waveform
4 distributions. This fit shows that the attenuation length of the bar is ~ 37 inches,
5 the longest attenuation length yet seen for the light guide technology.

6 There were 3 bars made in this batch of hand-dipped bars. One of those bars had
7 an attenuation length of ~ 31 inches, comparable to this result. One, however, had an
8 attenuation length of ~ 14 inches. It will be one of the objectives of next year's R&D
9 efforts to understand how to make light guides with consistently long attenuation
10 lengths.

11 Selected Results from the TallBo dewar facility

12 The TallBo dewar facility at Fermilab is described more fully in section 2.8.1. It
13 is a 450 liter dewar in lab PAB at Fermilab. It is large enough to hold 4 full PD
14 paddle frames loaded with 20-inch light guides. The TallBo dewar recirculates the
15 LAr and maintains its purity for weeks at a time. It is the test facility we use at IU
16 for longer-term comparison studies of many alternative technologies. The IU group
17 has run two experiments at TallBo so far, one in October-November 2013 and one in
18 February-March 2014. The goal of these experiments was to make inter-comparisons

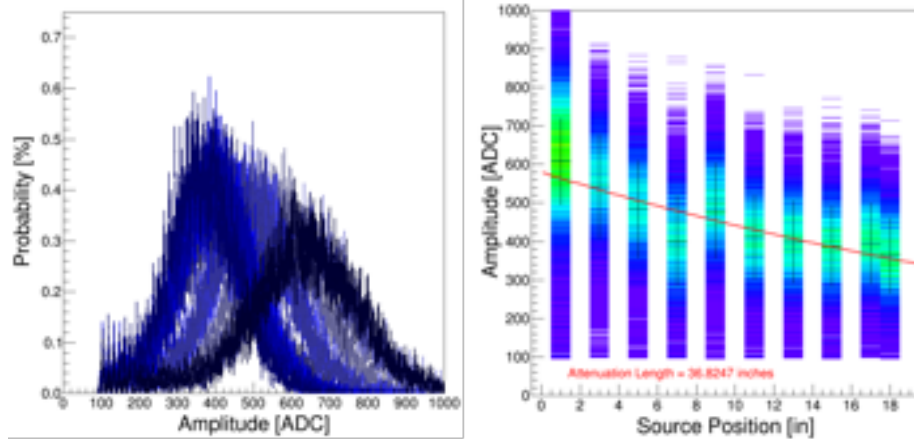


Figure 4.3: Left: Stacked waveforms for 11 positions of the α source along the bar. Right: The results of fitting a single exponential to the measurements on the left. The attenuation length is ~ 37 inches.

`fig:waveforms-`

of several light guide technologies under uniform conditions. In order to correct these comparisons for systematic effects, we constructed a Monte Carlo simulation of the experiment. First we made a model of the light guides; then we put this model into a full simulation of the TallBo dewar; finally, we tracked scintillation photons generated by cosmic muons to the light guides, into the light guides, and then down the light guides to the SiPMs.

The light guides were modeled as 20-inch acrylic bars with waveshifter embedded in their surfaces that convert 128 nm photons from LAr scintillation light to 430 nm light in the bar. The simulation then propagates the optical photons to the SiPMs at the end of the bar. The left side of Figure 4.4. shows the results of one such simulation in which the waveshifted light has been separated into the fraction of the total that propagates directly to the SiPMs and the fraction that is internally reflected to the SiPMs. Near the SiPM a significant fraction of the light propagates directly to the photodetectors. After 5-10 cm, the light comes mostly from internally reflected light.

The TallBo simulation was designed to answer two basic questions. The first of these questions is the way in which reflected light from the stainless steel walls Figure 4.5 affects the measurements. The results of that study are shown in the right side of Figure 4.4. Both the geometric corrections (black circles) and the corrections due to reflections (red circles) have been applied to the data. The results of the comparisons for 11 light guides made with 8 different technologies, including the

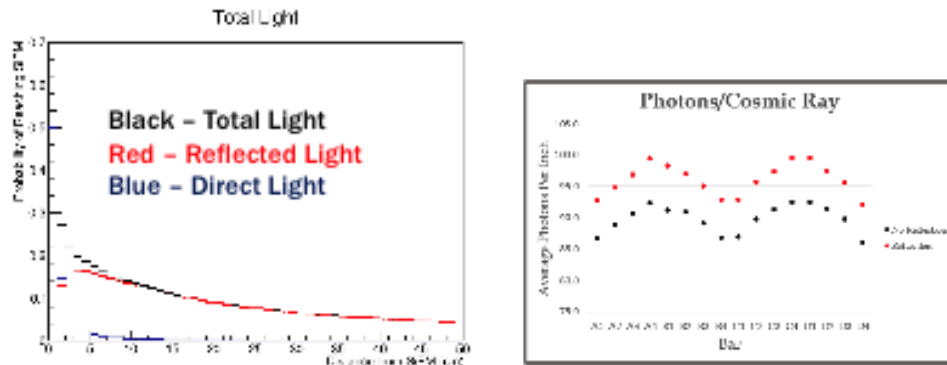


Figure 4.4: Left: Monte Carlo simulations of the 420 nm light seen by the SiPMs as a function of distance along the bar. Right: Increase in the light due to reflections in the TallBo dewar for the different light guide technologies.

`fig:mc-sim-and-tallbo`

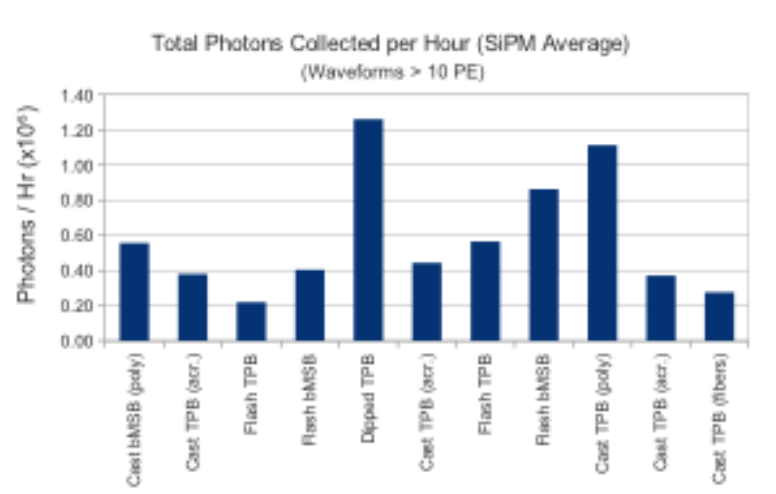


Figure 4.5: Comparison of several light guide technologies including the CSU fiber technology in the TallBo dewar. The corrections for systematics in Figure 4.4 (right) have been applied.

`fig:mc-sim-and-tallbo`

`fig:total-phot`

¹ prototype fiber light guide from CSU, during the February-March 2014 TallBo run
² are shown in Fig. 7. What seems to be clear from Fig. 7 is that the dipped tech-
³ nology pioneered by the MIT group has a better response than the flash heated bars
⁴ manufactured by the technology developed at IU. After these results were obtained
⁵ we have moved away from the flash heated technology and invested our R&D efforts
⁶ into our development of the dipping technology. These results have also motivated
⁷ the CSU group to modify their fiber design and produce a substantially improved
⁸ prototype fiber light guide.

¹ Chapter 5

² Installation and Commissioning

ch:install

³ 5.1 Introduction

⁴ This chapter discusses the LAr-FD Installation and Commissioning system's activities and responsibilities. LAr-FD construction and installation will occur in a series of distinct phases:

- ⁷ • installation planning and prototyping
- ⁸ • surface storage identification and operation
- ⁹ • excavation and outfitting of the cavern; this activity is the responsibility of the Conventional Facilities subproject (CF),
- ¹⁰ • construction and installation of the cryogenics system and cryostats by a construction management firm; this activity is the responsibility of the cryogenics system
- ¹¹ • construction of LAr-FD components at collaborating institutions and shipment to the Far Site
- ¹² • installation of detector components and installation management
- ¹³ • commissioning activities leading to CD-4

¹⁸ The Installation and Commissioning system will accept responsibility for the LAr-FD cavern, associated tunnels, infrastructure and above-ground facilities from Conventional Facilities upon completion of the Conventional Facilities contract. The cavern will be outfitted with the following utilities upon receipt of beneficial occupancy:

- 1 • ventilation in accordance with OSHA standards
- 2 • electrical power sufficient for the HVAC, cryogenics plant cooling and general
- 3 110-V service
- 4 • quiet power for the electronics with a double Faraday-shielded transformer lo-
- 5 cated some distance from the cavern to take advantage of the inductance of the
- 6 power lines. The primary shield will be connected to the main substation via
- 7 a grounded feed wire and the secondary shield will be connected to the Ufer
- 8 ground.
- 9 • communications consisting of telephone lines and computer network
- 10 • cavern lighting in accordance with OSHA regulations for industrial use
- 11 • tunnel lighting with battery-powered backup or emergency circuit backup
- 12 • environmental monitoring of oxygen, carbon monoxide, smoke and temperature
- 13 • dual isolation bulkheads separating the cavern from the existing Far-Site facility
- 14 • sump pumps for groundwater removal

15 After beneficial occupancy of the completed cavern from the CF subproject, the
16 cavern ventilation system will be tested to assure adequate performance with regard
17 to ODH requirements. The system will be tested with oxygen monitors distributed
18 around the cavern and a controlled argon spill. Remedial action will be taken if
19 required during cryostat and cryogenics construction.

20 The cryostat and cryogenics contractor will retain responsibility for the site during
21 construction of the cryostat and cryogenics system. The Cryostat and Cryogenics
22 System group will provide oversight during this phase. Upon completion of this
23 contract, the facility will be in the following state:

- 24 • the LN₂ refrigeration system will be constructed and commissioned with liquid
- 25 nitrogen
- 26 • the LAr systems and cryostats will be constructed and tested without the
- 27 introduction of cryogens
- 28 • the access hatches on the cryostat and the cryostat feedthroughs will be tem-
- 29 porarily sealed

- 1 • the APA- and CPA-installation support beams will be in place
- 2 • the cryostat will be connected to the steel roof structure thus connecting the
- 3 detector ground to the Ufer ground
- 4 The detector will utilize the cryostat pit rock bolts as part of the grounding
- 5 scheme. The rock bolts in the pit will extend through the shotcrete that lines the
- 6 cavern and be attached to the reinforcing steel network within the cryostat concrete
- 7 liner, forming an Ufer ground. The reinforcing steel will be connected to the steel
- 8 truss cover. The Ufer ground will be connected to the detector ground (the cryostat
- 9 SS liner) through a low-impedance connection.
- 10 The Installation and Commissioning group will be responsible for all LAr-FD-
- 11 related activities at the Far Site from this point in time until the end of the LAr-FD
- 12 project. Close coordination is clearly required between this group, system groups
- 13 that provide components and other Far Site construction activities.
- 14 On-project commissioning activities include the coordination of system-checkout
- 15 activities, culminating in the approval to introduce LAr into the detector modules,
- 16 and managing the steps required to meet the CD-4 goals.

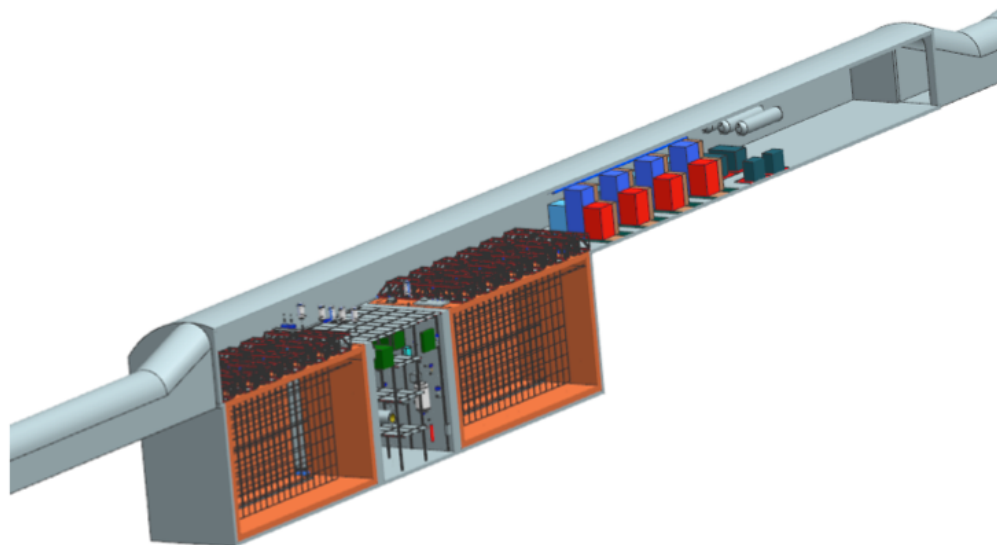


Figure 5.1: Cutaway view of two cryostats with TPC detectors installed

fig:tpc-in-two

5.2 Above-ground Pre-Installation

Editor's Note: The number of shipping containers listed in this section may not be accurate as of January 2015.

²

³ Detector components will be delivered to the Far Site over a period of many
⁴ months and will need to be stored in a surface-storage facility. This will allow
⁵ the supply of material to be maintained ready for installation. A facility for this
⁶ purpose will be identified and an agreement will be made for its use during LAr-FD
⁷ construction.

⁸ The initial surface-storage plan actually includes three facilities: a 4,000 ft² ware-
⁹ house structure for material receiving and unpacking, an on-site hardstand for storage
¹⁰ of a small number of cargo containers and an off-site hardstand area for the stor-
¹¹ age of a larger number of cargo containers. Material will be transferred from these
¹² areas to the cavern for installation, as required. Each system group is responsible
¹³ for delivery of its components to the local storage at the Far Site or to the off-site
¹⁴ location. The Installation and Commissioning group will provide the management
¹⁵ and labor resources for inventory control, material handling and transport from the
¹⁶ off-site and on-site storage facilities to the cavern.

5.2.1 Cryostat Materials

¹⁷ The on-site warehouse storage space will initially be made available to the cryogen-
¹⁸ ics system contractor who will construct the cryostats. The cryostat insulation will
¹⁹ comprise the largest bulk of material; approximately 2,500 m³. Figure 5.2 shows
²⁰ ^{Fig:gtt storage} membrane-cryostat components staged in the hull of an LNG tanker under con-
²¹ struction. Cryostat materials will come from overseas in approximately 100 shipping
²² containers that will be stored off-site. The containers will be brought to the shaft
²³ headframe building for unloading and transportation down the shaft.
²⁴

²⁵ Control of the storage area will revert to the Installation and Commissioning
²⁶ group when the cryostat-construction contract is completed.

5.2.2 TPC Materials

²⁷ APAs and CPAs, referred to as “TPC panels” in this chapter, will be constructed
²⁸ before arrival at the Far Site. The electronics will already be installed and the cold-
²⁹ testing performed. They will be shipped in sealed shipping containers to either the
³⁰



LBNE Conceptual Design Report
Figure 5.2: Membrane cryostat components staged in a LNG transport ship under construction.

fig:gtt_storage

1 on- or off-site hardstand area, depending on the TPC production rate. No significant
2 preparation or extensive testing of these components is required after arrival and
3 prior to installation. The entire set of TPC panels for the two-cryostat detector will
4 require approximately fifty shipping containers. Figure 5.3 shows a group of TPC
5 panels in a shipping container.

6 Whereas general material will be lowered in a lift cage, the TPC panels are too
7 long to fit in the lift cage and require special containers and special handling. The
8 TPC panels, grouped in their enclosed, special containers, will be lowered down the
9 Yates shaft since its lift has provisions to attach long objects to the bottom of the
10 cage. They will descend the shaft in a vertical orientation (the same orientation as
11 they will be installed), be rotated to a horizontal orientation, then moved along the
12 access drift on a cart or rail to the cavern. Figure 5.4 shows a TPC container exiting
13 at the bottom of the shaft. The TPC panels may be transported to the Far Site in
14 these special containers or transferred to them after arrival.

15 TPC-panel containers will be transported to the cavern and unloaded every few
16 days to supply the TPC components for installation. These containers may need to
17 be moved during off-work hours to avoid conflicts with other users of the shaft lifts.
18 TPC-panel containers may be stored in the cavern on the deck on top of the cryostat
19 trusses. Enough parts will be stored in the cavern to ensure that a sufficient supply
20 of TPC parts is always on hand for installation.

21 **5.2.3 Liquid Argon Receipt**

22 Delivery of LAr will occur over a one-year period for each cryostat, with approxi-
23 mately six tank trucks arriving on site per day. Each tank truck will have been
24 loaded with 18.8 tons of LAr which will be purity-tested by the vendor before the
25 truck departs. Minor losses of LAr will occur during shipment. The purity will be
26 checked again during unloading. If the impurities are found to exceed the required
27 specification, the partially emptied tank truck will be returned to the vendor.

28 LAr will be transferred to a buffer-storage vessel that allows the tank truck to
29 unload as quickly as possible. Under normal circumstances transfer of the LAr out of
30 each tank truck will require 1 hour, including the time for making hose connections
31 and purging the hoses. The storage vessel will deliver argon to the filtering loop that
32 processes argon from the cryostat recirculation and condensing loops.

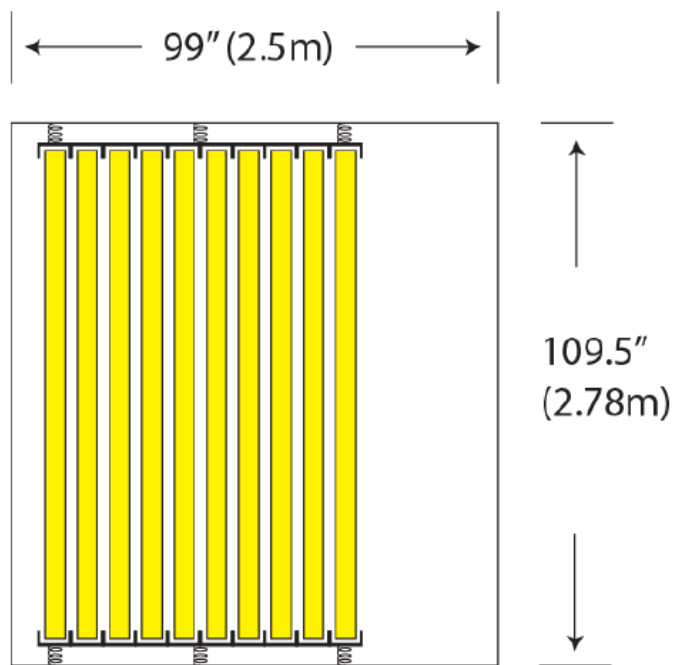


Figure 5.3: Concept for APA shipping containers - cross section view

LBNE Conceptual Design Report

fig:apa_ship

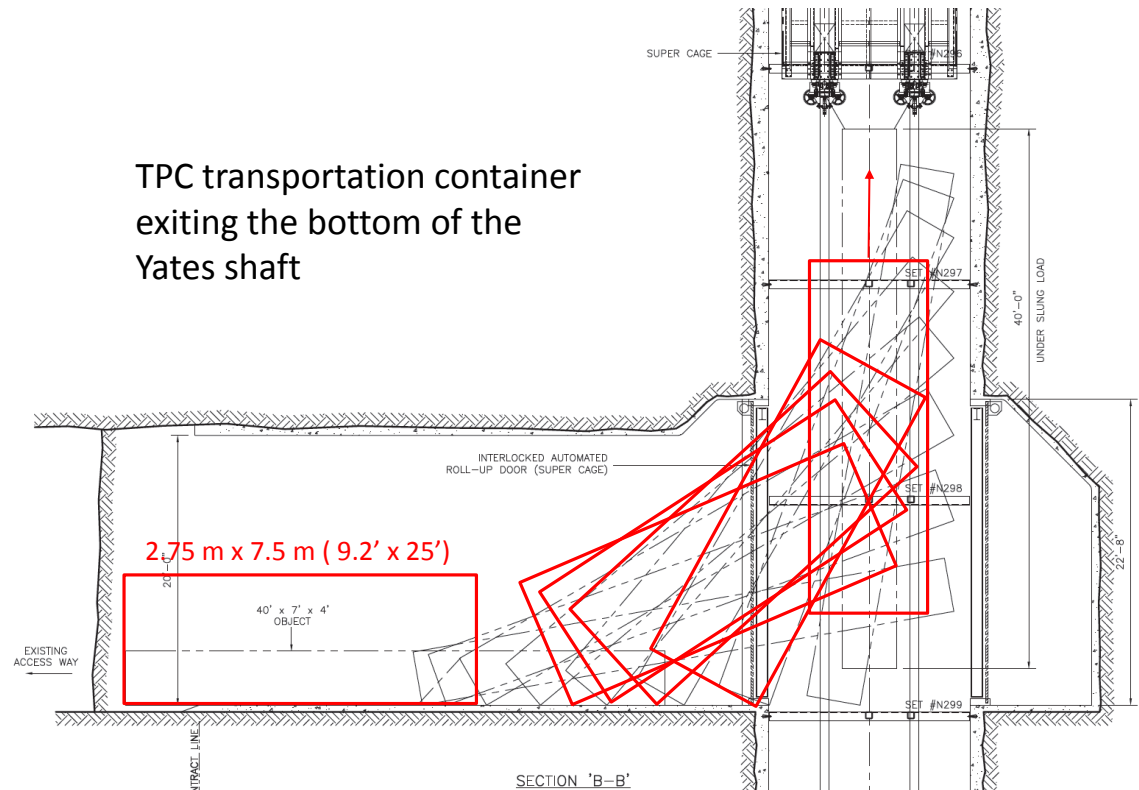


Figure 5.4: TPC-panel containers exiting the Yates shaft

fig:install-yates

5.3 Below-ground Pre-Installation

The below-ground pre-installation activities must be completed prior to the start of TPC installation into the cryostat. These activities include design, procurement and installation of detector-specific infrastructure such as man-lifts, lifting fixtures, catwalks, ladders, tools, and so on. The major items include the support rails for the TPC panels, the lower staging platform for joining two panels, installation monorails for moving the panels inside and outside of the cryostat, and a mobile scaffold for providing access to the top and middle of stacked TPC panels.

5.3.1 Equipment Required for Detector Installation

Several items will be installed for use during TPC installation, and removed afterwards.

- A temporary lighting system inside the cryostat with emergency backup lighting for TPC installation
- A ventilation system and air-monitoring sensors with alarms connected to the cryostat to assure adequate air quality for the personnel working inside the cryostat. The system will also include a high-sensitivity smoke-detection system that is interlocked to the power for all devices inside the cryostat.
- A raised-panel floor to protect the cryostat floor; see Figure 5.5. The raised-panel floor will have support spacers located between the convolutions in the stainless-steel primary membrane to provide a flat surface for moving equipment around within the cryostat. The pressure limit for the insulation in the floor is 0.5 MPa and the load of the vacuum that will be used to monitor leakage during installation reduces the effective limit to 0.4 MPa. The stock round spacers in the raised-panel floor are 10-cm diameter and would support a load of 310 kg. The load can be increased by adding larger-diameter plates under the standard spacers.
- A transfer rail with motorized trolleys to move TPC panels within the cryostat

5.3.2 Clean Area

A clean-area vestibule in the range of class 10,000 (ISO 7 equivalent) will be constructed in the septum area around the entrance to the cryostat to keep the area



Figure 5.5: Raised-panel floor to protect the cryostat's primary membrane

fig:raised_flo

1 around the open hatch isolated from the drift access. The vestibule will have an area
2 for personnel to gown with the appropriate clean-room clothing and safety shoes.
3 A large, closable door, next to which the TPC-storage containers can be parked,
4 will allow unloading of the TPC components directly from the container into the
5 vestibule.

6 A crane that operates inside the clean-room vestibule enclosure will be used to
7 transfer TPC panels from the vestibule into the cryostat. The crane will have a clean-
8 room-style hoist and trolley to prevent contamination of the cryostat or vestibule
9 area.

10 The Double Chooz detector developed a cleanliness plan to ensure that dust con-
11 tamination did not contribute more than a specified amount to the detector signal.
12 Measurements were made of the activity of rock in the underground laboratory which
13 was assumed to be the source of airborne dust. Maximum allowable dust concentra-
14 tions and the clean-room class and cleanliness practices were determined such as to
15 meet the requirements for contamination. The cavern for LAr-FD and many of the
16 access tunnels will involve new excavation with shotcrete covering the native rock.
17 The Installation and Commissioning group will need to evaluate the dust sources in
18 the LAr-FD cavern and determine if a similar approach to setting the clean room
19 requirements is appropriate.

20 **5.3.3 Rails for TPC-Panel Support and Transfer**

21 A set of five support rails, shown in Figures 5.11 and 5.6, permanently mounted in
22 each cryostat, will provide the support for the APA and CPA panels and a track for
23 moving the panels into position. Rods spaced at 5-m intervals will support the rails.
24 The rods will be hung from anchor points mounted in the top of the cryostat. The
25 rods will be adjustable to enable level installation of the rails, which will be done
26 in rail segments with the aid of a laser level. The rails shrink approximately 7 cm
27 along their entire length during cool-down. The rods will be installed with an angle
28 bias that allows the rails to return to level after the cryostat and TPC is cooled.

29 The mass of each stacked set of APA panels is 600 kg and the mass of each
30 stacked set of CPA panels is 250 kg. The load of the TPC on the support rails comes
31 to 200 kg/m for the APA rails and 100 kg/m for the CPA rails. The rail segments
32 will be constructed from 20-cm-deep laser-welded, W-shaped, stainless-steel beams.
33 The rail segments will be joined end-to-end with large pin connections. The upper
34 support rods will be made from 15-mm-diameter stainless steel.

35 The rail installation can be completed most efficiently while the large scaffolding
36 system used for cryostat construction is still in place, therefore it will be part of the

- ¹ cryostat-construction contract.

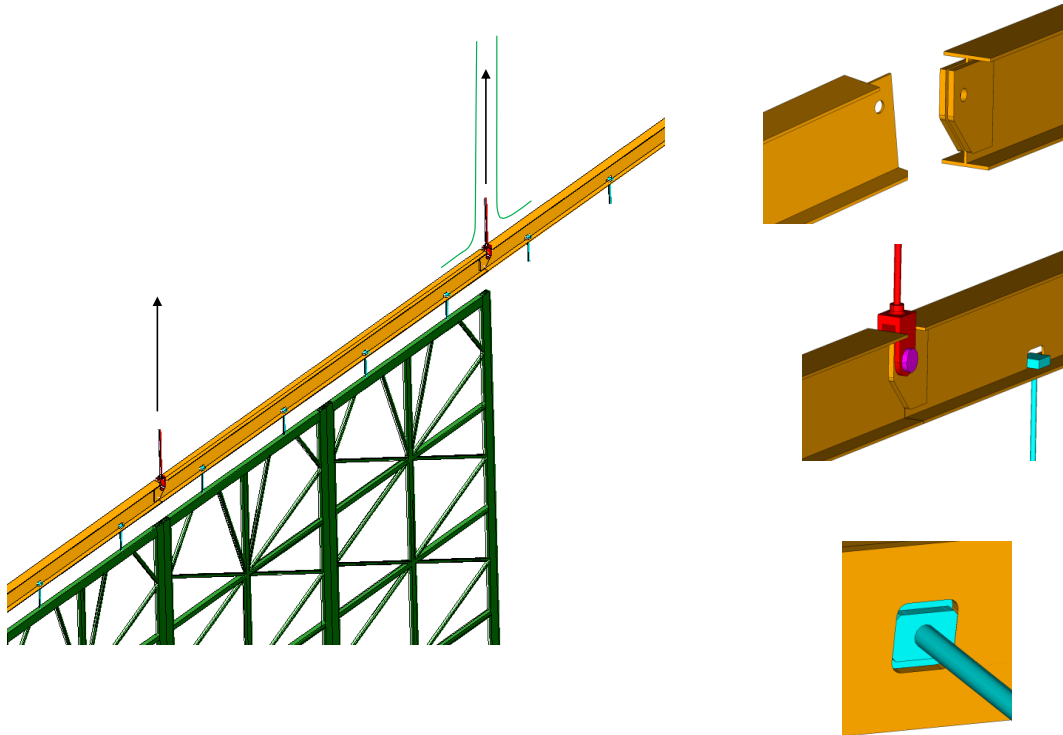


Figure 5.6: Support rails inside cryostat

fig:support-r...

- ² Signal and power cables will be installed from the cryostat feedthrough ports next
³ to the APA support rods, shown in Figure 5.7, along the rails to the point where
⁴ the connection to the APAs will be made. The cables will be preplaced and tested
⁵ before APA installation begins.

⁶ Editor's Note: Figure 5.7 is for a 17-kton fiducial mass cryostat. The
⁷ 5-kton cryostat is shorter and has fewer rows.

- ⁸ The top and bottom TPC panels of a stacked pair will be moved into the cryostat
⁹ separately, then connected together below the cryostat equipment hatch. The lower

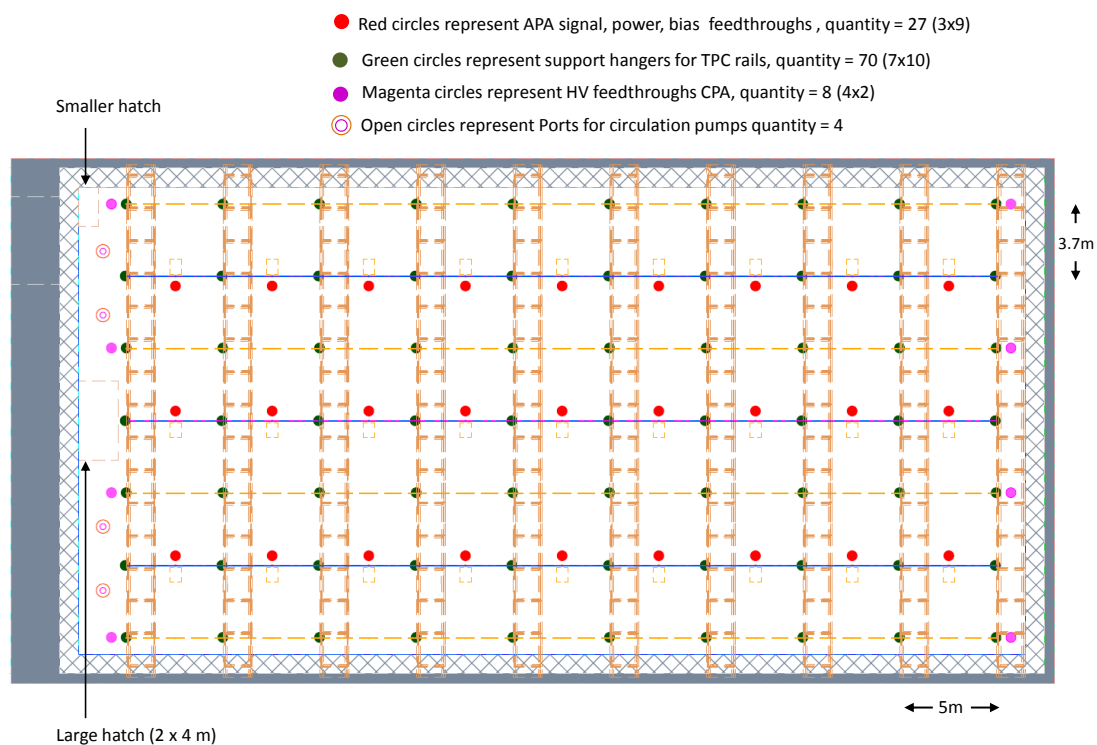


Figure 5.7: Feedthroughs

fig:feedthrough

- 1 panel is held temporarily with a staging platform while the upper panel is connected.
2 After connection, a motorized trolley will move the stacked panels from the hatch
3 area to the final position. Since the duty cycle of the trolley is rather low, the trolley
4 could be battery-powered to avoid the need for cable festooning. The trolley initially
5 moves along a transfer rail until it reaches the end where the stacked panel will be
6 permanently mounted. An arrangement of transfer switches is used to connect the
7 transfer rail to the final support rail. See Figure 5.8 for an example of a transfer rail.

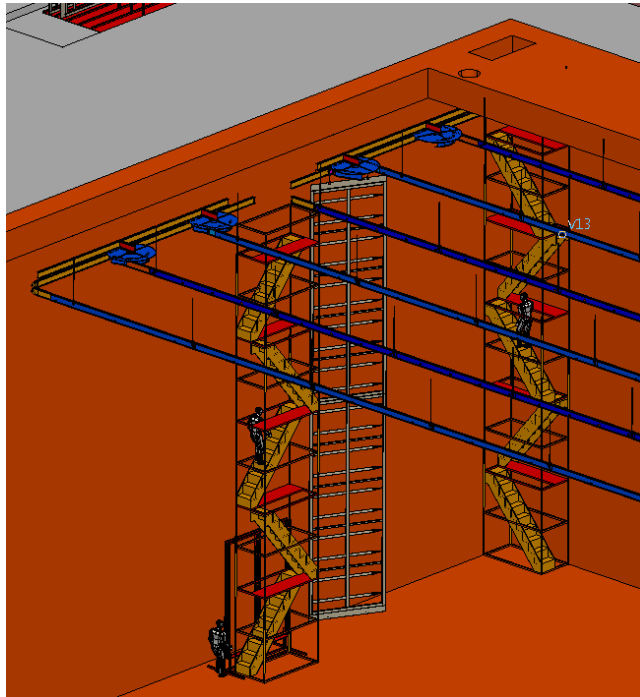


Figure 5.8: TPC installation monorail with APA moving to support rail

fig:installati

- 8 A rolling scaffold with an integral stair tower will allow personnel to access the
9 top of the stacked panel. Fixed scaffolds with stair towers will provide access into
10 the cryostat.

5.3.4 Detector Electrical Ground

The LAr-FD will have nearly a quarter million channels of electronics with an intrinsic noise level of less than 1,000 electrons. These channels will be connected to wires that are seven meters long. Thus, grounding, shielding and power distribution are critical to the success of the experiment. In the reference design the entire cavern will be treated as the detector ground for the following reasons.

The cryostat has a large number of penetrations for supporting the APAs that extend to the support structure above the cryostat. There are also 13 signal feedthrough ports which connect to racks located on the top of the cryostat. Achieving and maintaining adequate AC isolation on such a large structure during construction will be difficult. In addition, the cavern has very few connections to the outside world so it is much easier to isolate the cavern as a whole than the individual pieces.

Secondly, it is necessary to provide a conductive body with a large enough self-capacitance that its voltage changes only negligibly when electric charge flows onto it. In this way the cavern can serve as a sink of unwanted current without generating noise in the detector.

Reference Design

Earth ground will be provided by the Ufer grounding system in the concrete walls and other concrete support structures. This ground will be attached to the rock bolts in the cavern walls and augmented by the large amount of steel in the roof-support trusses and the upper metal floor. To be an effective ground, all of the steel support structure will be welded together. The welds need not be structural; their use is only to assure reliable long-term electrical connections.

In order for this system to work, the cavern must be kept noise-free, i.e., all connections, except AC power, between the cavern and the outside world must be electrically isolated either by dielectric breaks or optical isolators. Electric motors will be restricted to three-phase induction motors except for special, well-controlled cases. Electric heaters will be controlled by switches rather than SCRs. Digital equipment such as network switches will be run at frequencies of 30 MHz or higher whenever possible so that the noise remains outside the bandwidth of the TPC preamplifier. Some equipment, such as switching power supplies, will still need special attention to ensure that they do not generate noise in the detector.

As the only conducting link to the outside world, the AC power must be filtered to eliminate any electrical noise. Since the currents are large, it is most economical to implement a filter using the inductance of the power cable itself along with some capacitors to form a capacitor-inductor filter.

1 The reference design will keep the power for the conventional facilities and for
2 each cryostat independent of one another so that they can be operated independently.
3 As shown in Figure 5.9 (top), one 500-KVA transformer for each cryostat along with
4 a one-MVA transformer for the conventional facilities will be placed in a separate
5 utility room located a short distance from the detector cavern. These transformers
6 will have double faraday shielding with the primary shield returned on the ground
7 wire to the substation. The second shield will be connected to the local Ufer ground
8 and to the cavern by the required grounding wire.

9 A saturable inductor between the two shields serves to isolate the primary and
10 secondary shields and separate their grounds. The secondary shield and transformer
11 frame are connected to Earth ground at the transformer. The ground wire running
12 back to the substation is only locally grounded through the saturable inductor but
13 it is fully grounded at the substation. A fault between the secondary and primary
14 shields would trip the substation breaker due to current flowing in the return ground
15 wire. If this wire were disconnected, the current would flow through the saturable
16 inductor to Earth ground and also trip the substation breaker. Figure 5.9 (bottom)
17 shows an inductor used at D-Zero and the voltage developed across the inductor as a
18 function of the fault current. The inductance is completely saturated by 100 A and
19 the developed voltage is still safe.

20 The 480-V power will be transmitted from the utility room to a separate switch
21 gear for each detector module. The switch gear, located adjacent to its module,
22 will directly distribute power to all the 480-V loads. The switch gear will also feed
23 up to three 50-KVA single-faraday-shielded transformers. Two of these will provide
24 208-V power to the module and its associated cryogenic equipment, and the third
25 will provide additional cavern power. The number and size of the transformers may
26 change depending on the final load.

27 The filter on the conventional-facilities transformer will be similar to the one for
28 the detector modules. In addition to the conventional facilities, this transformer will
29 power all welding outlets. This arrangement would allow some minor welding on one
30 cryostat, if needed, while the other is taking data.

31 **Features**

32 It is important that all the components inside each detector module be connected to
33 a common ground. The best candidate for this common ground, and the one chosen
34 for the reference design, is the top of the cryostat. The APAs will have ground
35 braid connections to the roof at two points on each panel. The lower APAs will be
36 connected to the upper ones by their mechanical mounting connections. The front-

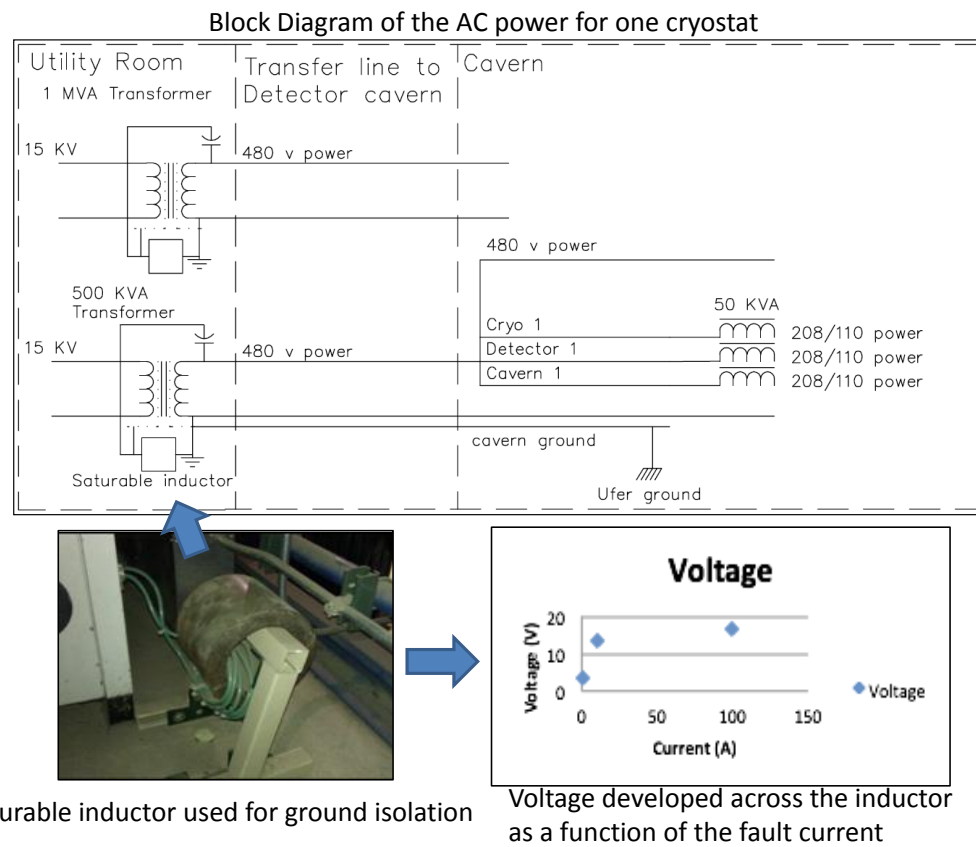


Figure 5.9: Block diagram of the AC power for one cryostat with a saturable inductor to separate the grounds of the transformer shields

fig:Saturable_

1 end boards, phototube ground and the reference ground for the bias voltages will all
2 be connected to the APA frame.

3 The top of each cryostat is made of 1.2-mm or 2.0-mm-thick stainless steel, a
4 poor conductor, and therefore does not serve as an adequate ground plane. The best
5 solution would be to add a copper sheet directly on top of the cryostat, however
6 this is difficult to do. Instead the copper sheet will be installed over the insulation
7 that is on top of the cryostat membrane, about one meter from the cryostat, and
8 connected to it via a grid of connections spaced 2.5 m apart. This spacing will give
9 good electrical performance up to 12 MHz – well above the input bandwidth of the
10 amplifier. The connections will be made with copper strips that fit in gaps in the
11 insulation. Power supplies and power-supply filters (including the cathode supply)
12 will all be grounded to this plane.

13 A port is located above every other APA junction and each port will serve the
14 four APAs located directly underneath it. Cables for the bottom two APAs will
15 be routed through the hollow cable frames to provide both mechanical support and
16 electrical shielding. The digital cables will be located in the left frame member,
17 and the power and bias lines will be routed through the right frame member. The
18 horizontal portion of the cable run will be outside of the wire planes, so the use of
19 doubly shielded cable such as Amphenol skew clear may be adequate. If not, then
20 custom metal shields will be mounted on the front-end circuit boards.

21 The racks will be mounted either directly over the ports or adjacent to them with
22 an extension to the rack that covers the port. All cables can be brought out of the
23 cryostat into a grounded and shielded enclosure. All cables to the APAs will be the
24 same electrical length to ensure uniformity of signal travel time. This will require
25 storing an extra 14 meters of cable for each top APA. The plan is to use 36-in-deep
26 racks and construct a shielded area on the back side of the rack to hold the excess
27 cable. Twenty-seven racks will be required for each cryostat, and rack space will be
28 shared between the TPC and photon-detection system readout and power supplies.
29 A modest number of racks will be required for the DAQ in the surface control room.
30 All relay racks will be equipped with rack protection and monitoring. The racks will
31 be supplied by the detector installation effort.

32 The digital electronics does not present a grounding issue in the strict sense, but
33 it does affect noise. The plan is to operate the digital system with at least a 32-MHz
34 clock that is well above the upper bandwidth of the input amplifier (the 3-db point
35 is less than 1 MHz).

5.4 Below-ground Installation Activities

- The following list of detector components and systems will be installed below-ground:
- Relay Racks with rack protection (10 on each cryostat plus a few in the control room)
 - Cable trays and power distribution to racks
 - Cable inside and outside of the cryostat including cable feedthroughs
 - DAQ crates and power supplies in the relay racks
 - The 52 APAs per cryostat with integrated photon detectors
 - The 78 CPAs per cryostat
 - Any cryogenic instrumentation not installed by the cryostat construction vendor (e.g. purity monitors)
 - Note: Support rails and hangers are installed during cryostat construction

5.5 TPC Installation

Each APA and CPA panel will be carefully tested after transport into the clean area at the septum and before installation into one of the cryostats. Immediately after a panel is installed it will be rechecked. Throughout the installation period it will be checked periodically. The serial stacking of the APA and CPA panels along the rails means that removing and replacing one of the early panels in the row after several others are installed would be very costly in effort and time. Therefore, to minimize the risk of damage, as much work around already-installed panels as possible will be completed before proceeding with further panels.

The installation sequence is planned to proceed as follows:

1. Install the monorail or crane in the staging area outside the cryostat, near the equipment hatch.
2. Install the relay racks on the top of the cryostat and load with the DAQ and power-supply crates.

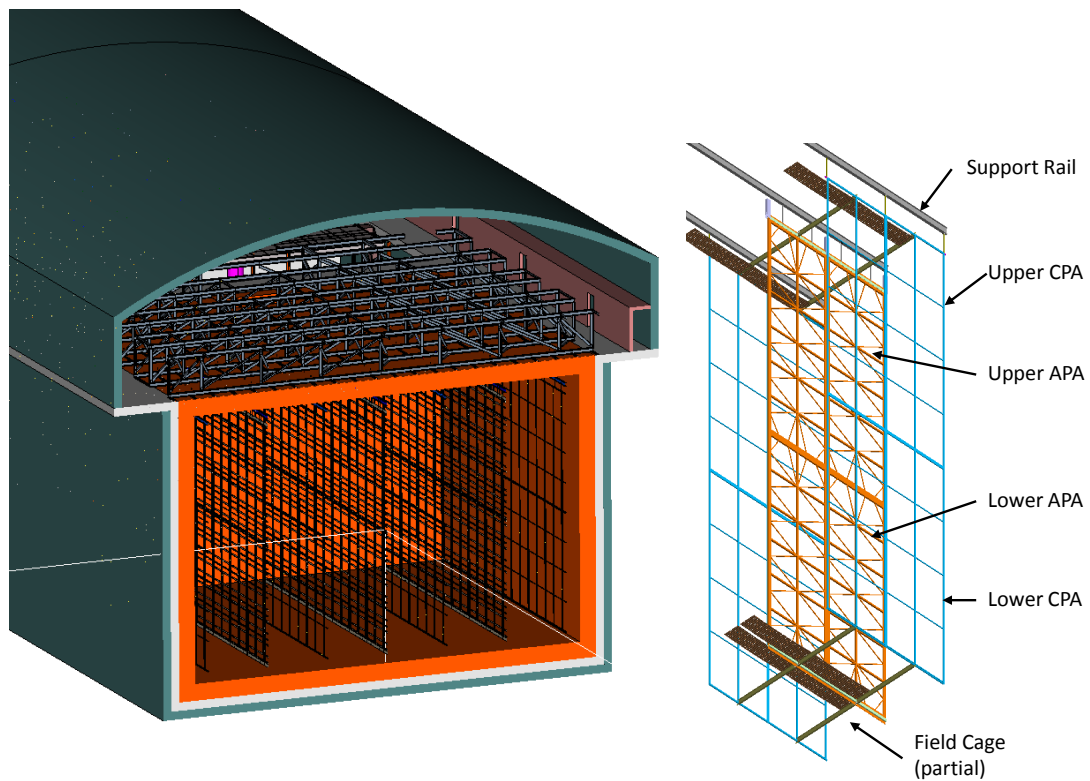


Figure 5.10: TPC panels installed in cryostat

fig:tpc-panels

- 1 3. Dress cables from the DAQ on the top of the cryostat to remote racks.
- 2 4. Construct the clean-room vestibule outside the cryostat hatch.
- 3 5. Install the raised-panel floor inside the cryostat.
- 4 6. Insert and assemble the stair tower and mobile scaffold.
- 5 7. Install the transfer rail with switches and the staging platform inside the cryo-
- 6 stat
- 7 8. Install protection on (or remove) existing cryogenics instrumentation in the
- 8 cryostat.
- 9 9. Install the cryostat feedthroughs and dress cables inside the cryostat along the
- 10 support beams.
- 11 10. Begin regular transport of TPC panels in shipping boxes into the cavern.
- 12 11. Install TPC panels panels:
 - 13 (a) Install a connected APA-CPA panel pair.
 - 14 (b) Connect power and signal cables.
 - 15 (c) Test each APA wire for expected electronics noise. Spot-check electronics
 - 16 noise while cryogenics equipment is operating.
 - 17 (d) Connect field cage in sections as the APA and CPA installation progresses.
 - 18 (e) Perform electrical test on CPAs and field cage.
 - 19 (f) Remove temporary floor sections as the TPC installation progresses.
 - 20 (g) Install sections of argon-distribution piping as the TPC installation pro-
 - 21 gresses.
- 22 12. Complete the field cage.
- 23 13. Remove the transfer rail, staging platform, moving platform and stair tower.
- 24 14. Temporarily seal the cryostat and test all channels for expected electronics
- 25 noise.
- 26 15. Seal the access hatch.
- 27 16. Perform final test of all channels for expected electronics noise.

1 In general, APA and CPA panels will be installed in order starting with the panel
2 furthest from the hatch side of the cryostat and progressing back towards the hatch.
3 The field cage will be installed in stages as the installation of APA and CPA panels
4 progresses. The only requirement for survey or alignment is to maintain the edges of
5 a row of APA panels to 3-mm alignment along each beam. A laser guide or optical
6 transit in combination with the adjustment features of the tie rods will be used to
7 establish the alignment. After the stacked panel is attached to the support rods the
8 electrical connections will be made to cables that were already dressed to the support
9 beams and electrical testing will begin. Periodic electrical testing will continue to
10 assure that nothing gets damaged during the additional work around the installed
11 panel.

12 The TPC installation will be performed in three stages, each in a separate location;
13 the locations, or zones, are shown in Figure 5.11. First, in the clean room
14 vestibule, a crew will move the APA and CPA panels from storage racks, rotate
15 to the vertical position and move them into the cryostat. Secondly, in the panel-
16 staging area immediately below the equipment hatch of the cryostat, a second crew
17 will transfer the lower panels from the crane to the staging platform, connect the
18 upper and lower panels together, route cables to the top of stacked panels and fi-
19 nally transfer the stacked panels on to the monorail trolley that moves within the
20 cryostat. A third crew will reposition the movable scaffolding and use the scaffold to
21 make the mechanical and electrical connections at the top for each APA and CPA
22 as they are moved into position. The monorails inside and outside the cryostat will
23 each have two motorized trolleys so that work can be conducted by all three crews in
24 parallel. The steady-state rate for installation, given this work plan and a single-shift
25 schedule, is estimated to be two stacked panels per day.

26 Wire integrity will be confirmed by measuring the Equivalent Noise Charge (ENC)
27 of each electronics channel and comparing it with the expected noise for a properly
28 connected wire. A properly connected wire provides an input capacitance of 240 pF
29 to the front-end amplifier resulting in an ENC at room temperature of 1,100 elec-
30 trons. The wire-integrity test also ensures that coherent noise sources, e.g., a me-
31 chanical connection between the detector ground and the Ufer ground, are discovered
32 promptly. Error budgeting, regular noise monitoring and mitigation will ensure that
33 the TPC reaches and maintains the required noise performance before the cryostat
34 is cooled down.

35 The detector installation system is also responsible for developing and implement-
36 ing the procedure for monitoring the integrity of the membrane-cryostat primary liner
37 during installation. The space between the primary liner and the secondary liner will
38 be held under vacuum during installation. The vacuum level will be automatically

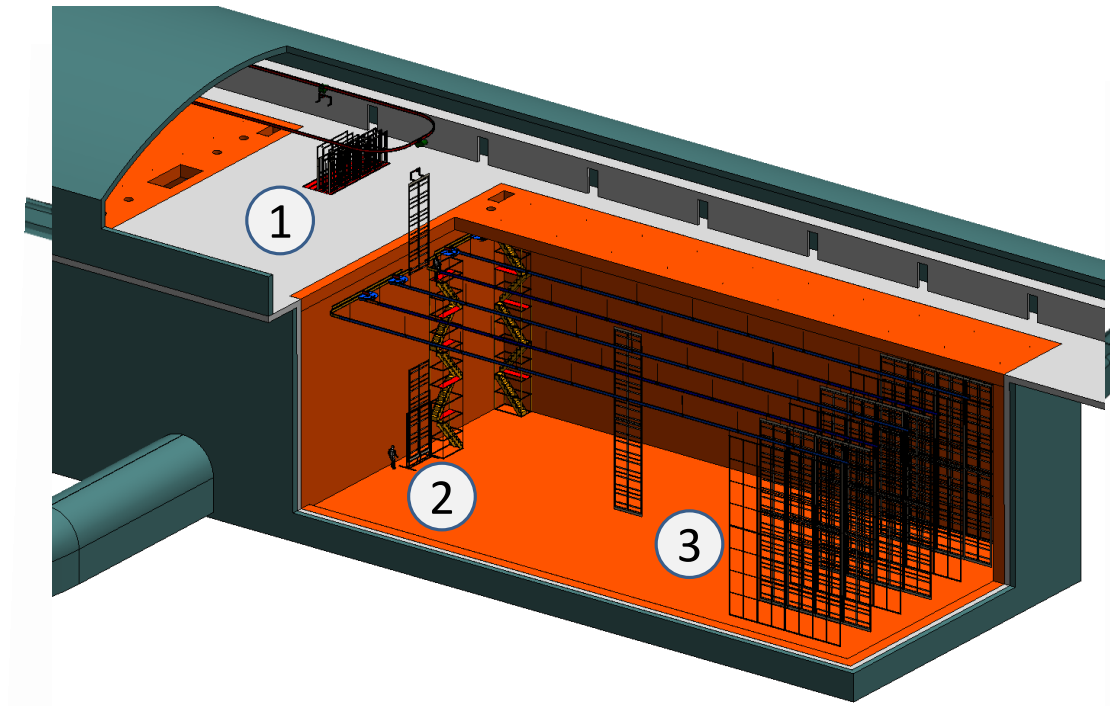


Figure 5.11: The three main work zones for TPC Installation. TPC components are lowered into the cryostat in zone 1. TPC components are connected together in zone 2, transferred to the support rails and then rolled into final position (zone 3).

fig:work-zones

- ¹ monitored and will alarm if any leaks develop in the primary membrane during TPC
² installation.

³ **5.6 Installation Prototype**

⁴ The goals of the installation prototype are to test and verify the key elements of
⁵ the equipment and process for TPC installation and to serve as a training tool for
⁶ personnel who will perform the TPC installation. The initial testing of the equipment
⁷ at Fermilab will be used to verify or refine the installation concepts. Complete testing
⁸ of the final equipment and operations will occur at Fermilab before the installation
⁹ equipment is moved to the Far Site.

¹⁰ For the installation prototype, a similar, 70%-height detector will be constructed
¹¹ in a suitable location at Fermilab, e.g. the Wideband lab or the CDF or DZero as-
¹² sembly hall. The cryostat mock-up will include a representation of a roof hatch,
¹³ APA and CPA rail supports and feedthroughs. Multiple mock-ups of APA and CPA
¹⁴ stacked panels will be installed. The APAs will include all mechanical mounting
¹⁵ points and electrical connections such as optical-fiber readout cables and power ca-
¹⁶ bles. Prototype versions of the special equipment required for TPC installation will
¹⁷ be used, including the lower panel staging platform, a transfer rail with trolley, and
¹⁸ rolling-cart scaffolding. Scaffolding elements will be rented and the scaffolding will
¹⁹ be erected by a contract or as part of a training program.

²⁰ Initial tests, where appropriate, will be performed at a low elevation. For example,
²¹ the installation trolley and single-switch rail segment will be tested at a low elevation
²² with a dummy weight. After successful demonstration of the features at low elevation,
²³ the components will be moved to a high elevation for testing with full size mock-up
²⁴ panels.

²⁵ **5.7 Training and Access Control**

²⁶ Installation and Commissioning will be responsible for the personnel, equipment and
²⁷ procedures for providing cavern-access controls. These controls will include a mech-
²⁸ anism for checking the training status of personnel, badge-in/badge-out procedures
²⁹ and closed-circuit-television monitoring of the entrance portal. Only trained person-
³⁰ nel will be allowed below-ground. Members of the installation crew will be trained
³¹ on specific installation tasks and must pass a qualification test. The training will
³² likely use mock-up APAs constructed for the installation prototype. The training

1 program will be modeled after the Fermilab “NuMI underground training” and will
2 be developed in collaboration with Sanford Laboratory ES&H personnel.

3 Installation and Commissioning will provide all of the general tools and equipment
4 needed to support the personnel in their installation work. It will include hand
5 tools, power tools, material-handling equipment, ladders, lifts, electrical meters and
6 personal protective equipment (PPE). The detector system groups will provide any
7 special equipment to check out or debug the power and read-out chain of the detectors.
8

9 **5.8 Detector Commissioning**

10 The construction of the two cryostats and the installation and commissioning activities
11 will be staged such that both TPCs can be tested cold while one cryostat
12 still remains available as a potential storage vessel. The LAr in one cryostat can be
13 transferred to the other, and back again, if necessary. Once both TPCs are known
14 to work properly at LAr temperature, the second fill will take place.

15 The commissioning sequence, illustrated in Figure 5.12, will start with the in-
16 stallation of the TPC in the east cryostat. During this time, construction of the
17 west cryostat will be completed. The east cryostat will be filled initially with room-
18 temperature GAr, injected from the bottom in order to displace the air upward
19 through the top ports. The procedure used for this gas purge will be developed during
20 prototype work. Following that, the LAr fill of the east cryostat will take four
21 to six months, assuming continuous LAr deliveries. LAr purification will begin when
22 the liquid level is high enough to start the recirculation pumps. The commissioning
23 of the cryogenics system can also begin at this point but its full commissioning will
24 require a fully loaded cryostat. When the cryostat is full, the TPC will undergo
25 testing for about one month. In-vessel purity monitors will operate during this time.

26 Construction of the west cryostat is expected to finish during the LAr fill of
27 the east cryostat. After the west cryostat is leak-checked and cleaned, its TPC
28 installation will begin. After TPC installation and testing, the purging and cooling
29 phases will proceed. Then the LAr from the east cryostat will be transferred to the
30 west one, at which point the west TPC will begin a month of testing. During this
31 time the east cryostat will be maintained cold via continuous GAr circulation. Once
32 tests on the west cryostat are completed successfully, the east cryostat will be refilled
33 with LAr, and its roughly five-month commissioning period begins.

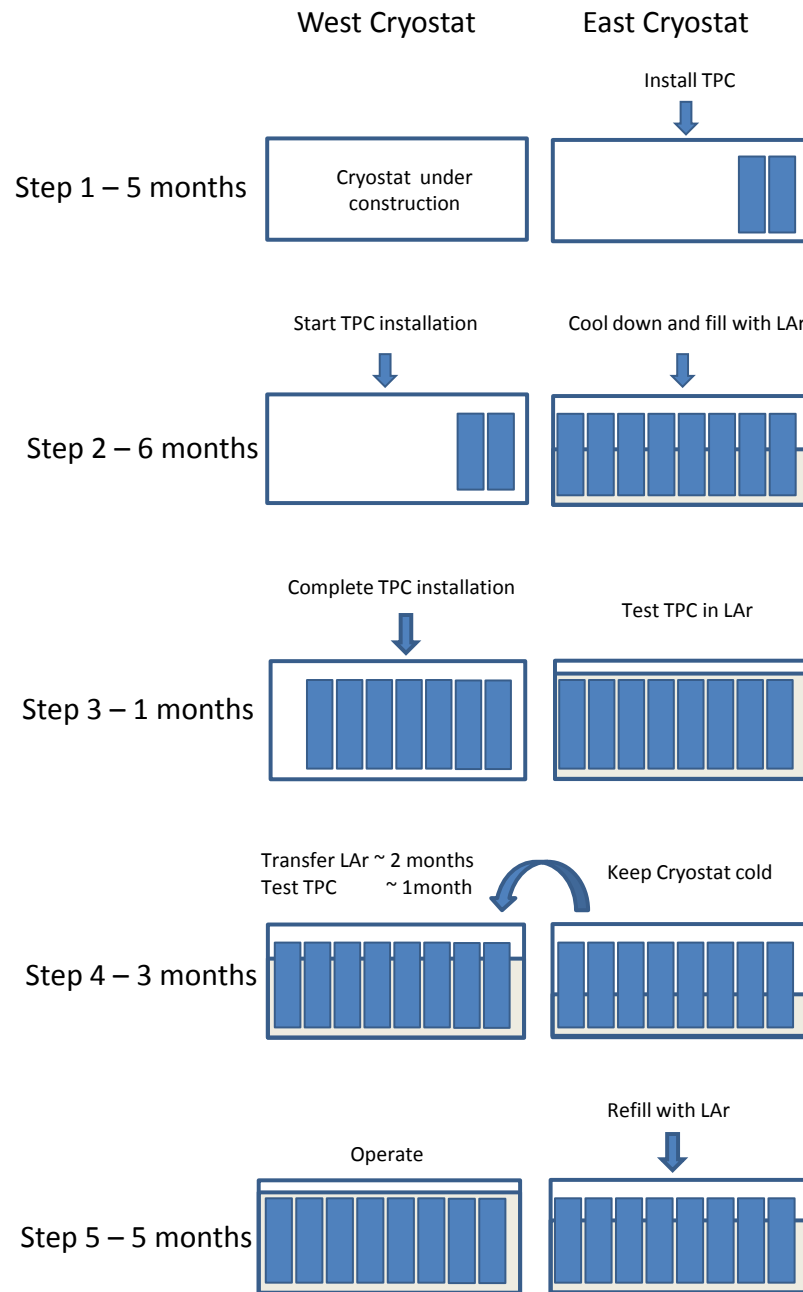


Figure 5.12: Startup and Commissioning Sequence

fig:startup_se

5.9 ES&H

- ² Careful consideration for ES&H will be demonstrated in the planning and execution
³ of the installation and commissioning. Safety professionals will be involved in all
⁴ phases. Hazards of note for the TPC installation are work at elevated heights and
⁵ working in the confined space of the cryostat.

¹ Chapter 6

² Detector Development Program

ch:randd

³ 6.1 Introduction

⁴ This chapter describes the development program designed to ensure a successful
⁵ and cost-effective construction and operation of the massive, dual-cryostat LArTPC
⁶ detector for LBNE and to investigate possibilities for enhancing the performance of
⁷ the detector. The feasibility of the LArTPC as a detector has been demonstrated
⁸ most impressively by the current state of the ICARUS experiment currently taking
⁹ data at Gran Sasso.

¹⁰ It is understood that for succesfull operation an LArTPC has stringent require-
¹¹ ments on

- ¹² • argon purity which must be of order 200 ppt O₂ equivalent or better
- ¹³ • long-term reliability of components located within the liquid argon; in partic-
¹⁴ ular, the TPC and field cage must be robust against wire-breakage and must
¹⁵ support a cool-down of over 200 K
- ¹⁶ • the front-end electronics which must achieve a noise level ENC of 1000e or
¹⁷ better

¹⁸ The design of the LBNE LArTPC has evolved significantly from earlier concepts
¹⁹ based on standard, above-ground, upright cylindrical LNG storage tanks which en-
²⁰ visioned single TPC sense and high-voltage planes spanning the full width of the
²¹ tank – essentially a direct scaling of previous detectors. Problems with the actual
²² construction of such massive planes and with the logistics of being able to construct
²³ the TPC only after the cryostat was complete are avoided in the present design. In
²⁴ our design, TPC ‘panels’ are fully assembled and tested – including the electronics –

1 independently of the cryostat construction. This modular approach is a key feature
2 of the design. It has the benefit not only of improving the logistics of detector con-
3 struction, but also the individual components can be of manageable size. It should
4 also be noted that the cryostat itself is formed of modular panels designed for quick
5 and convenient assembly.

6.2 Components of the Development Program

7 Programs of ongoing and planned development to allow the construction of massive
8 LArTPCs in the U.S. have been developed and described in the *Integrated Plan*
9 for LArTPC Neutrino Detectors in the US [?]. To advance the technology to the
10 detectors proposed for LBNE, the U.S. program has three aspects:

- 11 • a demonstration that the U.S program can reproduce the essential elements of
12 the existing technology of the ICARUS program
- 13 • a program of development on individual elements to improve the technology
14 and/or make it more cost-effective
- 15 • a program of development on how to apply the technology to a detector module

16 A summary of the items in the program is given in the following tables. Table
17 6.1 lists the activities that are part of the LBNE Project (“on-project”) described
18 in this chapter, a short description of the information needed and the LBNE mile-
19 stone corresponding to when the information is required. Table 6.2 lists off-project
20 activities, the aspect of these activities that is applicable to LAr-FD and the LBNE
21 milestone at which the information is required. These aspects will be described in
22 more detail in the following sections. As will be explained below, these are not R&D
23 activities, but rather elements of the preliminary engineering design process.

24 6.3 Scope and Status of Individual Components

25 6.3.1 Materials Test System

26 An area for LAr detector development, shown in Figure 6.1, has been established
27 in the Proton Assembly Building at Fermilab. The Materials Test System (MTS)
28 has been developed to determine the effect on electron-drift lifetime of materials
29 and components that are candidates for inclusion in LAr-FD. The system essentially
30 consists of a source of clean argon (< 30 ppt O₂ equivalent), a cryostat, a sample

Table 6.1: LBNE on-project development activities

Activity	LAr-FD Information	Need by
In-liquid Electronics	Low noise readout, long lifetime	CERN prototype construction
TPC Construction	Mechanical design	CERN prototype construction
35-ton Prototype	Cryostat construction	CERN prototype cryostat procurement
CERN prototype	detector integration	TPC construction

Table 6.2: LBNE off-project development activities

Activity	LAr-FD Applicability	Status	Need by
Yale TPC	None	Completed	NA
Materials Test System	Define requirements	Completed	NA
	Materials testing	Operating	As Req'd
Electronics Test Stand	Electronics testing	Operating	As Req'd
LAPD	Purity w/o evac.	Operating	LBNE CD-2
	Convective flow	Operating	LBNE CD-2
Scintillator Development	Photon Det. Definition	Completed	CERN prototype Construction
	Industrialization	Not started	LBNE CD-3
ArgoNeuT	Analysis tools	On-going	LBNE CD-2
MicroBooNE	Electronics tests	Construction	LBNE CD-3
	DAQ algorithms	In development	LBNE CD-3
	Analysis tools	In development	LBNE CD-2
	Lessons learned	Not started	LBNE CD-3

1 chamber that can be purged or evacuated, a mechanism for transferring a sample
2 from the sample chamber into the cryostat, a mechanism for setting the sample
3 height in the cryostat so that it can be placed either in the liquid or in the gas ullage
4 above the liquid, a temperature probe to measure the temperature of the sample,
5 and an electron-lifetime monitor. The system is fully automated and the lifetime
6 data are stored in a single database along with the state of the cryogenic system.



Figure 6.1: Liquid argon area at the Proton Assembly Building at Fermilab

PAB

7 A noteworthy feature is the novel bubble-pump filter inside the cryostat. In case
8 of argon contamination, this can filter the cryostat volume in a few hours, allowing
9 us to continue studies without having to refill. A schematic of the MTS is shown in
10 Figure 6.2.
MTS Schem

11 The major conclusions of the studies to-date are summarized here. No material
12 has been found that affects the electron-drift lifetime when the material is immersed
13 in liquid argon – this includes, for example, the common G-10 substitute, FR-4. On
14 the other hand, materials in the ullage can contaminate the liquid; this contamination
15 is dominated by the water outgassed by the materials and as a result is strongly
16 temperature-dependent. Any convection currents that transport water-laden argon

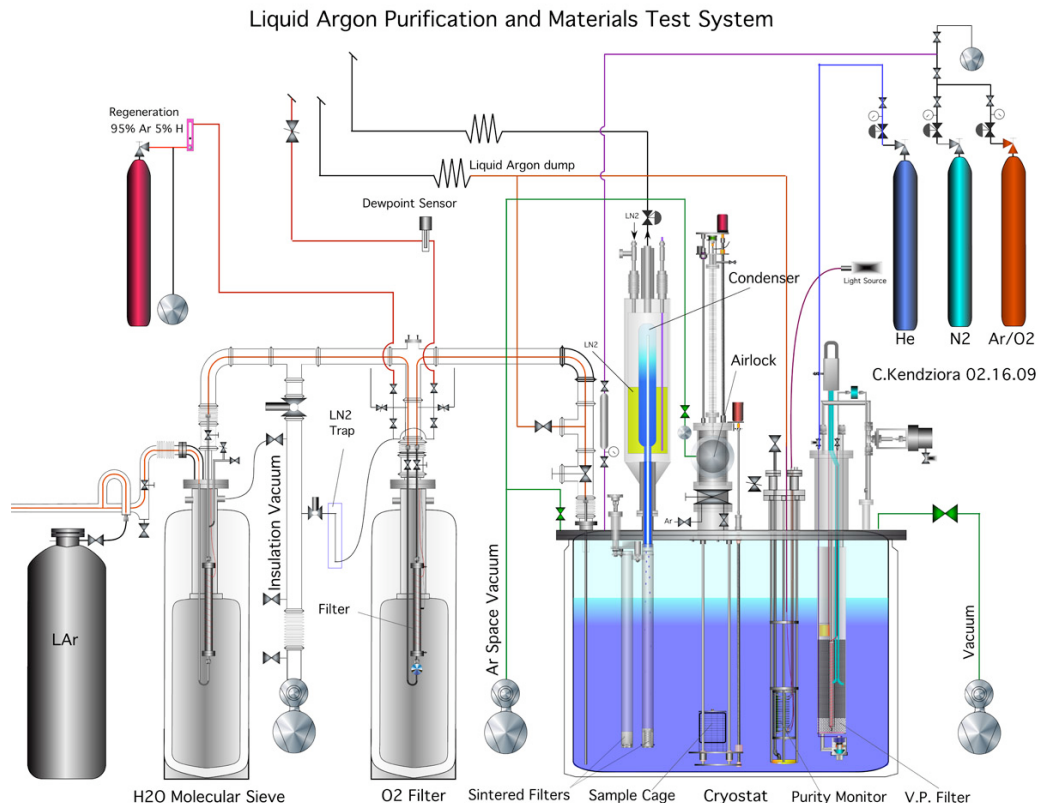


Figure 6.2: Schematic of the Materials Test System (MTS) cryostat at Fermilab

MTS_Schem

1 into the LAr and any cold surfaces on which water-laden argon can condense will fall
2 into the LAr and reduce the electron lifetime. Conversely, a steady flow of gaseous
3 argon of a few ft/hr away from the LAr prevents any material in the gas volume
4 from contaminating the LAr.

5 These results are taken into account in the design of both MicroBooNE and LAr-
6 FD. For LBNE they have been cast as detector requirements. The MTS will continue
7 to be used by MicroBooNE and LBNE to test detector materials such as cables that
8 will reside in the ullage.

9 **6.3.2 Electronics Test Stand**

10 The Electronics Test Stand is also installed in the Proton Assembly Building at
11 Fermilab. It consists of a cryostat, served by the same argon source as the Materials
12 Test System, and a TPC with a 50-cm vertical drift terminating in three planes of 50
13 wires each, arranged at 120 degrees. Figure 6.3 shows the TPC being inserted into
14 the cryostat. Two sets of small scintillation counters outside the cryostat are used to
15 trigger the system on cosmic rays. The data from this system provide a crucial check
16 of simulations of the electron drift and the signals induced on the wires.

17 The front-end electronics and the crucial shaping filters for the ArgoNeuT experiment
18 were developed on this system from the sort of data shown in Figure 6.4. These
19 data also led to the development of the FFT technique for reconstructing track hits.
20 A hybrid pre-amplifier has been successfully tested in LAr and has demonstrated
21 excellent noise performance.

22 The ASIC front-end amplifiers for LBNE will also be tested, providing assurance
23 that bench measurements are reproducible in a functional TPC.

24 **6.3.3 Liquid Argon Purity Demonstrator**

25 The Liquid Argon Purity Demonstrator (LAPD) is a significant-scale system, 30 tons,
26 consisting of a complete cryogenic recirculation system and a vessel capable of achieving
27 large-drift LArTPC purity specifications without initial evacuation. While large
28 cryogenic systems have been built by U.S. groups, this is the first with a purification
29 system intended specifically for an LArTPC. As such it is providing valuable experience
30 and data for the construction of future systems. Figure 6.5 shows the filtration
31 system and the LAPD tank in place at Fermilab's PC-4 facility.

32 The tank is instrumented with several systems. An array of sniffers measures the
33 oxygen concentration at six heights during the gas-purge; a system of temperature
34 monitors can be lowered and raised inside the tank to measure temperature gradients;



Figure 6.3: Electronics test TPC insertion into cryostat

TPC

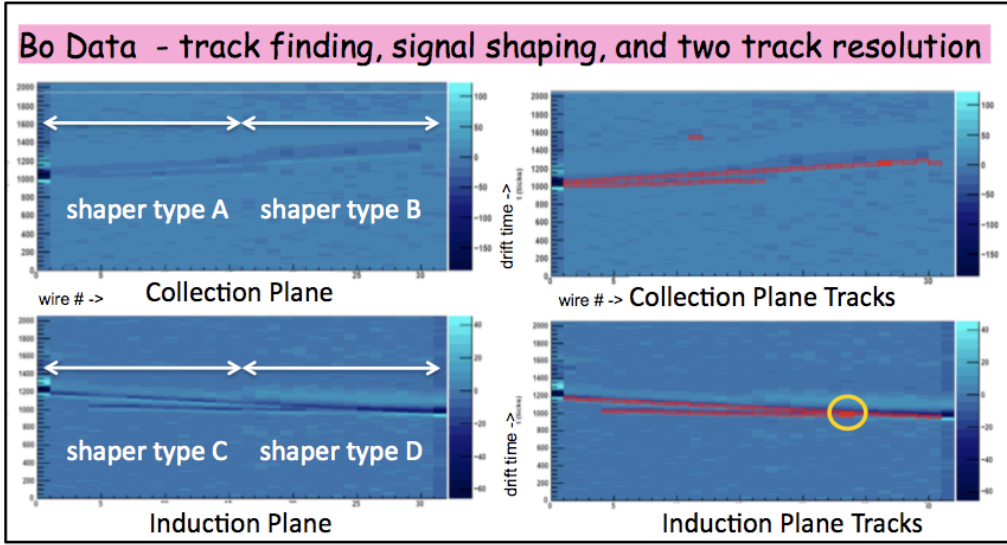


Figure 6.4: A cosmic ray with a delta electron as seen in the Electronics Test Stand TPC. Note the different width of the shaded portions along the tracks in the left panels. These are due to the two shaping circuits being tested. The readout scheme for MicroBooNE and LBNE uses digital signal processing and has minimal filtering before the ADC.

BoData

- ¹ an ICARUS-style purity monitor is deployed on the input line to the tank; and four
- ² ICARUS-style purity monitors measure electron-drift lifetime within the tank.

³ Analytic instrumentation includes a water meter and an oxygen meter, both
⁴ with ppb sensitivity, and a nitrogen meter with 10-ppb sensitivity, installed for the
⁵ purpose of taking measurements throughout the system. The scheme for displacing
⁶ the air (at atmospheric pressure) in the cryostat interior volume by introducing and
⁷ purifying LAr consists of several steps: a gas purge with argon, gas recirculation
⁸ with purification, an LAr fill while venting (to drive out any contaminants remaining
⁹ in the gas) and recirculation of the LAr through the purification system.

¹⁰ The primary motivation of LAPD is to demonstrate an electron-drift lifetime
¹¹ of several milliseconds, which has now been accomplished. LAPD began purging
¹² with argon gas in September 2011. The tank was filled with LAr to the 40% level
¹³ on November 1. A drift electron lifetime of 3 ms was achieved in late November
¹⁴ after some re-work was done on the filter material containment system. The filters
¹⁵ became saturated (with water) in mid December, were regenerated and were returned
¹⁶ to service in late January 2012. The drift-electron lifetime reached 3 ms after four
¹⁷ days of operation and has continued to improve as of February 2.

¹⁸ Now that high purity has been achieved, the effect of varying the conditions



Figure 6.5: Liquid Argon Purity Demonstration filtration and tank at the PC-4 facility

LAPD

1 (gas and/or liquid recirculation, different recirculation rates, no recirculation) can
2 be investigated. The size of the tank allows us to use the measurements from the
3 temperature-monitor system to check the accuracy of ANSYS simulations of the
4 temperature profile within the tank. This will check the simulations and should
5 confirm the small temperature gradients and resulting low velocities of the convection
6 flows predicted for large LArTPCs.

7 A problem was found with the building electrical system in early March 2012 that
8 necessitated ending the planned suite of LAPD tests prematurely. The current plan is
9 to perform additional re-work on the filter material containment system over the next
10 few months, followed by a second phase of testing. At this time, LAPD management
11 and operations will be transferred to LBNE to support the 35-ton membrane-cryostat
12 prototype described in Section 6.3.7.

13 **6.3.4 Photon Detection R&D**

14 The R&D program for Photon Detection is based on a promising, new, cost-effective
15 scheme for light collection in LArTPCs as described in a NIM article by Bugel et
16 al [?]. The design is based upon lightguides fabricated from extruded or cast acrylic
17 and coated with a wavelength-shifter doped skin. Multiple acrylic bars are bent to
18 guide light adiabatically to a single cryogenic PMT. Prototypes of the basic detector
19 elements have been shown to perform well. These lightguides have a thinner profile
20 than the usual TPB-coated PMT-based system, occupying less space in an LAr
21 vessel and resulting in more fiducial volume. Another advantage of this system is
22 that the bars are inexpensive to produce. The most convenient place for the paddles
23 is between the wire planes that wrap around the APAs.

24 Lightguide R&D has advanced rapidly since the initial publication resulting in
25 $\sim 3 \times$ higher light yields. The R&D is now sufficiently advanced to provide a technical
26 basis for the LAr-FD reference design. On-going design efforts at MIT, Indiana
27 University, and Fermilab are directed toward industrial-scale production and the
28 evaluation of lower-cost fluors that are effective in converting VUV photons. These
29 efforts also include investigating PMTs with increased quantum efficiency as well as
30 other efficient light-collection technologies, such as Geiger-mode avalanche photodiodes
31 (commonly known as Silicon Photomultipliers, or SiPMs).

32 **6.3.5 TPC Design**

33 The design for LBNE has adopted the basic ICARUS multi-plane, single-phase TPC
34 concept and has incorporated new features suitable for a very large detector. The

- 1 main emphasis of the development program is to develop a TPC design that is highly
2 modular, low-cost, robust and easily installed inside a finished cryostat.

3 A significant effort has been focused on minimizing the dead space between de-
4 tector modules to improve the fiducial versus total LAr-volume ratio. The APA
5 reference design accomplishes this goal but requires making ~ 2 million high-quality
6 wire terminations. The wire-termination scheme used by ICARUS has proven to be
7 very reliable but it is too labor-intensive to fabricate for a million-channel detector
8 system. We have adopted the wire-solder + wire-epoxy termination scheme that has
9 been used for decades on drift chambers and proportional wire chambers to mount
10 Cu-Be wires. The termination scheme was used to terminate 2.5 million anode wires
11 in the CMS end-cap muon system. Cu-Be wires have excellent mechanical properties
12 and the advantage of low resistance compared to stainless steel. A study is currently
13 underway within the LAr-FD subproject to identify the optimum wire-bonding pa-
14 rameters. The focus is currently on finding a commercial epoxy that optimizes the
15 qualities of bond strength, cure time and low-temperature operation.

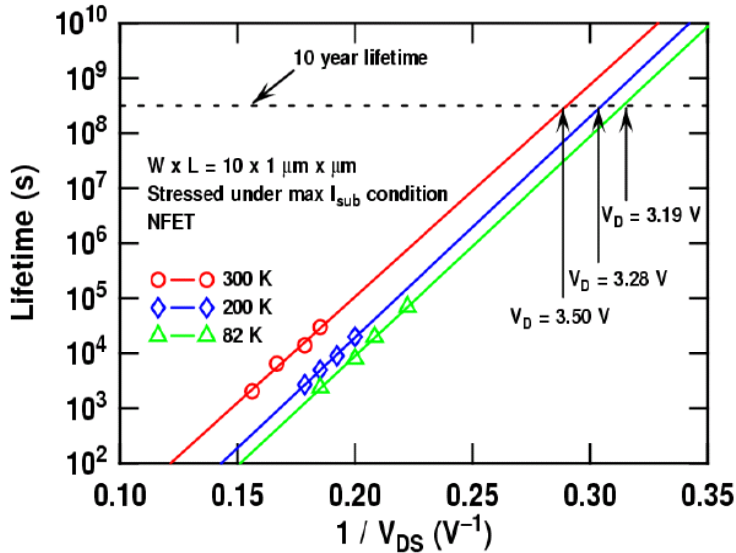
16 **6.3.6 Electronics Development**

17 The work to-date on cold electronics has established that no show-stoppers exist. The
18 remaining activities outlined here concern performance optimization of the CMOS
19 ASICs, the evaluation of several widely available CMOS technologies, and the devel-
20 opment of readout architectures appropriate and timely for various scenarios of very
21 large detectors.

22 **CMOS Transistors: Lifetime Verification and Technology Evaluation**

23 The results of the design of the CMOS electronics for operation at LAr temperature
24 (89 K), performed so far by the MicroBooNE and LBNE collaborations, as well
25 as by a large collaboration led by Georgia Inst. of Technology, are summarized in
26 Section 2.7.

27 Briefly, the fundamentals are: charge-carrier mobility in silicon increases at 89 K,
28 thermal fluctuations decrease with kT/e , resulting in a higher gain (transconduc-
29 tance/current ratio = g_m/i), higher speed and lower noise. For a given drain-current
30 density the same degree of impact ionization (measured by the transistor substrate
31 current) occurs at a somewhat lower drain-source voltage at 89 K than at 300 K.
32 The charge trapped in the gate oxide and its interface with the channel causes degra-
33 dation in the transconductance (gain) of the transistor and a threshold shift. The
34 former is of major consequence as it limits the effective lifetime of the device (defined
35 in industry and the literature as 10% degradation in transconductance). Thus an

Figure 6.6: Lifetime at different temperatures vs V_{DS}

DSV

1 MOS transistor has equal lifetime due to impact ionization at 89 K and at 300 K at
 2 different drain-source voltages. This is illustrated in Figure 6.6.

3 This feature offers a tool for accelerated-lifetime testing by stressing the transistor
 4 with both increased current and increased voltage, and monitoring the substrate
 5 current and the change in g_m due to impact ionization. In these conditions, the
 6 lifetime can be reduced arbitrarily by many orders of magnitude, and the limiting
 7 operating conditions for a lifetime in excess of ~ 20 years can be determined. With
 8 this foundation, more conservative design rules (lower current densities and voltages)
 9 can be derived and applied in the ASIC design, as has been done for the ASIC
 10 described in Section 2.7.1. The goal of this part of the program is to verify by
 11 accelerated testing the expected lifetimes for the several widely available CMOS
 12 technologies under consideration (TSMC, IBM, AMS). It should be noted that this
 13 is a standard test method used by the semiconductor industry. These methods are
 14 used to qualify electronics for deep space NASA missions as well as commercial PCs.

1 Readout Architectures, Multiplexing and Redundancy

2 A high degree of multiplexing after digitization of signals is essential for a TPC with
3 0.5 million wires in order to reduce the cable plant and the attendant outgassing.
4 Just how high a multiplexing factor should be chosen is a matter of study, considering
5 the risk of losing one output data link. A part of the program will include system
6 designs with redundant links and redundant final multiplexing stages to minimize
7 the risk of losing the data from a significant fraction of the TPC (note that even
8 with a multiplexing factor of 1/1024 and no redundancy, one failed link would result
9 in a loss of 0.2%).

10 6.3.7 Cryostat Development: 35-ton Prototype

11 The next step in the cryostat-prototype program is intended to address project-
12 related issues: (1) to gain detailed construction experience, (2) to develop the pro-
13 curement and contracting model for LAr-FD and (3) to incorporate the design and
14 approval mechanism in the Fermilab ES&H manual. (Membrane cryostats are de-
15 signed in accordance with European and Japanese standards.) At present, we are
16 in the process of procuring the cryostat components for a 35-ton membrane cryostat
17 from IHI.

18 The LBNE project has contracted with the Japanese company IHI to build a
19 small prototype membrane cryostat at Fermilab. This approximately 35-ton unit is
20 to be built and made operational in 2012 at Fermilab's PC-4 facility where LAPD is
21 located. It is intended to demonstrate high-purity operation in this type of cryostat
22 and the suitability of the planned LAr-FD construction techniques and materials.
23 The testing programs for LAPD and the small prototype will be similar. LBNE's
24 35-ton membrane cryostat will use a large portion of the cryogenic-process equipment
25 installed for LAPD.

26 The prototype membrane cryostat's total size, including insulation and concrete
27 support, is approximately 4.1 m × 4.1 m × 5.4 m, and will hold approximately
28 826 tons of LAr. The insulation thickness will be 0.4 m rather than the 1.0 m cho-
29 sen for our reference design. The techniques of membrane-cryostat construction will
30 be demonstrated to be a fit for high-purity TPC service. Welding of corrugated
31 panels, removal of leak-checking dye penetrant or ammonia-activated leak-detecting
32 paints, and post-construction-cleaning methods will be tested for suitability of ser-
33 vice. Residual contamination measurements at different elevations during the initial
34 GAr purge process will be compared to computational predictions and will validate
35 the purge-process modeling of a large rectangular vessel. The prototype membrane
36 cryostat will be filled with LAr. Purity levels of the liquid with time and electron-drift

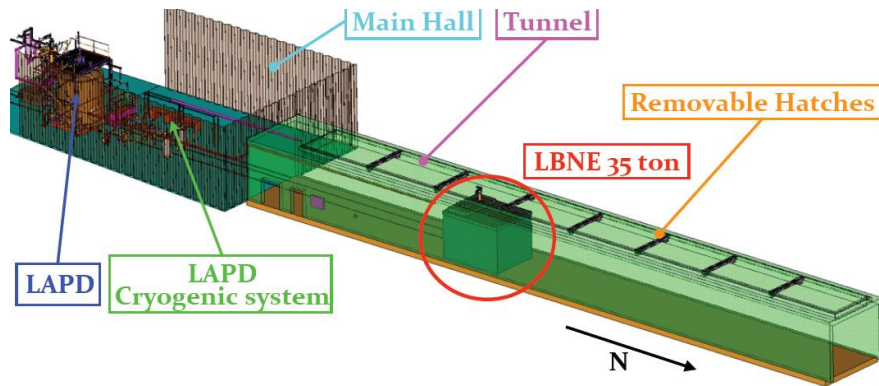


Figure 6.7: Layout of 35-ton prototype at Fermilab's PC-4 facility

fig:v5ch2-35ton

¹ times will be measured using purity monitors installed in the liquid bath. Heat-load
² measurements will be made and compared to calculations. Eventually, connectors
³ and feedthroughs, ports and other features that are planned for the reference design
⁴ will be incorporated into the prototype. Materials and cold-electronics testing can
⁵ be done along with electron-drift-time measurements.

⁶ In principle, a thin-walled membrane cryostat is as suitable as a thick-walled
⁷ cryostat for use with high purity LAr. Both would be constructed with 304 stainless
⁸ steel with a polished surface finish. Both would use passive insulation. The total
⁹ length of interior welds required for construction would be similar in both cases. The
¹⁰ leak checking procedure would be the same in both cases.

¹¹ The significant difference between membrane cryostats and thick-walled cryostats
¹² is the depth of the welds used to construct the vessel. The majority of membrane-
¹³ cryostat welds are completed in one or two passes with automatic welding machines.
¹⁴ A second difference, and a major advantage, is that the membrane cryostat is a
¹⁵ standard industrial design that has been in use for over 40 years. A thick-walled
¹⁶ cryostat vessel would be custom designed and would require significant engineering
¹⁷ and testing. A third difference, and another major advantage, is the ability to purge
¹⁸ the membrane cryostat insulation space with argon gas so that a leak cannot affect
¹⁹ the purity if it escapes detection and repair.



Figure 6.8: Membrane panel assembly and components

3panel

1 A 3-m × 3-m wall panel shown in Figure 6.8 was constructed at Fermilab using
 2 materials and technical guidance from GTT. The labor hours used in construction
 3 are consistent with the vendor estimates. The wall panel was leak tested (none were
 4 found) and vacuum tests were performed on the insulation system. We found that
 5 the insulation system is designed to allow vacuum pumping of the main cryostat
 6 volume to a hard vacuum. This result demonstrates that vacuum pumping of a
 7 membrane cryostat is feasible, if it is found to be required. No modifications to the
 8 vendor-supplied components are required to accomplish this.

9 6.3.8 One-kiloton Engineering Prototype: LAr1

Editor's Note: The far detector prototyping plan known as LAr1 has been replaced by a plan to build and test a prototype with full-size TPC components at CERN.

10

11 The last major project of the development program is the construction of a 1-kton
 12 cryostat, called LAr1, to be equipped with the same TPC and electronics as LAr-FD.
 13 The proposed cryostat will reside at Fermilab's D-Zero Assembly Hall using the LAr

1 and LN infrastructure already existing for the D-Zero detector, which is no longer
2 operating. The end of the Tevatron era allows LBNE to make immediate use of this
3 existing building and the existing cryogenic processes it houses. This prototype will
4 serve to test all the major components of LAr-FD, in particular:

- 5 • Gain further experience in cryostat construction and procurement
6 • Exercise the assembly and testing procedures for all the individual components
7 • Test the integration features of the detector design including:
8 – the TPC supports
9 – the cold electronics, signal feedthroughs and power feedthroughs
10 – the grounding scheme and control of electrical noise
11 – the purification system
12 – the cryogenic system and the cryogenic control system
13 • Exercise the installation procedure

14 The means of demonstrating that these goals have been met is via the acquisition
15 and reconstruction of a sample of through-going cosmic rays. LAr1 is being managed
16 as a semi-independent subproject. See Chapter [Ch:LAr1](#) for further details. The subproject
17 was subjected to a CD-1-style technical, cost, schedule and management review in
18 August 2011. LAr1 construction could be completed in early 2014 if both funding
19 and resources are available.

20 An attractive extension of the LAr1 goals would be to measure the cosmic-ray
21 spallation background rates expected in LAr-FD. A sample of cosmic-ray spallation
22 interactions in the LAr1 volume could be acquired in a relatively short period of
23 time. Charged kaons associated with the interaction could be identified and their
24 momentum measured. Charged kaons produced by K^o charge-exchange could also
25 be identified and their rate and angular distribution measured.

26 **6.3.9 Physics Experiments with Associated Detector-Development 27 Goals**

28 Two projects, ArgoNeuT and MicroBooNE, which are physics experiments in their
29 own right, are also contributing to the development of the LBNE experiment. Their
30 most important role is in providing data and motivation for the development of event
31 reconstruction and identification software.

1 ArgoNeuT - T962

2 The Argon Neutrino Test (ArgoNeuT) is a 175-liter LArTPC which completed a run
3 in the NuMI neutrino beam. The $0.5\text{ m} \times 0.5\text{ m} \times 1\text{ m}$ LArTPC was positioned
4 directly upstream of the MINOS near detector, which served as a muon catcher for
5 neutrino interactions occurring in ArgoNeuT.

6 ArgoNeuT began collecting data using the NuMI anti-muon neutrino beam in
7 October 2009 and ran until March 1, 2010. ArgoNeuT's $\sim 10\text{k}$ events motivate the
8 development of analysis tools, and are the basis for the first measurements of neu-
9 trino cross sections on argon. An event with two π^0 decays is shown in Figure 6.9.
10 ArgoNeuT was also the first LArTPC to be exposed to a low-energy neutrino beam
11 and only the second worldwide to observe beam-neutrino interactions. The Ar-
12 goNeuT collaboration is currently preparing (1) a NIM paper that documents the
13 detector performance using NuMI beam muons and (2) the first physics paper on
14 muon-neutrino charged-current differential cross sections on argon. See Figures 6.11
15 and 6.12.

16 A deconvolution scheme using an FFT has been applied to the ArgoNeuT data.
17 This procedure eliminates a problem with the ArgoNeuT electronics (which were
18 D-Zero spares and could not be modified for ArgoNeuT). Another more significant
19 benefit of deconvolution is that bi-polar induction-plane signals can be transformed
20 into uni-polar collection-plane signals. An example of this is shown in Figure 6.10.
21 A selection of figures from the draft NIM paper are reproduced below.

22 The applicability of ArgoNeuT is that it provides a set of data in the same range of
23 energy as the LBNE neutrino beam, enabling the development of analysis algorithms
24 that can be utilized for LAr-FD physics analysis with little or no modification.

25 MicroBooNE E-974

26 The MicroBooNE experiment is an 86-ton active mass LArTPC, (170-ton argon
27 mass) in the construction phase. It has both a physics program and LArTPC devel-
28 opment goals.

29 MicroBooNE received stage 1 approval from the Fermilab director in 2008, partial
30 funding through an NSF MRI in 2008 and an NSF proposal in 2009. MicroBooNE
31 received DOE CD-0 Mission Need in 2009 and CD-1 in 2010, and CD-2/3a review
32 in September 2011. It plans to start running in early 2014.

33 As well as pursuing its own physics program, MicroBooNE will collect a large
34 sample ($\sim 100\text{k}$) of low-energy neutrino events that will serve as a library for the
35 understanding of neutrino interactions in LAr. Because MicroBooNE is at the sur-
36 face, it will also have a large sample of cosmic rays with which it can study potential

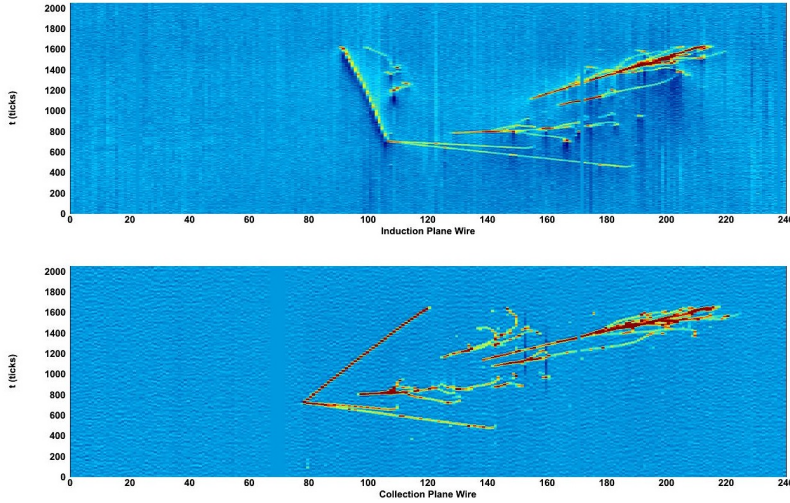


Figure 6.9: A neutrino event with four photon conversions in the ArgoNeuT detector. The top (bottom) panel shows data from the induction (collection) plane after deconvolution.

2pi0

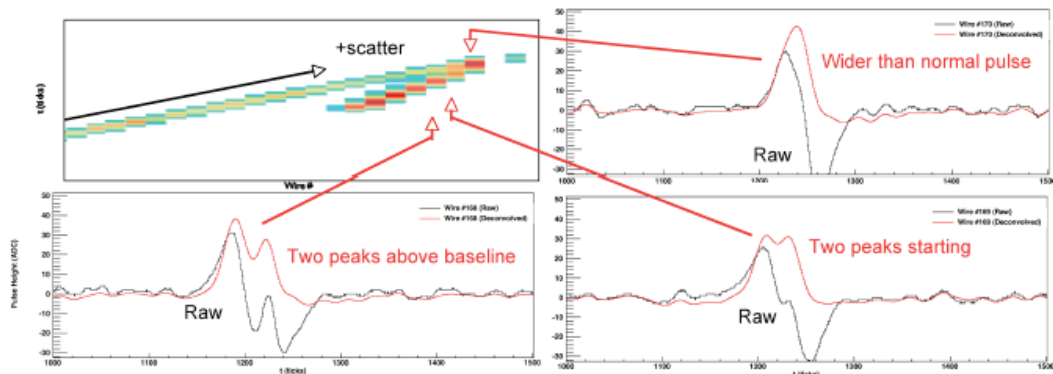


Figure 3: (Upper left) A set of tracks as seen on the (deconvoluted) induction plane. The wire views on three adjacent wires are also shown in order to demonstrate the effects of deconvolution on the raw wire pulses. The raw data can be seen in black and the deconvoluted data can be seen in red.

Figure 6.10: Figure from the ArgoNeuT draft NIM paper.

Argo-decon

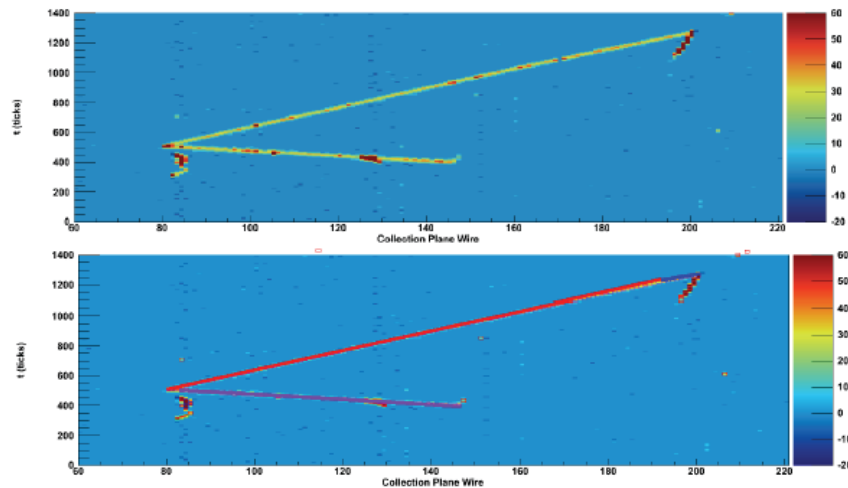


Figure 6: (Top) A neutrino candidate in ArgoNeuT as seen on the collection plane. (Bottom) The Hough lines found with the line-finding algorithm overlaid on the particle tracks.

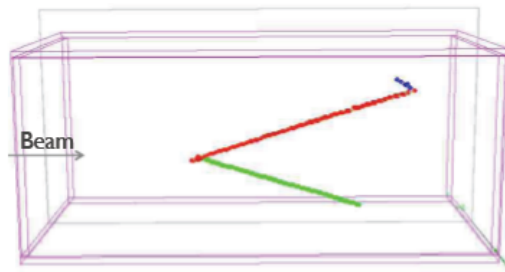


Figure 7: The neutrino event shown in Figure 6 reconstructed in three dimensions.

Figure 6.11: Figure from the ArgoNeuT draft NIM paper showing the status of 3D reconstruction

ArgoNeuT_3Drec

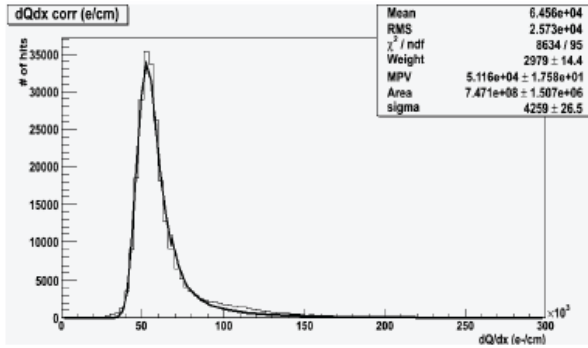


Figure 13: dQ_0/dx distribution (in ADC/cm) obtained for the through-going muon data sample having corrected for the electron lifetime and quenching effect on the ionization charge and properly taken into account the contribution due to δ -rays, as reported in the previous Section. A Landau-Gaussian fit is also reported.

Figure 6.12: Figure from the ArgoNeuT draft NIM paper showing the status of calorimetric reconstruction.

ArgoNeuT-calor

backgrounds to rare physics. The process of designing MicroBooNE has naturally stimulated several developments helpful to the LBNE program. Studies of wire material, comparing Be-Cu with gold-plated stainless steel in terms of their electrical and mechanical properties at room and LAr temperatures, and techniques for wire-tension measurement are immediately relevant. Expertise has been developed generating simulations of electrostatic-drift fields as well as simulations of temperature and flow distributions in LAr cryostats which is being applied to the LAr-FD TPC and cryostat. MicroBooNE will use the front end of the proposed in-liquid electronics as the wire-signal amplifiers and the DAQ developed for MicroBooNE will exploit compression and data-reduction techniques to record data with 100% livetime. In summary, MicroBooNE's LArTPC development goals that are pertinent to LAr-FD are

- large-scale testing of LBNE front-end electronics, similar in scale to the CERN prototype
- testing of continuous data-acquisition algorithms
- refinement of the analysis tools developed in ArgoNeuT
- provide costing and construction lessons-learned

6.4 Summary

Impressive progress has been made in the development of LArTPC technology over the last few years. All elements of the development program have completed the R&D phase. Credible conceptual designs exist for all systems in LAr-FD. The technical activities described in this chapter are properly characterized as preliminary engineering design.

The most significant deficiency is the lack of fully-automated event reconstruction. Algorithms have been developed within the LAr community and are being successfully applied to ArgoNeuT data as well as to simulated MicroBooNE data. The algorithms have individually shown that the high efficiency and excellent background rejection capabilities of an LArTPC are achievable. The task remains to combine them into a single package.

¹ Chapter 7

² Alternatives Not Selected

^{h:alternatives}

- ³ Alternative detector configurations and design parameters that were considered but
- ⁴ ultimately rejected for other designs are discussed in this chapter.

⁵ 7.1 Detector Configuration

⁶ 7.1.1 Double Phase Readout

⁷ The European GLACIER collaboration is pursuing a novel double-phase readout detector technology that has potential advantages. In this scheme, ionization electrons are drifted upwards under the influence of an electric field towards the liquid-vapor interface. The electrons are extracted from the liquid into the vapor by an electric field of 2.5 kV/cm. The electrons then drift to two stages of Large Electron Multipliers (LEM). Electrical signals are induced on segmented electrodes on the LEM.

¹⁴ This method requires far fewer readout channels than our reference design, however significant R&D is required to demonstrate the viability of this technique for a large detector. This design requires very long electron-drift lengths ($\sim 20\text{m}$) in order to be cost-effective.

¹⁸ 7.1.2 Cryostat Shape

¹⁹ Storage tanks can be classified by shape (upright cylinder, horizontal cylinder, rectangular parallelepiped) and means of support (self supporting, externally supported).

²¹ A horizontal cylindrical tank would require significant structural support to withstand the gravitational load. On the other hand, upright self-supporting cylindrical

1 tanks are commonly used for surface storage of cryogenic liquids. The proposed
2 above-ground LArTPC experiment FLARE utilized a tank of this configuration. An
3 upright cylindrical tank is also proposed for the 100-kton GLACIER underground
4 detector. In contrast, the 600-ton ICARUS detector is a rectangular parallelepiped.

5 A study was performed [?] to compare the cost for three configurations of equivalent
6 active mass: upright cylindrical cryostat (soup can), rectangular parallelepiped
7 externally-supported cryostat (membrane) and the rectangular parallelepiped self-
8 supporting cryostat (modular). The study considered the cost of rock excavation,
9 the cost of the total inventory of LAr required for a detector with a fixed active mass
10 and a rough estimate of the cryostat cost.

11 The active/total mass fraction for the three configurations ranges between 70%
12 and 74% and is therefore not a significant factor in the cost difference. The major
13 cost factor is the volume of rock that must be excavated for these configurations.
14 There is a significant amount of unused cavern space if an upright cylindrical tank is
15 located within a rectangular parallelepiped cavern. The amount of unused space can
16 be reduced by excavating a cylindrical cavern but the excavation cost would increase
17 significantly (~ 30%).

18 The study results show a cost range of 10% - 20% for the different configurations.
19 This is within the uncertainty of the estimates (~ 50%) so none of the options can
20 be rejected purely on economic grounds given our current state of knowledge. Given
21 sufficient resources, all configurations could be more fully developed to make a more
22 informed decision, however any potential value would be offset by the cost of pursuing
23 multiple design paths.

24 The study results also indicate that a membrane cryostat is the most cost-effective
25 solution. It clearly maximizes the use of the excavated rock volume. A membrane
26 cryostat is also inherently more cost-effective than a self-supporting cryostat since
27 the hydrostatic pressure of the liquid is constrained by the cavern walls and not the
28 cryostat walls, thereby reducing the amount of structural steel required.

29 **7.1.3 Modular Cryostat**

30 The modular LANND detector concept was considered. The main benefit of the
31 LANND concept is that the cryostat is evacuable. However, reinforcing members
32 within the cryostat would be required to withstand the vacuum load. Physics cuts
33 around these members would reduce the fiducial mass of the detector significantly
34 relative to the membrane-cryostat reference design. Results from the Liquid Argon
35 Purity Demonstrator have shown that cryostat evacuation is not required to achieve
36 excellent LAr purity.

7.2 Depth Options

7.2.1 Surface and 300L

Cosmic-ray backgrounds for accelerator-based neutrino analyses are negligible in an LArTPC located on the surface of the earth. The cosmic-ray rate on the top of an APA drift cell of size $2.5\text{ m} \times 5\text{ m}$ would be 2 Hz if it were located at the surface. A neutrino event is fully contained within the drift cell and the drift time is 1.5 msec, so the rate of accidental cosmic rays in a drift cell containing a neutrino event is 0.2%. The physics scope of either the surface or 300L options would be restricted to accelerator neutrinos since a competitive proton-decay search could not be performed with such a high background rate. The cost of underground construction is significantly higher than conventional surface construction so there is no clear benefit from the 300L option.

Significant cost savings (several \$100M) would result for the surface option. However, space charge build up due to the relatively high cosmic ray flux on the surface and the slow ion drift velocity may result in unacceptable distortions in the electric field using the long 3.7 m drift that is planned for the LAr-FD. This can be mitigated by reducing the drift length, which would result in a substantial increase in the number of channels and a modest reduction in the ratio of fiducial volume to total volume. These would, in turn, increase the cost of the detector, partially offsetting the cost reduction from moving to the surface.

7.2.2 800L

In addition to the reference design described in this CDR for a LAr-FD at the 4850L, a candidate design for the 800L was also developed [?]. At this depth, there is an unacceptable level of background to $p \rightarrow \nu K^+$ due to the creation of K0L by cosmic ray muons in the surrounding rock, which subsequently charge exchange within the LAr detector to create an isolated K^+ . To mitigate this effect, a large-area veto system was included in the 800L design, in order to tag muons which could generate such background and thereby eliminate candidate proton decay events in coincidence with a detected muon. Given the goal of essentially zero background for the proton decay search ([?] quotes a background rate on the order of 1 event in 30 years), the veto system would be required to be extremely efficient, and therefore essentially completely hermetic. However, due to the practical engineering considerations of how to implement a veto system extending 7 m into the rock at both top and bottom of the main detector, it proved difficult to achieve the required hermetic coverage. In addition, at the position of the proposed cavern at the 800L, the cosmic ray flux

1 $\Delta\phi$ angle and energy ΔE depend on the details of the surface topography, which
2 would require extensive simulations to be able to be assured of the efficacy of the veto
3 system for reducing the background to the required level. Moving the detector to the
4 4850L reduces the cosmic ray background by three orders of magnitude, essentially
5 eliminating these concerns.

6 Cosmic ray muons passing through the LAr detector itself can produce spalla-
7 tion products with lifetimes too long to allow signals resulting from their subsequent
8 decay to be vetoed by observing the muon that created them. These would create
9 backgrounds that could compromise low-energy physics searches, of which the ob-
10 servation of neutrinos from a distant core-collapse supernova is the prime, but not
11 only example. The spectrum of spallation products of argon is not well known, nor
12 is the spectrum of low-energy searches that the LBNE LAr-FD may be called upon
13 to do, so it is difficult to quantify the effect of such background. Since the spallation
14 backgrounds cannot be vetoed, the only way to reduce them is to move the detector
15 to greater depth.

16 Based on these considerations, as well as the fact that siting LBNE at the 4850L
17 would help enable other deep underground science in the U.S., the LBNE Collabora-
18 tion Executive Committee, in its meeting in December 2011, issued a statement that
19 “There was a very strong preference for siting the experiment at the 4850L depth.”

20 **7.3 Cryogenics Plant**

21 **7.3.1 LAr Supply using a Temporary Air-Separation Plant**

22 We have considered whether the provision of a temporary, dedicated air-separation
23 plant could be justified based on the elimination of LAr losses due to boil-off during
24 transportation, elimination of vehicle movements and the potential increase in the
25 supply reliability. These advantages must be offset against the net capital cost of
26 the temporary plant, the operating cost of the plant and the relative inefficiency of
27 the small temporary plant as compared to a large commercial plant. We have been
28 advised by LAr suppliers that this would not be cost-effective.

29 **7.3.2 LAr Storage**

30 It would be desirable to provide temporary storage of LAr to decouple the delivery
31 schedule from the detector construction schedule. Ideally, temporary storage could
32 reduce the schedule by six months since argon deliveries can occur in parallel with

1 detector construction. This is only possible if construction of the temporary storage
2 facility occurs concurrently with other activities.

3 Temporary storage would also mitigate the risk of a detector failure necessitating
4 access to the cryostat. If a sudden detector-wide failure occurred and temporary
5 storage were not available, the argon would be vented to the atmosphere and the
6 \$25M investment of LAr would be lost. The cryostat filling sequence described in
7 Chapter 5 effectively eliminates the likelihood of failure during detector commission-
8 ing. A sudden detector-wide failure occurring during operations is highly unlikely. It
9 is more likely, but still unlikely, that a gradual degradation of detector performance
10 would occur over an extended period of time, allowing time for a decision to be made
11 to construct a storage tank.

12 **7.3.3 Common Riser for LAr and LN**

13 The potential for the replacement of the two liquid cryogen risers (LAr and LN) with
14 a common cryogenic riser may be considered during later design phases. The fill lines
15 are not normally used during operation. After initial filling of the cryostat the argon
16 line is not planned to be used unless the cryostat is to be drained. The common line
17 would be configured in standby mode for LN service in case of unplanned outage of
18 the refrigeration plant.

19 **7.3.4 Common Vent Lines**

20 A common vent system could be adopted that would be suitable for both nitrogen
21 and argon. It would need to be sized for the peak combined flow rate. The proba-
22 bility of either argon or nitrogen being vented under normal operations is low, but a
23 Simultaneous Operations Study (SIMOPS) would be required to demonstrate that
24 cross-contamination could not occur during commissioning, or normal or emergency
25 operations. A greater level of design detail is required to support this study than has
26 been possible to-date and therefore separate vents have been included at this stage.

27 **7.4 Cryostat Insulation**

28 The original LANND modular cryostat included the use of a vacuum-insulated
29 space between the inner and outer tanks, resulting in a significant decrease in the
30 required refrigeration load. This benefit would need to be weighed against the added
31 capital cost of a vessel that can withstand the vacuum load. Arup eliminated the

1 vacuum-insulated option during the screening process, citing the benefit of not having
2 an outer tank designed for a full vacuum load.

3 The use of a vacuum-jacketed cryostat was rejected. The most serious concern is
4 an accident scenario that would result in a significant leak in the inner vessel. The
5 outer tank and the argon venting system would need to be designed to cope with the
6 large volume of released gas.

7.5 TPC

8 7.5.1 TPC Configuration

9 Reference Design 1a

10 The first proposed Reference Design, 1a, relied on a minimal extrapolation of the
11 MicroBooNE TPC module design. The detector would be installed in a cavern with
12 drive-in access and would consist of a rectangular stack of TPC modules that had
13 been constructed above-ground.

14 A modest extrapolation of the MicroBooNE module design parameters does not
15 introduce large cost uncertainty if done properly. The extrapolations are in di-
16 mensions that do not challenge the limits of the technology. Rather, this detector
17 configuration suffers from a poor fiducial/total mass fraction. Only 56% of the LAr
18 in the detector would be useful for physics and the cost is ~ 3 times the cost of the
19 selected reference design.

20 Reference Design 2a

21 Reference Design 2a is similar to the selected reference design. The major difference
22 is the use of room-temperature, accessible electronics. The concept is shown in
23 Figure 7.1.
fig:refdes2a

24 Short low-impedance cables route wire signals from the Anode Plane Assemblies
25 (APAs) to a cold feedthrough which is kept at ~ 120 K. The readout electronics
26 are located within the feedthrough. The benefit of this design is that the electronics
27 boards can be replaced without removing LAr from the detector.

28 There are a number of disadvantages to this concept, however. The cable lengths
29 must be kept to ~ 1 m, the wire spacing must be increased to 5 mm and the wire
30 angle reduced from 45^{deg} to 30^{deg} in order to achieve a marginally acceptable signal-
31 to-noise ratio. As a result, the track resolution in the vertical direction is ~ 1 cm. A
32 large number of feedthroughs are required in order to keep the cable lengths short.
33 One feedthrough containing 576 electronics channels is required for every 53 cm along

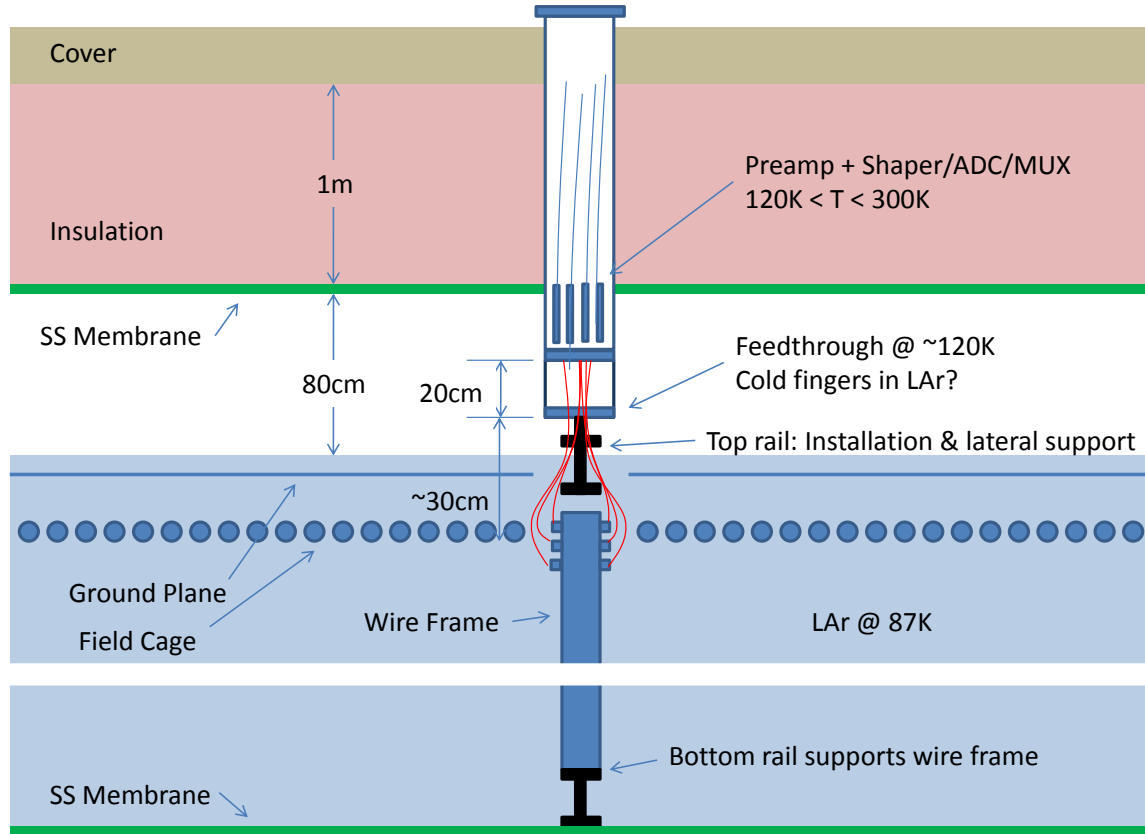


Figure 7.1: Reference Design 2a, showing cable routing from an Anode Plane Assembly to a cold feedthrough. The warm readout electronics are located within the feedthrough.

fig:refdes2a

- ¹ the top of each APA. Each feedthrough would be 34 cm \times 22 cm in cross section
- ² and would be \sim 2 m long.

³ 7.5.2 Wire Spacing

- ⁴ The distinguishing feature of the LArTPC is the ability to distinguish one MIP
- ⁵ electrons from 2 MIP electron-positron pairs close to the interaction vertex. A wire
- ⁶ spacing smaller than the design (5 mm) would have smaller signal-to-noise ratio
- ⁷ (S/N) commensurate with the wire spacing. The design S/N ratio could be restored
- ⁸ by decreasing the noise. The most direct means of accomplishing this would be
- ⁹ to reduce the wire length, thereby increasing the number of electronics channels.
- ¹⁰ Reducing the wire spacing below 5 mm will only offer minimal benefit since the

¹ background from NC π^0 events is already quite small.

² 7.5.3 Number of Wire Planes

³ The reference design includes three instrumented wire planes and one un-instrumented
⁴ grid plane. Reducing the number of instrumented planes to two would reduce the de-
⁵ tector cost by $\sim \$3M$ with a negligible loss of ν_e identification efficiency. This would
⁶ also reduce the readout redundancy, however, and potentially affect the long-term re-
⁷ liability of detector operations. We do not consider this a credible value-engineering
⁸ option.

⁹ The un-instrumented grid plane could be eliminated, saving $\sim \$1M$. The grid
¹⁰ plane is used to create equal signal levels in both induction planes. The signal level
¹¹ in the first induction plane would be reduced by ~ 2 times if the grid plane were
¹² eliminated. The grid plane also provides electrostatic discharge protection for the
¹³ instrumented wires. We do not consider this a credible value-engineering option.

¹⁴ 7.5.4 Drift Length

¹⁵ Selection of the design drift length is highly coupled with the expected LAr purity, the
¹⁶ wire spacing and the required ν_e identification efficiency and background rejection.
¹⁷ The ICARUS detector is currently operating with a drift electron lifetime of 6 to
¹⁸ 7 ms. We expect the LAr purity in LAr-FD to be equal or superior to ICARUS.
¹⁹ Increasing the drift distance beyond the reference design of 3.7 m would result in
²⁰ significant cost savings. The 5 mm wire spacing is well matched to this drift distance;
²¹ it is roughly twice the transverse diffusion RMS. As an example, if the drift distance
²² were increased to 5 m, the wire spacing could be increased to ~ 6 mm. The minimum
²³ signal-to-noise ratio would suffer a minor decrease from 36:1 to 30:1 if the electron
²⁴ lifetime was 6 ms. The effect of such a change on physics analyses has not yet been
²⁵ explored.

²⁶ 7.6 DAQ Cable Routing

²⁷ The concept of routing raw signals from all wires out of the cryostat, as ICARUS
²⁸ does, was considered. The large data rate would require a huge number of cables and
²⁹ feedthroughs with little benefit since the vast majority of the sampled wire signals
³⁰ have no information. The large cable plant would be a major contributor to LAr
³¹ impurities.

7.7 Installation & Commissioning

² The initial Installation and Commissioning concept was to support the TPC on the
³ floor of the cryostat. Cross-bracing in both directions would be required to ensure
⁴ mechanical stability and would compromise the TPC design. Hard points in the
⁵ cryogenic insulation would be needed which would likely require design modifications
⁶ to the standard vendor-supplied membrane-cryostat insulation system.

⁷ Several alternatives for accessing the top of the detector during installation were
⁸ considered. A scissors lift was considered and rejected due to concerns that the lift
⁹ could sway and damage detector components. Consideration was given to a moveable
¹⁰ platform that would traverse the top of the detector on rails, or alternatively, using
¹¹ a temporary catwalk. These systems would provide access to the top of the detector
¹² but not at intermediate heights.

¹³ Several installation sequences were considered; row-wise versus column-wise in-
¹⁴ stallation of APAs and CPAs. The current installation sequence was deemed superior
¹⁵ in that it minimizes work activities in previously installed sections of the detector.
¹⁶ This reduces the risk of damage during installation.

7.8 Photon Detection

¹⁷ Most LArTPCs use TPB-coated PMTs to detect scintillation light. Light emitted
¹⁸ more than a few meters from a PMT is diffused by Rayleigh scattering ($\lambda \approx 90$ ccm),
¹⁹ so PMTs would need to be placed between drift cells. This configuration is not
²⁰ compatible with the APA concept. Conceptually, each interior cathode plane can be
²¹ replaced with two cathode planes separated by sufficient space for an array of PMTs.
²² This would increase the width of the detector and the cavern by $\sim 1\text{m}$ and result in
²³ a lower fiducial mass.

²⁴ A variety of options were considered for the wavelength-shifting scheme and the
²⁵ light guides. These options suffer from lower light-collection efficiency and result in
²⁶ higher cost for the same performance.

7.9 LAr1 Prototype

²⁷ A variety of alternatives to the LAr1 prototype have been considered, e.g. con-
²⁸ structing a series of smaller prototypes to validate the integration of the detector
²⁹ systems. However, smaller prototypes may not catch some unknown issues that this
³⁰ technology, in its current state of maturity, may present.